DYNAMICAL SOURCE PROCESS OF MICROEARTHQUAKES DEDUCED FROM P WAVEFORMS AND THE STRUCTURE OF THE FRACTURED REGION WITHIN THE CRUST

By

Tameshige TSUKUDA

A Thesis Submitted to the University of Tokyo
for the Degree of
Doctor of Science

1979

ABSTRACT

In order to elucidate the dynamical process at the source of a microearthquake occurring within the crust of the earth, a method for waveform analysis and source modelling has been applied to initial P waves observed at some stations.

Data were supplied by the telemetering system of the Tottori Micro-earthquake Observatory of Kyoto University. The observation network covers some seismic active zones in the eastern Chugoku and western Kinki districts, southwest Japan, especially in the following active fault zones as the Shikano and Yoshioka faults in Tottori prefecture and the Yamasaki fault in Okayama and Hyogo prefectures. The region covering the above faults is the target area of the present study. Along the fault traces many spots of microearthquake sources are distributed at an interval of about 3-5km and at a depth of about 10km; each spot has a dimension of several hundreds of meters, which is considered to be a fractured region within the crust.

The telemetered system which contains a multi-channel magnetic-tape recording system provides us with seismograms of high quality: Recording at a central station yields accurate timimg, in particular, relative time relations, and the waveforms of ground velocity, having frequency components ranging from 1 to 60Hz and a dynamic range from several μ-kine to 350μ-kine , can be reproduced by the reproducing system into visible forms.

The waveform analysis can be devided into two steps. The first is to deal with analog data inspecting either similarity or dissimilarity in waveforms from different events originating at almost the same place. This inspection is quite requisite not only for preliminary analysis but also for precise location of hypocenter or the initiation point of the fracturing. The second step is concerned with the digital form of seismograms.

Digital data processing involves following procedures: digitization; Fourier transform; deconvolution for instrument, attenuation due to anelasticity of the medium and other frequency dependent medium responses; numerical integration; and so on. Attenuation quality factor Q has been estimated to be 200 - 300 by a spectral ratio method and simulation method using microearthquake waveforms. As a Q-filter it is convenient to employ the most simple formulation designed by Hamano(1970), which is appropriate for digital processing. Although the effect of the layering in the crust just beneath the stations is examined for a simple layered structure model, it is not incorporated into the analysis of actual waveform data because of some ambiguity in the crustal structure which, at any rate, is supposed to have only a slight effect on initial P waveforms. Geometrical spreading due to inhomogeneity of the crustal structure is also examined by a simulation. After removing the effect of instrument and anelasticity, ground velocity signals are integrated numerically and the Q-corrected ground displacements are obtained.

Radiated waveforms due to spreading shear dislocation source over a specified fault for an infinite medium are calculated by the method of Sato(1975, 1976). Rupture is assumed to start at a point and extends circularly at a constant velocity over the fault. The source time function at each point on the fault is assumed to be of a ramp-type with a constant rise time and final dislocation displacement. The shape of the radiated seismic pulse observed can be mainly ascribed to the fault shape and mode of rupture propagation, i.e., either unilateral or bilateral. Triangular and rectangular faults are modeled successfully in this study. Those are representatives of faults of arbitrary shape. In the modelling the rupture velocity is assumed to be 2.0 km/s.

Typical examples of simple P waveform seemingly almost free from distortion by medium response provide a key for dealing with more complex waveforms. It is found that the

effect of the inhomogeneous medium is so large as the observed wave that has traveled over a distance of more than about 30 kilometers cannot be corrected satisfactorily by a simple deconvolution. However the initial part of the wave just after the onset may considerably keep the origial form at the source. Some simple waveforms observed were transformed by deconvolution into the ground displacements, whose shape can be approximated by a triangular pulse with a width of about 30ms. But other example with a similar pulse width shows roughly trapezoid shape. The former is attributed to a relatively large rise time of 20ms and a triangular fault, the latter a small rise time of 10ms and a rectangular fault.

Fault dimensions obtained by comparison between theoretical and observed waveforms range from 40m to 120m. Those of relatively large events whose waveforms are all saturated on the seismogram traces have been investigated in the light of aftershock occurrences. The shocks of magnitude 3.7 and 3.1 which occurred at Yasutomi along the Yamasaki fault on September 30, 1977, has aftershock areas of 300 and 200m in diameter, respectively. The latter can be interpreted as a unilateral fault.

The fractured region, where microearthquakes frequently occur in a cluster, is found to be composed of small faults in echelon. At the Shikano fault, the source of the Tottori Earthquake of 1943(M7.4), more than 100 events with their linear dimensions less than about 60m were registered in June and July, 1977. The integrated source region extended long 500-600m in length and nearly along the active fault trace. This region is supposed to be elongated up to 1km for longer time interval.

One of the principal achievements in the present study is discovering the evidence of stick-slip in microearthquake faulting. At the source region near Tottori at a depth of about 10km, the fault with a length of 100m has made slip over the whole length either two times or three times generating

earthquakes of magnitude 2. Similar stick-slip faults have been observed for smaller events in the Yamasaki and Yasutomi regions as well as Tottori. High frequency components superimposed on P wave pulses correspond to one another for events originating from the same fault, indicating some asperity inherent to the fault. This nature is important for discussing seismic wave spectra.

Dislocation displacement $\bar{D}$, seismic moment Mo and stress drop $\Delta\sigma$ were evaluated for microearthquakes of magnitude ranging from 0.0 to 2.0 as follows;

$$\bar{D}=0.1\text{-}2 \text{ cm}, \quad M_o=10^{17}\text{-}10^{19} \text{ dyne-cm}, \quad \Delta\sigma=10\text{-}500 \text{ bars}.$$

Source parameters including the fault shape and rise time show distinctive regional variation. The effective stress exerted on the source region in the Yamasaki fault area seems to be higher than in the Shikano fault area. This may perhaps be partly due to the difference of source depths.

The validity of the present procedure for obtaining source parameters of a microearthquake has been fairly established inspite of some difficulties remained. Among these is the distortion effect of an inhomogeneity of the crust on seismic waveforms, which is evident from travel time irregularities, appearance of some crustal phases and splitting between SV and SH waves. The amount of the variation of the medium constants is up to 3%.

The present study is the first step to make clear the nature of microearthquake sources in a quantitative manner. The results are relevant to not only experimental studies on fracturing of rocks but also theoretical works on a realistic model of an earthquake source. Owing to a large number of events, researches on microearthquakes are remarkablly promising, especially in the earthquake source study.

TABLE OF CONTENTS

PREFACE

Development of high-sensitivity seismographs have revealed microearthquake activity in the earth. Pioneering works were done by Asada et al. who investigated magnitude distribution and established a similar relation with Gutenberg and Richter's or Ishimoto and Iida's formula for microearthquake events(Asada , 1957). Hypocentral distribution and focal mechanisms of microearthquakes have been investigated extensively utilizing data from routine observation at array stations by many workers (e.g.,Hashizume, 1970; Kishimoto and Nishida, 1973). Abundant data of hypocenters and focal mechanisms have promoted discussions concerning the relationship between tectonic structure and micro-seismicity(Mizoue et al., 1973; Oike, 1976),and orientation pattern of the tectonic stress(Nishida et al., 1974).

On the other hand detailed studies on source process has been remained to be undertaken. Recent development in recording apparatus and telemetering system enables us initiate comprehensive research on the mechanism of microearthquake generation. Major problems assigned to the present study are as follow:

1) Is a simple dislocation source model applicable to microearthquakes?
2) To what degree of details about source structure and dynamical process we can approach?
3) What kind of waveforms are analyzable?
4) What is the most simple and efficient technique dealing with seismograms?

The present thesis puts forward a fundamental technique appropriate to investigation of microearthquake sources in Chaper I. Applications are given in Chaper II, where source parameters are determined and fine structures of source regions will be fully discussed. Chaper III is a supplement to the preceding chapers, discussing and evaluating the medium effect on seismic waves.

The data were supplied by the Tottori Microearthquake Observatory, Disaster Prevention Research Institute, Kyoto University.

CHAPTER I

WAVEFORM ANALYSIS AND SOURCE MODELLING FOR MICROEARTHQUAKES

1.1 INTRODUCTION

Microearthquakes ordinarily occur so deep in the earth compared with their source dimensions that any static deformation at the ground surface cannot be detected and excitation of surface waves is very small. Under this circumstances we must make use of body waves for obtaining any information about the source.

For the purpose of deducing the time history at an earthquake source in detail, studies on waveforms are necessary. The most simple consideration about waveforms was made by Komura (1956), who found that the time interval between initial onset and a certain phase which appears on the early part of seismic waves shows a regular geographical distribution for Fukui earthquake of 1948(M7.3), and presented such a hypothesis that a great crack runs in a given direction along one of the nodal lines with a velocity of 2.1km/s. More advanced studies would be based on comparison of waveforms with synthesized seismograms derived from a theory of earthquake source.

In this chapter a systematic procedure to study the source process of microearthquakes is presented. we shall deal with a analog waveforms in the first step, then digital waveforms in the second step. In the last step an earthquake source model will be constructed.

1.2 OBSERVATION SYSTEM

A seismometric apparatus conventionally used in microearthquake observation is made up of an electro magnetic transducer or seismometer and compound electronic devices. Seismic signals are transformed into electric currents by the transducer, and then the electric signals are transmitted, modified and stored by various electronic devices such as transmitter, detector, amplifier, frequency modulator, frequency demodulator, analog-digital converter, digital-analog converter and memorizing devices or recording apparatus. It is convenient to designate this complex form of observing apparatus as observation system. The total system is divided into several sub-systems. The fundamental constitution is as follows; (1) transducer and amplification system, (2) transmitting system, (3) data accumulating system or recording system, (4) reproducing system. The last system is necessary for reproducing waveform data available for various purposes. An example of the constitutions of observation system is shown in Fig. 1.

Moving-coil type transducers have the property that their output voltage is proportional to the ground velocity for frequencies beyond the natural frequency of the pendulum. When a velocity impulse $\delta(t)$ (Dirac delta function) is entered in this transducer, following voltage is excited:

$$E_o = G\left[\delta(t) - \left\{2\varepsilon\cos\left(\sqrt{n^2-\varepsilon^2}\,.t\right) + \frac{n^2-2\varepsilon^2}{\sqrt{n^2-\varepsilon^2}}\sin\left(\sqrt{n^2-\varepsilon^2}\,.t\right)\right\}e^{-\varepsilon t}\right]$$

$$\text{when} \quad n \geq \varepsilon$$

$$= G\left[\delta(t) - \left\{2\varepsilon\cosh\left(\sqrt{\varepsilon^2-n^2}\,.t\right) + \frac{n^2-2\varepsilon^2}{\sqrt{\varepsilon^2-n^2}}\sinh\left(\sqrt{\varepsilon^2-n^2}\,.t\right)\right\}e^{-\varepsilon t}\right]$$

$$\text{when} \quad n < \varepsilon \qquad (1.1)$$

where G, n and ξ are sensitivity, natural angular frequency and damping constant, respectively. The above formula is easily obtained by solving the ordinary differential equation of motion of the pendulum. As shown in Fig. 1 the generated electric current is entered into the pre-amplifier passing through the registor of the coil attached to the pendulum and the shunt registor. The resultant voltage supplied to the electronic devices is turned to be

$$E = \frac{Rs}{Rc+Rs} \cdot E_o \qquad (1.2)$$

where Rc and Rs are coil and shunt registances respectively. These registances have an effect on determining the value of the damping constant. It is convenient to express the damping characteristic with $h(=\frac{\xi}{n})$ rather than ξ. In the frequency domain the response of the seismometer is formulated as

$$\bar{E}(\omega) = G \frac{-\omega^2}{n^2-\omega^2+2\xi\omega i} \qquad (1.3)$$

The sensitivity G has a value of several volts per kine, where kine means velocity unit of cm/s and will be used throughout this thesis for the sake of convenience. When the unit appears in either the text or figures we can immediately be acquainted with descriptions concerning velocity seismograms. The damping constant h is usually taken as $h^2=0.5$ which is a critical value taking position between over damping and peaking at the natural frequency. At almost all the routine stations for microearthquakes in our country seismometers with pendulum frequency of 1Hz are installed(

Suzuki et al., Microearthquake Observatories in Japan, second edition, 1979).

It is not practical to calculate an impulse response to the integrated series of electronic devices and transmission lines in terms of electric circuit theory. Thus we examine the system response by an experimental procedure: The frequency characteristic or transfer function can be obtained by measuring the spectra of both output and input signals. This procedure is namely deconvolution which will be discussed in a later section with respect to waveform analysis. Combining the low-cut characteristic of seismometer and the high-cut characteristic of electronic devices the overall characteristic is obtained as shown in Fig. 2, which is derived from the telemetering observation system operated at the Tottori Micro-earthquake Observatory(hereafter abreviated as T.M.O). All waveform signals analyzed in the present thesis are passed through this system. We can see from the figure the effective frequency band of 1-60Hz(-3dB drop).

Quality of data largely depends upon the ground noise at observing sites. The irregular noises at the array stations of T.M.O. have frequency components of 10-20Hz and its level is lower than 10μ-kine except for one or two stations. Tremors orginating from seashore have dominant frequencies of 0.5-1Hz and sometimes exceed the level of several hundred μ-kine during the time of stormy weather.

Consistency of the accumulated data is another aspect of their quality. Details about data accumulating system and monitoring system at T.M.O. are described by Kishimoto et al. (1978).

1.3 INSPECTION OF SEISMOGRAM

Primitive forms of seismic wave data or seismograms alone instruct us some important facts for seismological problems. In this section some examples of typical seismogram data are presented serving as elementary understanding of microearthquake sources and medium effects on waveforms.

Microearthquake waveforms are generally so complicated that it is difficult to deduce the real form of either P or S waves originated from the source. The first step we must take in the study of source process in terms of waveforms is to search for seismograms providing simple waveforms. Among over thousands of microearthquake events only several tens of events have a solitary P waveform shown in Fig. 3. Such simple data all belong to nearby earthquakes such an S-P time of 1-2.5sec. S waves are always complicated and contaminated by late arrivals. These velocity waves show very simple sinusoidal forms with one-cycle duration , suggesting their displacement waveforms as a triangular pulse like. These waveforms clearly demomstrate that the seismic waves are quite simple in an original form. This nature also indicates that the dynamical process at a microearthquake source is quite simple and can be modeled by a simplified treatment. Moreover complicated waveforms which appear on the most of seismograms may be intertreted as composed of various wave packets with simple forms, being superimposed by each other.

Fig. 4 shows another type of simple forms of P wave which are quite different from those of Fig. 3. Their shape is almost rectangular rather than sinusoidal. The initial rectangular pulse is accomanied by another rectangular pulse with opposite polarity after a short intermission. The displacement waveforms derived from them are supposed to be like a trapezoid. Existence of the above two types of body wave shape has been predicted by a simplified dynamical dislocation theory which will be discussed in a later section.

The most important procedure in the stage of inspection of waveforms is to compare a waveform of an event with that of another event with almost the same origin. This procedure will enhance releiability of observed data as well as inform us both source process and medium response. Fig. 5 demonstrates a typical set of similar waveforms. Let us observe the minor crests and troughs appearing after the initial large pulse. The coincidence of appearance time of either each crest or trough among the three events is excellent with an accuracy of time within 5ms. Such adjustment of arrival times of later phases results in disagreement of the onset times indicated by arrows in the figure. Enlarged traces of initial waves are given in Fig. 6 where the discrepancy of duration times are clearly seen though it is very small amount of 5ms.

The observational facts above discussed provide an important clue to making clear the structure of the source region of the pertinent events. Firstly the fine agreement of high-frequency late arrivals indicates that the origins of these events are closely located: We can roughly estimate the distance range about 30m assuming the P wave velocity as 6km/s and the time difference within 5ms. By the way the source dimensions of the individual events will be deduced as 30-40m in Chap. II. Combining these results we can conclude that the events have a common source region. The second implication inferred from the waveforms is the variation of pulse width from event to event originating from the same source. Is similar phenomenon recognized for ultra-microrarthquakes with a dominant frequency of more than about 100Hz? Ito(1977) investigated such earthquakes which occurred at Matsushiro, central Japan. Fig. 7 is the seismograms complied by Ito. The initial waves have different duration time; the longer the time the larger the amplitude. However it should be noted that so called scaling law by Aki(1967, 1972) is necessarily applicable to all the earthquakes as comfirmed by Chouet et al.(1978).

There are such cases that in spite of large difference of amplitudes the duration times show only slight difference as shown in Fig. 8.

We have inspected some typical waveforms of natural microearthquakes so far. Here let us examine artificial earthquakes or explosions for the sake of comparison. We choose two events detonated at almost the same site but about several hundred meters apart from each other and compare the waveforms of these events. As seen from Fig. 9 the first and second events have almost the same initial P waveform at every station in both amplitude and duration time, but their late arrivals are somewhat different from each other. This fact indicates that although the source time function is commom to the two events, the medium effects on their waveforms can be clearly distinguished. This means that the detonation points are separately located. By the method of hypocenter location based on P times, which will be discussed in the next section, the distance between the shot points is found to be about 500m.

1.4 HYPOCENTER LOCATION AND FAULT PLANE DETERMINATION

The most fundamental procedures in earthquake seismology are hypocenter location and fault plane determination. For they provide such important source parameters as coodinates of rupture initiation point, origin time or rupture initiation time, fault plane orientation and slip direction. Conventional methods for calculating the hypocentral parameters are based on a least squares technique with large amount of arrival time data, which is typified by the method of Bolt(1960). These methods are not applicable in the case of few data. Moreover it is not reasonable to use the data from distant stations because their reading times are not accurate compared with those of nearby stations. The method presented below gives a precise solution for necessary and sufficient input data and given medium constants and do not involve any approximation. The purpose of this method is to assure the relative positions of hypocenter among events of near sites. For this purpose we only use P arrival times at fixed four stations.

Let us assume that the medium is in a semi-infinite space with a horizontal surface and its constants are functions of only z which is the coordinate of vertical direction for the rectangular coordicate system x, y, z.. Then the travel time of a P wave can be calculated by some methods and expressed as a function of epicentral distance r and focal depth h. By the inversion of this travel time relation we can calculate epicentral distances r_1, r_2, r_3 at stations of 1, 2, 3, respectively, for a certain h(=-z) and a certain t(origin time) as follow:

$$x^2 + y^2 = r_1^2 \tag{1.4}$$

$$(x - x_2)^2 + (y - y_2)^2 = r_2^2 \tag{1.5}$$

$$(x - x_3)^2 + (y - y_3)^2 = r_3^2 \tag{1.6}$$

where (x, y) and (x_i, y_i), $i=1, 2, 3$ denote the coordinates of epicenter and stations, respectively, and $(x_1, y_1)=(0.0)$. Subtracting (1.5) and (1.6) by (1.4), respectively, we obtain

$$x = \frac{(r_1^2-r_2^2+x_2^2+y_2^2)y_3-(r_1^2-r_3^2+x_3^2+y_3^2)y_2}{2(x_2y_3-x_3y_2)}$$

$$y = \frac{(r_1^2-r_2^2+x_2^2+y_2^2)-2x_2x}{2y_2} \tag{1.7}$$

where we assume that $x_2y_3 \neq x_3y_2$ and $y_2 \neq 0$.
Substituting (1.7) into (1.4) the following relation is established:

$$f(t, h) \equiv \frac{r_1^2}{x^2+y^2} - 1 = 0 \tag{1.8}$$

where x and y are given by (1.7). In terms of the relation(1.8) we can determine the hypocenter for any given h. Of cource there is the case that no solution is found. The hypocenter as a function of h describes a locus in the semi-infinite space as illustrated in Fig. 10. In this stage we have no measure to determine the focal depth. In order to do

this another set of tripartite stations, for instance, stations 2, 3, and 4 must be incorporated and the same manner should be followed. The intersection of the two loci is the final result. Computational procedure involves solving the Eq. (1.8) numerically by iteration which must be continued until demanded accuracy is attained. The pair of loci are traced from the surface to a certain depth until they intersect each other. Some applications of this method to actual data have been attempted by Tsukuda et al.(1977a).

If the medium is homogeneous and the seismic wave velocity is V_o, then the fundamental equations are given by

$$(x - x_i)^2 + (y - y_i)^2 + h^2 = V_o(t_o + p_i)^2 , \qquad (1.9)$$

$$i = 1, 2, 3, 4$$

where P_i denotes relative arrival time at station i and t_o means relative origin time. Eqs. (1.9) can be easily rewritten as

$$2(x_i-x_1)x+2(y_i-y_1)y=V_o^2\left\{(t_o+P_1)^2-(t_o+P_i)^2\right\}+x_i^2-x_1^2+y_i^2-y_1^2$$

$$\text{for } i=2, 3, 4 \qquad (1.10)$$

$$h^2=V_o^2(t_o+P_1)^2-(x-x_1)^2-(y-y_1)^2$$

This is the system of linear equations and can be easily solved by matrix formulation. Eqs. (1. 10) are also treated by a similar manner previously mentioned. Details of such computational procedure are described by Tsukuda et al.(1977c).

As will be discussed in Chap. II microearthquakes generally occur at a depth around 10km in the granitic layer with a P wave velocity of about 6.0km/s and this layer has a considerable thickness more than 10km. Therefore the medium

model required for hypocenter location in terms of arrival times at near stations may be considered to be homogeneous. Some examinations assure this conclusion: Deviation from the result for a more realistic medium model is found be within about 1km. Because our concern is the relationship between the positions of clustering events, we shall adopt the homogeneous model of the medium for the sake of simplicity.

Estimation of hypocentral errors due to reading errors is important for discussing the fine structure of a source region of similar events. A simple procedure relevant to this problem is based on a simulation as presented by Tsukuda et al.(1976b, 1977d). The simulation of hypocenter determination has been carried out as follows. Let P_i(i=1, 2, 3, 4) be reading times of P wave at the four stations. We assume that P_i takes one of following values; P_{io}, $P_{io}-\varepsilon$ or $P_{io}+\varepsilon$ for i=2, 3, 4 and that the value of P_1 is fixed as P_{10} in order to reduce the frequency of iteration. Then $27(=3^3)$ hypocenters corresponding to the respective perturbed reading times are determined.

After obtaining the hypocentral parameters we must settle down determining the fault planes with respect to the partinent event. Available data for this purpose includes mainly polarities of initial motion, amplitudes of P and S waves and polarization angles of S waves. In most cases of current microearthquake observation, seismograms of horizontal components are not available. Therefore we must use S wave data incompletely. Initial motions, P wave amplitude and a special set of S wave properties would determine the fault plane solutions. If necessary several assumptions should be made concerning to such constraints as type of faulting, strike direction and dip angle. Such constraints are inferred from the solutions of other similar events. The above principle can be explained as follows. Let us take two sets of A and B. A contains all revealed focal properties

belonging to a certain definite event and B those of another minor event originating slightly apart from it. If the relation $B<A$ holds, we regard the two events equivalent to each other. The more the number of elements of B is the more the two events are similar to each other. If there are some elements of B that are not contained in A, the equivalency is not hold. Calculations of take off angles at foci are based on the horizontally layered crustal model derived from the Kurayoshi and Hanabusa explosions(Hashizume, et al., 1966).

1.5 WAVEFORM ANALYSIS

Seismic signals are initiated at the source and propagated through the medium taking various ray paths in the form of elastic waves and finally transformed into electric signals by an observation system. Signals within a narrow time interval are considered to be propagated along a narrow band of rays in the medium. Under this condition the medium along this band can be regarded as a linear system in response characteristic, which consists of sub-systems in series corresponding to every portion of the medium. As similary as in the study of large earthquakes(Ben-Menahem et al., 1965) the response of the medium may be represented by the following transfer function;

$$T(\omega)=G\cdot T_A(\omega)\ T_L(\omega)\ T_O(\omega) \qquad (1.11)$$

where $T_A(\omega)$, $T_L(\omega)$ and $T_O(\omega)$ are the transfer functions for the attenuation effect of the medium, reverberation due to layers just beneath the ground surface and observation system, respectively, and G is the diverging factor or geometrical spreading factor.

For a semi-infinite medium the geometrical spreading factor is given by

$$G=\sqrt{\frac{V_h\,\rho_h\,\sin i_h}{V_o\,\rho_o\,\cos i_o\cdot D}\left|\frac{di_h}{d\,D}\right|} \qquad (1.12)$$

where V_h, ρ_h and i_h are seismic wave velocity, density and take off angle at the source, respectively, and V_o, ρ_o and i_o are velocity, density and incident angle at the surface,

respectively; D denotes epicentral distance. The transfer function for the layering is readily calculated by the matrix formulation given by Haskell(1962) provided that the medium model has been established. Before discussing other transfer functions of (1, 11) let us review some aspects of spectral analysis and digital processing.

Let $f(t)$ be a waveform observed during the time $0 \leq t < \tau$. Extending the values of $f(t)$ over $t<0$ and $t \geq \tau$ periodically we get a periodic function of period τ. Then $f(t)$ can be represented by a Fourier series:

$$f(t) = \sum_{k=-\infty}^{\infty} c_k \, e^{ik\omega_0 t} \quad , \quad \omega_0 = \frac{2\pi}{\tau} \tag{1.13}$$

with

$$c_k = \frac{1}{\tau} \int_0^{\tau} f(t) \, e^{-ik\omega_0 t} dt \tag{1.14}$$

When $f(t)$ is digitized at an interval of $\Delta t (= \tau/N)$ into a time series x_n, it is convenient to define the Fourier coefficient as follows(Brillouin, 1962):

$$c_k = \begin{cases} \frac{1}{N} \sum_{n=0}^{N-1} x_n \exp(2\pi i \frac{kn}{N}), & |k| \leq \frac{N-1}{2} \\ 0 \quad , & |k| > \frac{N-1}{2} \end{cases} \tag{1.15, 1.16}$$

The above condition means that the higher harmonics are

regarded as negligible. In this case the inverse relation is

$$x_n = \sum_{k=0}^{N-1} c_k \exp\left(2\pi i \frac{kn}{N}\right) \qquad (1.17)$$

Computations concerning to (1. 15) and (1. 17) can be easily carried out by way of the algorithm of the Fast Fourier Transform(Cooley and Tukey, 1964). On the other hand the Fourier transform for the time series of a transient wave y_n is defined to be

$$Y(\omega) = \Delta t \sum_{n=-\infty}^{\infty} y_n \exp(-i\omega n \Delta t) \qquad (1.18)$$

where $y_n = x_n$ when $0 \leq n \leq N-1$ and $y_n = 0$ when $n<0$ or $n>N-1$.
From (1.15) and (1. 18) we can deduce the relationship between the Fourier coefficents for a periodic function and the Fourier transform for the corresponding transient wave as follows:

$$c_k = \frac{1}{N\Delta t} Y\left(2\pi \frac{k}{N\Delta t}\right) \quad \text{when } |k| < \frac{N-1}{2} \qquad (1.19)$$

Hereafter we shall use the Fourier coefficents regarding as the Fourier transform in the above sense. The time t and frequency f $(=\omega/2\pi)$ are expressed as

$$\begin{aligned} t &= n\Delta t \qquad n = 0, 1, \cdots, N-1 \\ f &= k\Delta f \qquad k = 0, \pm 1, \cdots, \pm\left(\frac{N-1}{2}\right) \end{aligned} \qquad (1.20)$$

where $\Delta f = \frac{1}{N\Delta t}$. The frequencies are bounded by the limit or

Nyquist frequency $f_N=\frac{1}{2\Delta t}$. We must remove beforehand the higher frequency components beyond this limit from the original wave data. Taking account of the response of the observation system as shown in Fig. 2 it is reasonable to choose the Nyquist frequency as 100Hz for this study. Accordingly the sampling time interval Δt and frequency interval Δf are 5ms and 0.391Hz, respectively. In what follows the formulation of the several transfer functions in digital forms will be presented.

Transfer Function for Attenuation

We want to construct a transfer function for attenuation due to anelasticity of the medium. The attenuation factor in seismic wave amplitude is conventionally given by

$$\left|T_A(\omega)\right| = e^{-\frac{\omega}{2Q}t} \qquad (1.21)$$

where t is the duration time for propagation and Q denotes the quality factor for attenuation. The Q value seems to be nearly constant for a wide frequency range according to field observations and laboratory experiments for rocks(e. g., Attewell et al., 1966). However, the recent experimental study of Berkhemer et al.(1979) shows a tendency for a general increase in Q with frequency ranging from o.ol to 1Hz, which is obtained by analyzing the spectra due to a step-like stress exerted on the mantle peridotite at a high temparature of 1200° and 1300°c. Although it is not certain that the above tendency would be found for the crustal materials and for the frequencies higher than 1Hz, let us model this characteristic for the transfer function. According to Hamano(1970) it is convenient to adopt such a form of transfer function as

$$T_A(\omega) = \exp\left\{ -\frac{t}{Q\,\Delta t}\sin\left(\frac{\omega\,\Delta t}{2}\right) + i\phi(\omega) \right\} \tag{1.22}$$

$$\phi(\omega) = -\frac{t}{\pi Q\,\Delta t}\sin\left(\frac{\omega\,\Delta t}{2}\right)\ln\frac{1+\cos\left(\frac{\omega\,\Delta t}{2}\right)}{1-\cos\left(\frac{\omega\,\Delta t}{2}\right)}$$

where Q is taken as a constant: $\phi(\omega)$ is the phase angle, which is determined by causality relations proper to a linear system (Futtermann, 1962); $T_A(\omega)$ should be extended over $|\omega|>2\pi f_N$ periodically as indicated from (1. 18). As seen from (1. 22) the transfer function is characterized by a dimensionless parameter $\frac{t}{Q\cdot\Delta t}$ or $\frac{r}{VQ\Delta t}$, where r and V are propagation distance and seismic wave velocity, respectively, provided that either t or f_N is specified. Amplitude characteristics of $T_A(\omega)$ are presented in Fig. 11. Dotted lines show the characteristics of (1. 21). Discrepancy between the two transfer functions is small for lower frequencies. The raised amplitudes in the transfer function(1. 22) at higher frequencies have a role to depress high frequency numerical noises when the transfer function is used in deconvolution or inverse operation. This is another reason for employing the transfer function or Q-filter presented in (1. 22).

Transfer Function for Observation System

The frequency response or transfer function for the transducer or velocity type seismometer takes a form similar to the expression (1. 4). As easily seen from (1. 4) the transfer function vanishes at $\omega=0$, which causes division by

zero in inversion process or deconvolution. In order to avoid such difficulty, an approximate substitute should be employed. For this purpose we turn back to the impulse response (1. 1), the Fourier transform of which gives the transfer function. The transformation was carried out numerically by the use of the Fast Fourier Transform. The delta function $\delta(t)$ in (1. 1) is approximated by a spike with a height of $1/\Delta t$. The numerical result turns out to be satisfactorily precise with its deviation within 3%, and the difficulty previously mentioned is removed. The transfer function for the electronic devices was also obtained by the same procedure, where the impulse response waveform was experimentally deduced. Multiplying the transfer functions for the seismometer by that for the electronic circuit the overall transfer function is eatablished in a numerical form. Its frequency characteristic for the system operated at T.M.O. is presented in Fig. 2.

Numerical Differentiation and Integration

The transformation of a velocity signal into the corresponding displacement signal and vice versa is made by numerical integration and differentiation, respectively, rather than by convolution and deconvolution in frequency domain, avoiding the accumulated errors in the prosses. Such operations in time domain are applied to the appropriate part of the whole waveform assuming the other parts negligible to assure the stability of the operation. The differentiation is formulated by

$$y_n=(x_{n+1}-x_n)/\Delta t \qquad n=1, 2, \cdots, N \qquad (1.\ 23)$$

and integration by

$$y_n = \Delta t \sum_{n=1}^{N} x_n \qquad (1.\ 24)$$

where we assume the signal x_n for $n<0$ and $n>N$ vanishes or is negligible. In the above formulation a pseudo phase lag due to above representation arises. However this phase lag would bring about merely a shift of a waveform along the time axis.

In addition to the above operations in time domain it is convenient to use an interpolation technique based on the sampling theorem. A digital form of waves is a descrete function of time with an interval of Δt. When we want to obtain its analog version or more smoothed waveform, the waveform $f(t)$ for arbitrary time t is calculated by the formura

$$f(t) = \sum_{n=1}^{N} x_n \frac{\sin\pi(t/\Delta t - n)}{\pi(t/\Delta t - n)} \qquad (1.\ 25)$$

for $t>0$

where $x_n = f(n\,\Delta t)$ and $f(0)=0$. This formula is based on the limited frequency band with its width f_N, the Nyquist frequency. Throughout this thesis waveforms are plotted at an interval of $\Delta t/2$ by the interpolation method above presented.

Convolution and Deconvolution

In the frequency domain the spectrum $F(\omega)$ or Fourier transform of an input wave is transformed into the spectrum

$G(\omega)$ of its output wave by the relation:

$$G(\omega)=T(\omega)\cdot F(\omega) \qquad (1.\ 26)$$

where $T(\omega)$ is the transfer function of the linear system concerned. Above transformation is equivalent to so called convolution. The inverse relation of (1. 26), that is,

$$F(\omega)=T(\omega)^{-1}\cdot G(\omega) \qquad (1.\ 27)$$

exhibits the deconvolution procedure.

Let us examine the response of the linear system including the absorptive medium and the observation system by convolution. A triangle-shaped seismic displacement wave as shown in the top of Fig. 12 changes its form variously according to the attenuation parameter for the observation system of T.M.O. As seen from Fig. 12 the position of the zero-crossing point on the seismogram waveform moves with the value of the attenuation parameter. Fig. 13 is another representation of the effect of the system, where the various input waves and its responses are described for a fixed value of the attenuation parameter. These diagrams are very useful for estimating the duration time of seismic pulses from the inspection of seismograms, especially when the seismogram traces are saturated in their amplitude due to the limitted amplitude range of observation system.

On the contrary deconvolution procedure is applied for removing the effect of the system from seismogram waveforms. Fig. 14 describes a typical example of this procedure presenting deconvolved waveforms together with the original waveform. Firstly the observed

waveform was converted into the true ground velocity at the observing point by the deconvolution for the observation system. Next, the attenuation effect due to absorption in the medium was removed. Finally the Q-deconvolved ground velocity was transformed into the ground displacement in the case that the medium were not anelastic. The above procedure does not include the deconvolution for layering medium. In the present study we shall not dwell on this problem partly because the structure model of the upper most crust is not so definite and partly because it is supposed that the effect is rather weak as noticed from some simple waveforms observed. For example the displacement waveform in Fig. 14 has a quite simple shape except for the later portion that indicates high frequency oscillation, which may be due to the source process rather than the crustal response because of the difference in frequency contents between the main part and the later part.

The above example is one of the most simple P waveforms observed, which are isolated from later waves. In the case of more complicated waveforms showing no marked quiescence after their initial wave packet it is difficult to decide the trace point beyond which we must cut off the later waves. Some examinations for actual data in the extreme cases of very short cut on the one hand and rather long cut on the other indicate that the amplitude deviations for the final displacement waveforms amount to more than several per cent but general shapes of the initial waves are scarecely changed.

1.6 MODELLING OF MICROEARTHQUAKE SOURCE

Earthquakes are considered to be caused by either brittle fracturing of the rock or stick-slip movement on a preexisting fault. In either cases shear faulting may occur at the source. The mathematical formulation for seismic waves due to this type of source is based on dynamical elastic theory on dislocation or its equivalent force system, i. e., the double couple source(Maruyama, 1963).

It is quite probable that an initial rupture or slip arises at a certain point and at a certain moment of time, then the rupture spreads radially on a surface radiating seismic waves, and finally the slipping ceases after some time leaving a fault with a certain finite dimension. Let us construct an ideal model for an earthquake source having above nature. We assume that the rupture is initiated at a point and extends circularly at a constant velocity Vr(rupture velocity) over a fault. The dislocation displacement D(t) as a function of time t at each point on the fault can be approximated as

$$D(t)=\begin{cases} 0 & t<0 \\ (t/\tau)\bar{D} & 0\leq t\leq \tau \\ \bar{D} & \tau<t \end{cases} \qquad (1.28)$$

where $\bar{D}$ denotes the final displacement and τ means the rise time of the source time function. We assume that the values of $\bar{D}$ and τ are constant over the entire fault.

The generated fault has a definite boundary surrounding it, which may take various shapes. Let us consider following two types of fault; triangular fault and rectangular fault. Any rounded or generally elliptical shape is approximately described by a certain rectangle with an appropriate aspect

ratio, and a triangle represents a typical peaked shape. The triangular fault will be used for modelling P waveforms with gradual onset. For simplicity we treat merely an isosceles triangle with a height a and the length of its base 2b as shown in Fig. 15. On the other hand the rectangular fault is specified by a length a and a width 2b. Taking rupture initiation point into account we will study the following respresentative fault models; (1) unilateral triangular fault, (2) unilateral rectangular fault, and (3) bilateral rectangular fault. The positions of initiation points of rupture and fault geometries assumed are shown in Fig. 15. It is reasonable to take a a representative length of the fault rather than 2b and the relation $a>2b$ holds, because the observed pulse-width changes largely in the case of horizontal rupture propagation; the vertical propagation is insensitive. Since the purpose of this model construction is to interpret the seismic pulse in terms of fault parameters and the data available are limitted in number, then the number of the parameters or degree of freedom must be reduced as small as possible. Hence we assume that $b=a/4$.

Our problem is to determine rise time τ, final dislocation displacement $\bar{D}$, fault shape, and fault size a by comparing the observed seismic waves with theoretical ones.

Theoretical waveforms are readily computed by the method presented by Sato(1975, 1976), where expressions are derived to obtain displacements due to a fault with an arbitrary shape in an infinite medium not by the double numerical integration but by the single integration with less computation time than the conventional method. Let us express the displacement at the station(r, θ, ϕ) as (u_r, u_θ, u_ϕ) for the polar coordinate system taking the origin at the hypocenter of a microearthquake, where r is the hypocentral distance, θ inclination angle of the radial axis from the vertical and ϕ azimuth. In the case of far field observation the transversal components of a P wave are considered to be negligible leaving the substantial

displacement of u_r, the radial component. We compute u_r at the pertinent stations. Figs. 16(a), (b), (c), (d) show some examples of the computational results. These are diagrams for modelling the microearthquake source at Tottori as will be discussed in Chap. II. The pulse shapes are roughly classified into either triangular and trapezoidal types. The latter occurs in the either cases that the fault length $\underline{a}$ is sufficiently small for both triangular and rectangular faults or that the fault length is sufficiently large for rectangular faults. The former appears in case of triangular faults for a wide range of $\underline{a}$ and τ. For suitable values of $\underline{a}$ and τ the displacement due to a rectangular fault shows a symmetrical triangular shape. We notice that triangular faults bring forth asymmetrical triangular pulses with peaks at their later portions; the slope of the onset is gradual in comparison with the similar triangular pulses due to rectangular faults. The initial slope of an observed P wave would be an important element for fitting the observed wave to the theoretical ones.

The radial component displacement computed for the infinite homogeneous medium is related to the vertical component ground displacement at the observing point in such a way that the former is incident on the bottom of the superficial layer just beneath the pertinent station and transformed into the latter. According to the result given in Chap. III the amplification factor (ratio of output amplitude devided by the input) range from 1.2 to 2.5 for incident angles from 0° to 70°. The assumed crustal model is given in Fig. 39. The frequency characteristic of the transfer function for this structure model has merely slight effect on the P waveforms. Since the thickness of the layer is very small(2.2km) compared with epicentral distances, then existence of this layer is neglected in the computation of theoretical displacements.

1.7 DISCUSSIONS

Our fundamental source parameters are rise time τ, dislocation $\bar{D}$ and fault dimension $\underline{a}$ for given fault shape as presented in the last section. From these parameters some other source parameters are derived. The static moment acting on the fault is

$$Mo = \mu S \bar{D} \qquad (1.29)$$

where μ is the rigidity of the medium and S the fault area(Aki, 1966); $S=a^2/4$ for the triangular fault and $S=a^2/2$ for the rectangular fault. The stress drop $\Delta\sigma$, which is another static parameter of the dislocation source, is formulated as

$$\Delta\sigma = c\,\mu\frac{\bar{D}}{a} \qquad (1.30)$$

where c is a dimensionless shape factor(Kanamori and Anderson, 1975). It is so difficult to obtain the expression of c for faults of arbitrary shape that we should be satisfied with some substitutes for them. For the rough estimation it may be convenient to use following formula for a circular fault derived from the theory of Eshelby(1957) assuming the Poisson's ratio as 0.25:

$$\Delta\sigma = \frac{7\pi}{16}\mu\frac{\bar{D}}{r} \qquad (1.31)$$

where r is the radius of the fault. In our case we put $r=a/2$ for triangular faults and unilateral rectangular faults and $r=a$ for bilateral rectangular faults.

On the other hand the effective stress σ_e, which accelerates the dislocation movement, is a dynamical parameter determined by $\bar{D}$, τ and S wave velocity β as follows,

$$\sigma_e = \frac{\mu \bar{D}}{2\beta\tau} \qquad (1.32)$$

for infinite rupture velocity(Brune, 1970) and

$$\sigma_e = \frac{\mu \bar{D}}{2\beta\tau} \left(1 + \frac{\beta}{V_r} \right) \qquad (1.33)$$

for finite rupture velocity V_r(Kanamori, 1972).
Such dynamical parameter cannot be determined by conventional studies based on amplitude spectra of seismic waves.

Microearthquakes have been investigated by way of spectral analysis of seismic body waves, for instance, for the moment range 10^{18}-10^{19} dyne-cm by Douglas and Ryall(1972). Their method is based on the relationship between the corner frequency introduced by Brune(1970) and source dimension, and on the measurement of amplitude. Ishida(1974) also applied this method to small earthquakes with their moment 10^{22}-10^{24} dyne-cm, and at the same time attempted a waveform analysis, where a more simple source model than that of the present study was used. Her method does not involve the fault shape effect, and is based on convolution technique rather than deconvolution.

Which is the better, the convolution method or the deconvolution method, is the point of an argument. Convolution technique, that produces theoretical ground motions from either assumed or theoretical source time function , has been employed widely in waveform analysis, in particular, in body wave studies(Bollinger, 1968; Mikumo, 1969). On the other hand deconvolution, that deduces source time functions from observed waveforms, has been also applied to the studies on deep-focus

earthquakes(Fukao, 1972) and on shallow earthquakes(Langston, 1976). Since the transfer functions for medium and instrument have low-cut or high-cut characteristic of frequency, the convolved signals are deprived of lower and higher frequency components outside the frequency band of the transfer function. This is the same with observed seismograms. Generally it is impossible to recover such components by deconvolution. However those signals cannot bedealt with even by the convolution method. Hence we cannot conclude that the deconvolution method would be inferior to the convolution method. At any rate, we can only discuss waveforms assuming the signals concerned are limitted in their frequency bands. Under this assumption the deconvolved signal and its original one show one-to-one correspondence. Really the convolution for the deconvolved signal results in producing the same signal as the original one. The most remarkable merit in the deconvolution method is that it is convenient to compare the seismic waveforms from various observing points in the same condition and to understand the properties of seismic pulses, which oan be easily classified into some typical types when they are deconvolved.

It is interesting to compare the studies of large earthquakes with those of microearthquakes with respect to waveform analysis by deconvolution. Let us take an example from the study on P waveforms from the large deep-focus earthquake of 1963 in the western Brazil by Fukao(1972). The depth of focus is 577km; the epicentral distance ranges from 47° to 92°, which is substituted by hypocentral distance range from 4885km to 8770km ; and representative pulse width of seismic P waves is 10s. The instrumental response characteristic of the long-period seismograph for the World-Wide Standardized Seismograph Network is shown in Fig. 17 together with that of microearthquake observation. The digitization interval Δt is 0.7s giving the Nyquist frequency

f_N as 0.714Hz. Attenuation factor $r/(V\ Q\ \Delta t)$ ranges 1.4 to 2.5 putting v=10km/s and Q=500. In the study of microearthquakes the focal depth and hypocentral distance are 5-10km and 10-40km, respectively. The pulse width of P waves is about 30ms and 60ms for magnitude of about 0 and 2, respectively. Δt and f_N are 5ms and 100Hz in this study. The attenuation factor ranges from 2.0 to 4.0 for v=6km/s and Q=200-300(Chap.III). Generally speaking microearthquakes are small in time and space by about 1/100 compared with large deep-focus earthqakes. However the procedures for dealing with waveforms are almost identical when taking the scaling factor into account.

The theoretical dislocation model presented in section 1.5 is besed on the assumption that the dislocation time function is uniform on the fault plane. Sato and Hirasawa(1973) presented such a model that the center of the fault slips for a longer time than the edges and consequently a greater relative displacement takes place near the center, and formulated the far-field displacement in the case of a circular fault with the rupture initiation point being at the center. This model produces a gradual onset slope on a seismic pulse. This property can be also produced by our triangular fault model.

The method presented in this chapter is summarized in Fig. 18. Its applications to some interesting problems on microearthquakes will be given in Chap. II.

CHAPTER II

SOURCE PROCESSES OF MICROEARTHQUAKES THAT CLUSTER IN A SMALL CONFINED REGION WITHIN THE CRUST

2.1 INTRODUCTION

Microearthquakes tend to occur successively within a small confined region for a certain time interval. Watanabe(1964) pointed out this nature and attempted to interprete this phenomenon in terms of rheological deformation within the crust. Such sequential events would provide valuable data for studying the mechanism of earthquake generation, in particular, the fracturing process and/or stick-slip sliding(e. g., Mogi, 1967; Brace, 1972). From this point of view the detailed studies on the seismological properties of these events are required. For the first step Tsukuda et al. (1976b, 1977 d) carried out precise hypocenter location for clustered microearthquake events using P arrival times and found that the size of the source region is within several hundred meters.

However it is necessary for obtaining more detailed structure of the source region to investigate seismic waveforms determining the source dimensions of individual events. One of the purposes of this chapter is to clarify the fine structure of the source region where microearthquakes successively occur in a cluster and to confirm whether the stick-slip faulting would occur in reality. Another purpose is to deduce the dynamical source process for many microearthquakes events with special attention to the regional difference in properties of earthquake generating mechanism.

For such purposes the data from the telemetered observation system of the Tottori Microearthquake Observatory(T.M.O.) are excellent. One reason for this is that the observation network covers following very interesting active-fault zones as the Shikano and Yoshioka faults in Tottori prefecture, which is a typical example of the earthquake fault(the Tottori earthquake of 1943, M7.4), and Yamasaki fault in Okayama and Hyogo prefectures, which is conspicuous left lateral strike-slip fault with its length being greater than 60km(Fig. 19).

Fig. 20 shows epicentral distribution of earthquakes of magnitude greater than or equal to 2. We can see linear configulations of epicenters along the above mentioned faults, and vacant area surrounding the fault systems. Such distinct regional contrast in seismicity may indicate relatively simple features of earthquake generation as well as of crustal structure. Another reason for the excellency is that the observation system has high detectability of microearthquake events and high quality of waveform data(Kishimoto et al., 1978; Fig. 1; Fig. 2).

In this chapter we shall deal with clustered events from following sites; Horadani, the Shikano fault; Kuchihosomi, the Shikano fault; Tottori; Yamasaki; and Yasutomi, the Yamasaki fault. The most simple forms of P wave were observed from the events originating from Horadani(Fig. 27). This region is slightly apart northward from the main trend of Shikano fault. At Kuchihosomi a number of ultra-microearthquakes occurred in a cluster along the trace of the Shikano fault. At Tottori relatively large events of magnitude 2 occurred successively. From the Yamasaki region, which is located within the aftershock area of the earthquake(1973, M5.1; Tsukuda et al., 1977a), remarkable P waveforms were observed(Fig. 4). This region is isolated from the microearthquake spots along the Yamasaki fault. At Yasutomi, near the Yamasaki fault, occurred remarkable seismic activity in 1977(e. g., Kishimoto, 1978). The pertinent earthquakes are listed in Table 1.

2.2 HYPOCENTRAL DISTRIBUTION AND FAULT PLANE SOLUTIONS

Utilizing the method presented in section 1.4 hypocenters of events which occurred around the region concerned have been determined assuming the medium as homogeneous and putting the P velocity as 6.0km/s. Figs. 21 and 22 are hypocentral maps for the Shikano and Yoshioka fault area and for the Yamasaki and Yasutomi region near the Yamasaki fault, respectively. From those figures we notice many spots of hypocenters, that are distributed separately at an interval of 3-5km. Detailed descriptions on hypocentral distribution and fault plane solutions are given in what follows. Estimated hypocentral errors due to uncertainty of P arrival times are given in Table 2 together with station parameters. Errors in focal depth are considerablly large compared to epicentral errors.

Horadani, Shikano fault

At the spot near Horadani, the Shikano fault, relatively widespread distribution of hypocenters are observed from Fig. 21. Microearthquakes originating from this spot offer P waveforms of simple shape when observed at SN station as shown in Fig. 3. Fig. 27 shows a typical example of these events. The waveform observed at TT station is as simple as at SN. We cannot determine uniquely the fault plane solution of this event for the sparsity of push-pull data. According to the principle presented in section 1.3 we refer to the relatively large event from almost the same region as shown in Fig. 25. In addition to this reference the geographical distribution of amplitudes were examined and the solution, a normal fault type, was obtained. It is not always the case that events in this region have this property(Tsukuda, 1978b). One of the reason why prominent P waveforms, compared with late arrivals, are detected might be that the station is located nearly in the direction of dilatational axis.

Kuchihosomi, Shikano fault

This region is characterized by occurrence of very small events with magnitude less than 1.0 and rather long size of about 1km. From Jun. 27 to Jul. 26, 1977 many shocks of small magnitude occurred. More than 100 events were registered by the telemetered observation system. In Table 1 only the events whose signal amplitudes exceeded ordinary triggering level(10μ-kine) are listed. Epicentral region of small events, hypocenters of which could not be determined, were estimated by the travel time difference between SN and TT stations. Thus the activity in this period turned out to cover the region A and B as shown in Fig. 24. Fault plane solutions are roughly classified into two types; K1 and K2(Fig. 25; Table 3). In determining the solutions a nearly strike-slip type was assumed. Strike directions of both solutions are not in harmony with the trend of either epicentral configulation or the trace of Shikano fault, and the two types occurred in both A and B. The earthquake faults of a very small size may be distributed along the nearly E-W trend in echelon.

Tottori

At Tottori there had been a remarkable microearthquake activity during the period from Aug. 22, 1976 to Jan. 12, 1977. The sequential microearthquakes are isolated from other events in both time and space. The events of No. 1, No. 2 and No. 16 (Table 1) had epicenters apart from the source of other clustered events by 1-2km. All of the events took almost identical focal depths. The hypocenters were already located by the previous studies(Tsukuda et al., 1976b, 1977d). In the present study relocation of hypocenters was carried out taking the waveforms into account and excluding ambiguous data: The principle that the same waveforms indicate the same hypocenters was applied as discussed in section 1.3. In this way the rather broad distribution in the previous studies become small in size down to about 150m in linear dimension.

The fault plane solutions are given in Fig. 25 and in Table 3. The T1 type occurred in the regions B and C; T2 in A; and T3 in C(Fig. 24). In determining the solution T1 following points were taken into account: ---

(1) It is supposed that CZ station is located near the P nodal line because the polarity changes with event to event.
(2) At SN station S waves are predominantly polarized in SH motion. This means that the P nodal plane with nearly E-W strike direction is almost vertical.
(3) The epicentral distance of CZ is roughly equal to that of SN and maximum amplitudes of vertival component S waves of CZ is about five times greater than those of SN.
(4) Distribution of P wave amplitudes at several stations was taken into account.

Other solutions are based on the assumption that the fault type is approximately strike-slip type.

Yamasaki

This region is within the aftershock area of the shock of M5.1, 1973. The aftershock activity has continued intermittently for more than 6 years. In this study a typical sequence was dealt with. The fault plane solution is assumed to be a strike-slip type.

Yasutomi, Yamasaki fault

The region around Yasutomi had been an inactive region in seismicity before 1977. As seen from Fig. 22 three distintive spots of earthquakes had appeared during the period from March to Octovor, 1977. The largest spot is the objective of the present study. The spatial distribution of hypocenters are shown in Fig. 24. The epicenters are apart from the trace of the Yamasaki fault by about 3km but the trend of their distribution is nearly paralled to the trace.

Enlarged hypocentral map reveals that the distribution is separated into two spots(A and B). Earthquakes occurred in

numeral order as indicated in Fig. 24. The principal shock(No. 1, M3.7) was accompanied by many aftershocks. The aftershock area extends 300-400m in length. By the event of No. 15 the activity of another spot was initiated.

After the largest aftershocks(event5 and event 15, M3.1) some small events subsequently occurred. These events might be regarded as aftershocks of the master events. Thus we can estimate the aftershock area or source area of the events of magnitude 3. As indicated in Fig. 24 the size of the two sources is about 200m in diameter. The source of event 5 may be unilateral fault as shown in Fig. 24.

Fault plane solutions are roughly classified into two types. Y1 is the solution of the principal shock. This is almost unique solution owing to a number of data including those of distant stations. Either Y2 or Y3 is that of the event of No. 15, which cannot be uniquely determined. The solutions of smaller events are supposed to be between Y1, Y2 and Y3.

2.3 INSPECTION OF SEISMOGRAMS

The first step to study waveforms is the general comparison of seismograms from clustered events. Fig. 26 shows seismograms for Tottori region. The two examples generally resemble each other in waveform, in paricular, for such a distant station as OY, epicentral distance of which is about 40km. However some differences are observed from the figure. For example the polarities of initial motions at CZ station are opposite to each other.

The next step is the detailed comparison of waveforms. In this study we concentrate our attention to P waveforms. It is important to investigate the change in waveform with hypocentral distance and epicentral azimuth. Fig. 27 is a typical example of P waveforms originated from Horadani, Shikano fault. The hypocentral distances at SN, TT and CZ are about 10km, 16km, and 29km, respectively. The initial wave packet observed at CZ is apparently simple in its form. But its duration time or predominant period is longer than that observed at the nearby stations by about three times. This fact means that it is impossible to be ascribed to directivity effect of the moving source alone. The difference in duration time for various epicentral azimuths amounts to 2L/V at the most, where L is the length of the source and V is the seismic wave velocity. In this case 2L/V is estimated to be about 20ms. This example clearly shows significance of the medium effect. As will be made clear this deformation cannot entirely be corrected by deconvolving the attenuation effect of the medium. An interpretation of this nature is that the P wave packet of CZ is composed of the initial wave propageted along the direct path and other waves propagated along the paths slightly different from that of the initial wave. At any rate the effect of inhomogeneity of the crust is so significant that the observed P wave propagated over a distance

of about 30km cannot be corrected satisfactorily by a simple deconvolution.

By inspection of seismograms some groups of events that are very familiar with each other in their waveforms were found. These groups are marked by a, b, etc. for each region in Table 1 and also described in Fig. 24.

2.4 REDUCTION OF OBSERVED P WAVEFORMS AND COMPUTATION OF THEORETICAL WAVEFORMS

The seismic signals stored on magnetic tapes were reproduced by the electro-magnetic oscillograph having a natural frequency of 270Hz into visible records with an allowance limit of trace amplitude of 40mm p-p and a paper speed of 1mm/ms. The fluctuation in paper speed is within 1%. The frequency response of the oscillograph is nearly flat for 0-100Hz. Each seismogram was digitized at an irregular time interval of about 1ms by X-Y digitizer(Fig. 1) and interpolated numerically at a constant interval of 5ms. Seismogram data were cut off above the time point where the first quiescence appears after the initial prominent waves, generally about 60-80ms after the initial onset. The resolving power of the digitizer is 0.25mm. The reading error in digitization amounts up to 0.5mm on the trace. In the present study we only deal with vertical component seismograms.

The digitized seismograms were transformed by deconvolution into the Q-corrected ground displacements(section 1.5). The attenuation quality factor Q for P waves was assumed to be 200 for the Shikano fault zone and 300 for the Yamasaki fault zone. Deconvolved P waveforms for various source regions are given in Figs. 14, 28, 29, 30, and 31.

Theoretical P waveforms were computed assuming the P velocity as 6.0km/s. For convenience the focus of each event belonging to a small confined region is fixed at the focus of the principal event. The amplification factor due to a superficial layer beneath observing sites(See section 1.6) was assumed to be 2.0 for all the cases neglecting its frequency and incident angle dependence. In modelling the source the diagrams, presenting theoretical displacement pulses for various source parameters and for various observation stations, were employed(Fig. 16).

2.5 MODELLING OF MICROEARTHQUAKE SOURCES

2.5.1 Typical Seismic Pulses

Fig. 32 describes the way of fitting the theoretical waveforms to observational waveforms for the event from Horadani. The fault plane solution and assumed direction of rupture propagation are shown in Fig. 25. The fault shape, rupture mode, rise time and fault length are changed successively. The best fit is obtained for the case of a triangular fault with rise time τ=20ms and fault length a=40m. Observe the gradual onset slope of the pulses at SN and TT. Rear part of the those pulses are contaminated with small higher frequency waves. The observed waveform at CZ is not in harmony with the theoretical one except for the initial part.

This example presents a typical form of seismic pulse, which is characterized by a triangular shape with gradual onset slope. Another typical example is trapezoid-shaped pulse from Yamasaki(Fig. 33), which is modeled by a rectangular fault with rise time τ=10ms and fault length a=60m. In this example rather high frequency disturbance is superimposed on the general form.

Some other typical examples are seen from Fig. 30, which shows deconvolved P waveforms from Tottori. The events 1, 12 and 14 have a rather sharp onset slope compared to other events. The waveform of event 15 shows a typical triangular shape.

Some representative waveforms from regions concerned were made comparison with theoretical waveforms. Fault shape, rise time and fault length were estimated in the way presented above. The final dislocation displacement $\bar{D}$ was obtained by comparing the amplitude for each station and averaged. Seismic moment M_o and stress drop $\Delta\sigma$ were calculated using the formulas (1.29) and (1.31) assuming $\mu=3.3\times10^{11}$dyne/cm^2 and listed in Table 4 together with fundamental source parameters.

2.5.2 Elongated Source Region of Ultra-Microearthquakes

The sequential events from Kuchihosomi are all very small in magnitude. Even the largest shocks have a magnitude of 0.9. One of these is the event 30, whose waveforms are shown in Fig. 34 together with the theoretical ones. The source of this event is estimated to be a triangular fault with τ=20ms and a=60m. This source may bring about moment of 1.1×10^{18}dyne-cm and stress drop of 58bars. It is interesting to compare this values with those of an adjacent region, Horadani. The moments and magnitudes of the two events are nearly comparable. However the stress drop is 150bars in Horadani, which is higher than in Kuchihosomi. The difference in stress drop is directly related to the source sizes of the two. The Kuchihosomi event is relatively large in its source dimension. Other events from Kuchihosomi also have similar properties(Table 4). Every event has a source dimension less than about 60m.

The integrated source region at Kuchihosomi is as long as 1km for all the events and 500-600m for the sequence during the period from Jun. 27 to Jul. 26, 1977. As noticed from Table 1 the activity migrated along the elongated zone irregularly toward east at one time and west at other time. The fault plane solutions show no regional characteristic. The two types of solutions occurred in every region. The waveforms observed at the nearby station SN show great difference from event to event. This may be due to temporal change of the source location. Microearthquake faults in this region seem to be configulated in echelon. That elongated source region is located nearly on the trace of the Shikano fault. Such a micro-seismic activity with relatively large source region compared to their magnitude scale may be closely related to the quaternary fault. Along such a fault very small slips may occur in a comparatively large scale.

2.5.3 Azimuthal Variation of Pulse Width

The displacement pulses of initial motion from Tottori show distinctive change of pulse-width with epicentral azimuth(Fig. 29). As shown in Fig. 35 these pulses are interpreted in terms of either a unilateral or bilateral fault. The event 3 (M2.0) is the first shock that occurred in the concentrated region of many events as plotted in Fig. 24. The event 6 is another main shock(M2.2) that occurred in this region. Fault plane solution can be regarded as the same for the two. The choice of the fault orientation was based on the configulation of foci, which is extended in the north and east directions. The large difference in the pulse widths of the two events at TT can be attributed to the rupture mode. The waveform at CZ of the other main shock(No. 11, M2.1) indicates somewhat complicated feature. It cannot be interpreted in terms of a simple fault model. We must consider at least two faults with different orientation. When we assume that the source is composed of two sheets of fault, one of them is T1 type in fault plane solution and the other T2. The latter fault started to slip about 20ms after the break of the former. The parameters of this compound source are given in Table 4.

2.5.4 Stick-Slip Sources of Microearthquakes

The fault dimensions and the positions of the three main shocks at Tottori are described in Fig. 24. The source of the event 3 is a bilateral fault with the total length $2a$=120m and that of event 6 is a unilateral triangular fault with a=100m. The hypocenters of the two events take nearly the same position, the focus of the second shock is slightly displaced toward north by about 50m. It may be presumable that the two shocks occurred on the common fault plane, because the source areas of the two shocks are large enough compared to the distance between the two hypocenters. As to the third main shock we cannot give a definite answer to the question whether its source had a common region with the others.

These three events are almost the same in magnitude but slightly different as shown in Fig. 37.

As previously mentioned there are many groups of earthquakes with similar waveforms. Fig. 31 shows two examples of these, which are from Yasutomi, the Yamasaki fault. The displacement waveforms in the left column in the figure resemble each other even for high frequency ripples in spite of large difference in amplitude; the top is four times as large as the bottom. These events are also considered to be originated from the same source. The right column is similar as the left, but the frequency content is not the same between the large event and the small ones. Similar groups are also found for the events from Tottori. The most typical example is the group of events 5,7 and 10, as noted in section 1.3.

These examples may indicate the repetitive slip on the fault, that is, a similar phenomenon as stick-slip sliding observed in the laboratory experiment on rocks.

2.5.5 High Frequency Radiation from the Source

So far we have inspected many examples of observed seismic pulses. The pulses are as a first approximation, classified into two shapes: triangle and trapezoid. These overall pulse shape is superimposed by higher frequency ripples. Such an example as the event 15 in Fig. 30 is almost free from such ripples. But most of the events are suffered from this disturbance. These high frequency components are also recongnized at other stations. Fig. 36 shows such examples. The waveforms at CZ and TT are comparable to each other. Fig. 33 also shows this nature.

Similarity of these high frequency waves among clustered events as shown in Fig. 31 might suggest that the radiation of these components is closely related to the property of the source or fault.

2.6 DISCUSSION AND CONCLUSION

In this chapter some typical forms of seismic displacement pulse for microearthquakes have been presented. Such relatively simple waveforms are also observed for large deep-focus earthquakes. Kasahara(1963) deduced simple displacement pulses for S waves from deep focus events by using as analog computer circuit removing the seismograph effect. His procedure does not include deconvolution for attenuation. Therefore we cannot compare directly his waveforms with ours. Nevertheless we can recognize the same features: Triangular shapes and trapezoid shapes are seen.

In most cases seismic pulses are associated with high frequency disturbances superimposed on the general form of the pulse. Some phases of these disturbances are interpreted in terms of multiple shocks in the study of deep-focus earthquakes(Fukao, 1972; Sasatani, 1976). Some are supposed to have relation to return motion generated locally on the fault plane(Kikuchi and Fukao, 1976). The present study on microearthquakes have revealed the repetitive occurrence of the earthquakes with almost the same waveforms including high frequency components. This feature may be reasonablly explained in terms of stick-slip and asperity inherent to the pertinent fault. The asperity involves existence of barriers where static friction or fracture strength is higher than other part of the fault surface(Das and Aki, 1977; Miyatake, 1977; Mikumo and Miyatake, 1978). Far field radiation from such a fault model was computed using the finite difference method by Miyatake(1979). Fig. 38 shows P displacement pulses for the rectangular fault with random barriers, a line barrier, a block barrier and constant strength. Appearance of the high frequency disturbance is quite similar to our observational waveforms.

So called "earthquake family"(Hamaguchi and Hasegawa,

1975) may involve the following implication: Some of the earthquakes would have a common source region or make repetitive slips on the same fault surface; and such faults would have orientations slightly different from each other and be distributed adjacently forming an integrated source region, or a fractured region, for the family of earthquakes. Such a fine structure of the source region, the source of the "earthquake family", has been revealed by nearby observations as presented in this chapter. At far distant stations the observed seismic waves show so similar forms that we cannot discriminate between events from different origins.

Source parameters of microearthquakes obtained in this study are as follow: rise time τ=10-20ms, fault length $\underline{a}$=40-60m, dislocation displacement $\bar{D}$=0.1-1cm, seismic moment Mo=10^{17}-10^{18} dyne-cm, stress drop $\Delta\sigma$=10-150bars, for events of magnitude M 0.0; τ=20ms, a=100-120, $\bar{D}$=0.5-1cm, Mo=8-9x10^{18} dyne-cm, $\Delta\sigma$=50-100bars, for events of M 2.0. Anderson and Fletcher(1976) determined the source parameters of a Blue Mt. Lake earthquake with a magnitude of 2.2 by both spectral and waveform methods using an S wave accelerogram observed at a station with its hypocentral distance of about 1km and obtained τ=20ms, Mo=8.4x10^{18} dyne-cm and source dimension of 40-80m in diameter. These values are fairly consistent with our results. The parameters of microearthquakes having magnitude less than 2 had never measured before the present study. Another parameter, the effective stress σ_e, is evaluated by the expression (1.33). The calculated effective stress using the result presented in Table 4 is always smaller than the stress drop by about factor of two or three. However we cannot conclude that this difference has a significant implication because of great uncertainly in the determination of both stress drop and effective stress. On the contrary rise time is a reliable dynamic parameter of the source. It is comfirmed that the rise time is less than 30ms for microearthquakes having magnitude less than or equal to about 2.

The regional difference of the source parameters revealed in this study may be summarized as follow: ---

(1) Comparison between the Shikano fault area and the Yamasaki fault area was made using the microearthquakes from Horadani at a depth of 6km, near the Shikano fault and those from Yamasaki at a depth of 14km, near the Yamasaki fault. The source model for Horadani is characterized by a relatively large rise time of 20ms and a triangular fault, whereas the sources for Yamasaki have such properties as a small rise time of 10ms and a rectangular fault. The effective stress and ambient stress in the Yamasaki fault area seems to be higher than in the Shikano fault area. One of the reason for this may be the difference of source depths.

(2) Comparison between the fractured region along the active fault trace and the region outside the trace of the fault or along the sub-faults associated with the main fault was made for the Kuchihosomi and Horadani regions corresponding to the former and the latter cases, respectively. The events from Kuchihosomi has relatively large source dimensions causing low stress drops compared to those from Horadani.

The source regions of microearthquakes in a stationary state of crustal seismic activity are separately distributed within the crust at an interval of 3-5km. Each region has a dimension ranging from several hundreds of meters up to 1km. The activity at a certain region has a close relation to other regions around. Tsukuda(1977b) pointed out such phenomena as nearly simultaneous occurence of earthquakes between the spots and successive migration of activity from spot to spot in the Yamasaki fault area. The life time of the activity at each source region would be an important quantity relevant to not only the mechanism of earthquake generation but also such properties as ambient tectonic stress and inhomogeneity of the medium.

CHAPTER III

ON THE INHOMOGENEOUS AND ANELASTIC CRUST OF THE EARTH

3.1 INTRODUCTION

The crust of the earth is not only the origin of microearthquakes but also the medium of seismic waves that deliver the information about source process. According to the results of explosion seismology fairly homogeneous layers i. e., granitic layer and basaltic layer are developed thickly and widely. For instance the Kurayoshi and Hanabusa(Hashizume et al., 1966) revealed the granitic layer in southwest Japan, its thickness and P wave velocity being 13km and 6.1km/s, respectively. Microearthquakes occur in this layer. Thus theoretical seismograms are computed usually assuming that the medium is uniform and infinite. However microearthquake waveforms are, in some cases, considerably complicated even for the initial P waves. This may be due to inhomogeneous and anelastic nature of the crust. In order to deduce the source function from observed waveforms it is very important to estimate quantitatively the degree of inhomogeneity and anelasticity.

Since our concern is the nearby observation of microearthquakes, we restrict this study to the upper crust. For simplicity we divide the properties of the upper crust into following three points: (1) reverberation effect due to superficial layers just beneath the observation site; (2) heterogeneity and anisotropy in the granitic layer; (3) anelasticity in the upper crust. In what follows above properties are described for the case of Tottori area and the surrounding regions.

3.2 SUPERFICIAL LAYER

In this section we deal with the portion of the crust between the ground surface and the top boundary of the granitic layer. The transfer function for this portion is used for bridging between the theoretical far field radiation in an infinite medium and the observational ground motion.

For simplicity the layer is assumed to be homogeneous. The problem is to determine the P and S wave velocities and the thickness of the layer. Constraints for the layer model are as follow: -----

(1) Intercept time t_o of the travel time curve

$$t=t_o + \Delta/V_p \qquad (3.1)$$

where t, Δ and V_p are travel time, epicentral distance and P wave velocity, and V_p=6.06km/s, for the Kurayoshi and Hanabusa explosions, is 0.60sec.

(2) Apparent velocity of P for the upper most layer is 4.7km/s (Tsukuda, 1976a).

(3) V_p/V_s ratio (V_p and V_s mean P and S wave velocities respectively) is 1.69(Tsukuda, 1976a).

Thus we obtain the structure of the layer as shown in Fig. 39. The P and S velocities and the thickness are 4.7km/s, 2.78km/s and 2.2km, respectively.

This layer turns out to have no serious effect on the seismic initial pulses from microearthquakes. For the appearance of the reflected wave on the seismogram is at least about 90ms after the initial onset. The transfer function for this layer was computed by the matrix method(Haskell, 1962). An example of the frequency characteristic is shown in Fig. 39.

3.3 INHOMOGENEITY OF THE GRANITIC LAYER

The relation(3.1) expresses the first order approximation for the travel time curve. Using the data from telemetered observation system of the Tottori Micro-earthquake Observatory the travel times of the quarry blasts at Aoya, Tottori prefecture, have been examined. In this procedure the shot time was not measured and the relative travel-time was used. The results show that the deviation from the linear relation(3.1) amounts up to 0.08sec for an epicentral range from 13km to 65km along nearly the same path of the Kurayoshi and Hanabusa explosions. This fluctuation of travel times is partly due to the local structure near the stations.

Furthermore the travel times for the Aoya blasts show azimuthal variation as shown in Fig. 40. The path along MZ, IZ, HM stations, in the southeast direction from the shot point, indicates lower P velocity than the path along TT, CZ and OY stations, in the nearly east direction by about 3%. This is an evidence of lateral heterogeneity in the granitic layer.

There are some evidences to indicate the existence of additional layers locally seated in the upper crust, which may not be revealed by the travel time analysis of explosions. P pulses from microearthquakes occurring at Kuchihosomi, the Shikano fault, are always acompanied by a preceding small wave which emerges 30-40ms before the onset of the pulse and shows the same polarity as the main pulse when observed at TT station(See Fig. 34). This wave is not the direct P wave because its amplitude is so small compared with the theoretically expected wave from the source model presented in Chap. II. The above precursor wave is probably a refracted wave from a local dipping layer with a relatively high velocity. Similar phenomenon was found for the microearthquakes from Fukusaki, the Yamasaki fault. On seismograms observed

at OY station, its hypocentral distance being about 40km, the precursor wave appears at 70-80ms before the main P wave (Tsukuda et al., 1977d).

Another inhomogeneous property is anisotropy of the medium constants. Fig. 41 presents an example of seismograms showing splitting of SH and SV waves, the evidence of anosotropy in the granitic layer. The time difference between SH and SV is about 0.1s. Taking the hypocentral distance and S wave velocity as 11km and 3.5km/s respectively, the fluctuation in the S wave velocity is estimated to be 3%. This amount is comparable with the examples presented in Gupta's paper(1973), where hypocentral distance and the time difference are about ten times greater than our case.

The phase termed PxP on the vertical component seismogram in Fig. 41 is interpreted as a reflected P wave from the local layer at a depth of about 12km.

3.4 MEASUREMENT OF Q

The frequency dependence of attenuation due to anelasticity of the crust is modeled by

$$A(r, f)=S(f)\cdot R(\theta, \phi)\ \exp\left\{-\alpha(f)\cdot r\right\}$$
$$\alpha(f)=\frac{\pi f}{v Q} \qquad (3.2)$$

where $A(r, f)$ means amplitude of seismic waves at a hypocentral distance of r and for a frequency f; $S(f)$ is the source spectrum and $R(\theta, \phi)$ represents radiation pattern; V and Q are constants and denote seismic wave velocity and attenuation quality factor, respectively. Here the azimuthal change of the source spectrum is assumed to be negligible. We use observed spectra at two stations originated from the same source(comparative path method, after Okada, 1977). Assuming V and Q are constant in the whole medium, the spectral ratio is given by

$$\frac{A(r_2, f)}{A(r_1, f)}=C\ \exp\left\{-\alpha(f)(r_2-r_1)\right\}$$
$$C=\frac{R(\theta_2, \phi_2)}{R(\theta_1, \phi_1)} \qquad (3.3)$$

where 1 and 2 indicate stations 1 and 2, respectively.

The most favorable data for this spectral method are pulse like waves which contain wide-range frequency components. The Horadani event may be a good example. The difference of hypocentral distance is 5.4km between SN and TT stations. From the spectral ratio as shown in Fig. 42 we can estimate average Q value in the upper crust for P waves as 173 assuming the P velocity as 6.0km/s. Another example is from around the western end of the Shikano fault. The P waves observed SN and TT are quite complicated but have a very high frequency

components. It this case analog data processing was applied. The analog filters used are the same as Tsukuda(1978a). This data give Q=265 putting r_2-r_1=11.9km. Combining the two results the average Q value of the upper crust in the Shikano fault area is considered to be about 200 for P waves.

Another technique to estimate Q values involves simulation by which we calculate a synthesized seismic wave propagated through an absorptive medium and compare it with an observed wave. The most simplified manner in this line is to examine what frequency components the observed wave posseses. Let us inspect some examples of seismogram waveforms originated from Tottori and Yasutomi along the Yamasaki fault. As seen from Fig. 5 the Tottori events have high frequency components of about 60Hz immediately after the initial P pulse when observed at TT, its hypocentral distance being 12km. These waves are not transmitted to other distant stations. For TT station the dimensionless attenuation parameter $\frac{r}{V \cdot Q \, \Delta t}$ (See section 1.5) takes the value 2.0 provided that the Q value is 200, whereas the values of the parameter for other stations are more than 4.0. Thus we conclude that such high frequency waves as mentioned above can be detected at stations whose hypocentral distances are short enough to give the attenuation parameter of less than 3.0 or so. These waves also appear on the seismograms for the events from the Yasutomi region, the Yamasaki fault, when observed at MZ station. Therefore the dimensionless parameter for the Yamasaki fault area is estimated to be less than 3.0 or so which results in giving the Q value as 300-400. The difference of Q values between the Shikano fault zone and the Yamasaki fault zone may be due to the difference of focal depths between the two regions.

3.5 DISCUSSION

In section 3.2 we assumed that the near surface layer is homogeneous. However it may be probable that the crustal material just beneath the ground surface changes its own properties with depth. Really the P velocity at the top of the crust is estimated to be 3-4km/s for the site of TT station(Tsukuda, 1976a). Above result was inferred from the angles of incidence of P at the station. The existence of such a low velocity layer at the upper most crust should affect severely the geometrical spreading factor(section 1.5). In order to estimate the diverging effect we assume the following crustal model:

Depth(km)	P velocity(km/s)	Density(g/cm^3)
0.0-0.2	3.5	2.0
0.2-2.2	4.8	2.0
2.2-	6.06	2.7

Based upon this model the angle of emergence was calculated as a function of epicentral distance D for a given focal depth. Then the derivative $d\, i_h/d\, D$ was obtained by numerical differentiation. It is easy to calculate the geometrical spreading factor using above result and eq. (1, 12). The deviation of the factor from 1/r, where r is the hypocentral distance, amounts up to 50% for focal depths of 5-10km.

Q values obtained in this study are extremery small compared with the result by Hashizume(1979), who analyzed explosion seismic waves and estimated the Q value for the upper and the lower crust beneath southwestern Honshu, Japan, as 1000-2000. This discrepancy may be mainly derived from the difference of frequency band; 1-15Hz in the case of Hashizume and 1-50Hz in our case. In Hashizume's case the frequency range is too narrow to discuss the frequency

characteristic of seismic waves. On the other hand Hamaguchi and Hasegawa(1975) estimated the average Q value in the crust beneath Tohoku districts, Japan, as 400 by a simulation. This result is in harmony with the present study.

CONCLUDING REMARKS

The results of the present study on microearthquakes with moment from 10^{17} to 10^{19} dyne-cm are summarized into the following points: ———

(1) The source process of microearthquakes can be interpreted, as a first approximation, in terms of a relatively simple fault model. The model adopted is specified by such properties as fault shape, fault dimension, propagation direction of rupture, rise time of source time-function and final dislocation displacement. Exceptionally there is such an event that its source would be modeled with more than one sheet of fault, and multiple shock.

(2) Clustered microearthquakes reveal the fractured region within the crust. It is possible to discuss the relationship between locations of individual events in the integrated source region or the fractured region and to make a comparison of the sizes of individual sources with the dimension of the fractured region, provided data from nearby observations are available. Such phenomena as repetitive occurrence of faulting like stick-slip sliding, extensive distribution of microearthquake faults in echelon, and high frequency radiation from the same source are remarkable.

(3) Inhomogeneity of the crust is the cause of complicated feacures in seismic waves. The amount of the variation of the medium constants derived from regional difference of P travel times, appearance of some crustal phases and splitting between SV and SH waves is up to 3%. To avoid this medium effect we should only use the initial P waves observed at nearby stations their hypocentral distance being less than about 30km.

(4) In dealing with seismic signals in a digital form it

is of use to transform them into displacement signals by deconvolution for understanding the essential properties of either seismic waves or earthquake sources. It is difficult to deduce various properties from spectra of seismic waves. The deconvolution method is turned out to be not inferior to the convolution method. In addition to the above digital processing, the inspection of analog data is also important for discussing the details of waveforms.

The present study is the first step to make clear the nature of microearthquake sources in a quantitative manner. The results are relevant to not only experimental studies on fracturing of rocks but also theoretical works on a realistic model of an earthquake source. Owing to a large number of events, researches on microearthquakes are remarkably promising, especially in the earthquake source study.

ACKNOWLEDGEMENTS

I wish to express my gratitude to Prof. Ryosuke Sato for giving me valuable suggestions and critically reviewing the manuscript. Thanks are also due to Professors Toshi Asada and Yoshimichi Kishimoto for their encouragement throughout the present study, Dr. Yasunori Suzuki for some revision of computer program of the theoretical seismogram programed by Prof. R. Sato, Dr. Yozo Hamano for instructing me the derivation of Eqs. (1.22), Drs. Kei Takano and Ryohei Nishida for critically reading the manuscript, Drs. Kazuo Oike, Jun'ichi Ito and Takashi Miyatake for permitting me to use their figures. Discussions with the members of the Geophysical Institute , the University of Tokyo, and Disaster Prevention Research Institute, Kyoto University, were helpful. My thanks also extended to Mrs. Yoko Tsukuda for assistance in preparing the manuscript. Computations were made on a HITAC 8700/8800 at the Computer Center, the University of Tokyo.

REFERENCES

Aki, K., Generation and propagation of G waves from the Niigata earthquake of June 16, 1964, part 2. Estimation of earthquake moment, released energy, and stress-drop from the G wave spectrum, Bull. Earthq. Res. Inst., Tokyo Univ., 44, 73-88, 1966.

Aki, K., Scaling law of seismic spectrum, J. Geophys. Res., 72 1217-1231, 1967.

Aki, K., Scaling law of earthquake source time-function, Geophys. J., 31, 3-25, 1972.

Anderson, J. G. and J. B. Fletcher, Source properties of a Blue Mt. Lake earthquake, Bull. Seism. Soc. Am., 66, 677-683, 1976.

Asada, T., Observation of near-by earthquakes with ultra sensitive seismometers, J. Phys. Earth, 5, 83-113, 1957.

Attewell, P. B. and Y. V. Ramana, Wave attenuation and internal friction as functions of frequency in rocks, Geophysics, 31, 1049-1056, 1966.

Ben-Menahem, A., S. W. Smith and T. L. Teng, A procedure for source studies from spectrum of long-period seismic-body waves, Bull. Seism. Soc. Am., 55, 203-235, 1965.

Berckhemer, H., F. Auer and J. Drisler, High-temperature anelasticity and elasticity of mantle peridotite, Phys. Earth Planet. Inter., 20, 48-59, 1979.

Bollinger, G. A., Determination of earthquake fault parameters from long-period P waves, J. Geophys. Res., 73, 785-807, 1968.

Bolt, B. A., The revision of earthquake epicenters, focal depths and origin-times using a high-speed computer, Geophys. J., 3, 433-440, 1960.

Brace, W. F., Laboratory studies of stick-slip and their application to earthquakes, Tectonophysics, 14, 189-1972.

Brillouin, L., Science and information theory, Second edition, Academic press, Chap. 8, 78-80, 1962.

Brune, J. N., Tectonic stress and the spectra of seismic shear waves from earthquakes, J. Geophys. Res., 75, 4997-5009, 1970.

Chouet, B., K. Aki and M. Tsujiura, Regional variation of the scaling law of earthquake source spectra, Bull. Seism. Soc. Am., 68, 49-79, 1978.

Cooley, J. W. and J. W. Tukey, An algorithm for the machine calculation of complex Fourier series, Math. Comp., 19, 3019-3022, 1964.

Das, S. and K. Aki, A numerical study of two dimensional spontaneous rupture propagation, Geophys. J. Roy. astr. Soc., 50, 643-668, 1977.

Douglas, B. M. and A. Ryall, Spectral characteristics and stress drops for microearthquakes near Fairview Peak, Nevada, J. Geophys. Res., 77, 351-359, 1972.

Eshelby, J. D., The determination of the elastic field of an ellipsoidal inclusion and related problems, Proc. Roy. Soc., London, A241, 376-396, 1957.

Fukao, Y., Source process of a large deep-focus earthquake and its tectonic implication ---The western Brazil earthquake of 1963, Phys. Earth planet. Inter., 5, 119-126, 1972.

Futterman, W. I., Dispersive body waves, J. Geophys. Res., 67, 5279-5291, 1962.

Gupta, I. N., Dilatancy and premonitary variations of P, S travel times, Bull. Seism. Soc. Am., 63, 1157-1161, 1973.

Hamano, Y., Waveform change due to attenuation, Programme and Abstracts, Seism. Soc. Japan, No. 2, 81, 1970(in Japanese).

Hashizume, M., O. Kawamoto, S. Asano, I. Muramatsu, T. Asada, I. Tamaki and S. Murauchi, Crustal structure in the western part of Japan derived from the observation of the first and second Kurayoshi and Hanabusa explosions, Part 2, crustal structure in the western part of Japan, Bull. Earthq. Res. Inst., Tokyo Univ., 44, 109-120, 1966.

Hashizume, M., Investigation of microearthquakes - On earthquake occurrence in the crust -, Bull. Disas. Prev. Inst., Kyoto Univ., 20, 1-12, 1970.

Hashizume, M., Q of the crust beneath southwestern Honshu, Japan, derived from explosion seismic waves, phys. Earth Planet. Inter., 20, 25-32, 1979.

Haskell, N. A., Crustal reflection of plane P and SV waves, J. Geophys. Res., 67, 4751-4767, 1962,

Ishida, M., Determination of fault parameters of small earthquake in the Kii peninsula, J. Phys. Earth, 22, 177-212, 1974.

Ito, J., Some anomalous characteristics of extremely small earthquakes, Ph. D. Thesis, Tokyo Univ., 1977(in Japanese).

Kanamori, H., Determination of effective stress associated with earthquake faulting, The Tottori earthquake of 1943, Phys. Earth Planet. Inter., 5, 426-434, 1972.

Kanamori, H. and D. L. Anderson, Theoretical bases of some empirical relations in seismology, Bull. Seism. Soc. Am., 65, 1073-1095, 1975.

Kasahara, K., Waveform analysis of S-pulse from deep focus earthquakes, 1, Bull. Earthq. Res. Inst., Tokyo Univ., 41, 209-216, 1963,

Kikuchi, M. and Y. Fukao, Seismic return motion, Phys. Earth Planet. Inter., 12, 343-349, 1976.

Kishimoto, Y. and R. Nishida, Mechanisms of microearthquakes and their relation to geological structures, Bull. Disas. Prev. Res. Inst., Kyoto Univ., 23, 1-25, 1973.

Kishimoto, Y., On anomalous phenomena in some kinds of observations incidental to a small earthquake at the Yamasaki fault on Sept. 30, 1977, Disas. Prev. Res. Inst., Annuals, Kyoto Univ., No. 21B, 1-9, 1978(in Japanese).

Kishimoto, Y., K. Oike, K. Watanabe, T. Tsukuda, N. Hirano and S. Nakao, On the telemeter observation system of the Tottori and the Hokuriku Microearthquake Observatory, Zisin, 31, 265-274, 1978(in Japanese).

Komura, S., A consideration about the mechanism of the occurrence of severe earthquakes, Zisin, 9, 175-181, 1956 (in Japanese).

Langston, C. A., A body wave inversion of the Koina, India, Earthquake of December 10, 1967, and some implications for body wave focal mechanisms, J. Geophys. Res., 81, 2517-2529, 1976.

Maruyama, T., On the force equivalents of dynamical elastic dislocation with reference to the earthquake mechanism, Bull. Earthq. Res. Inst., 41, 467-486, 1963.

Mikumo, T., Long-period P waveforms and the source mechanism of intermediate earthquakes, J. Phys. Earth, 17, 169-191, 1969.

Mikumo, T. and T. Miyatake, Dynamical rupture process on a three-dimensional fault with non-uniform frictions and near-field seismic waves, Geophys. J. R. astr. Soc., 54, 417-438, 1978.

Miyatake, T, Numerical simulation of dynamical faulting process, Zisin, 30, 449-461, 1977(in Japanese).

Miyatake, T., Numerical simulation of dynamical faulting process (4) - Seismic waves from a three dimensional fault -, Programme and Abstracts, Seism. Soc. Japan, No. 2, 57, 1979(in Japanese).

Mizoue, M., M. Nakamura and K. Kotani, Characteristics of seismicity in the northwestern part of the kii peninsula, - in special reference to the active fault system as inferred from spatial distribution of small and micro-earthquakes -, Bull. 50th Anniversary of the Great Kanto Earthquake, 1923, Earthq. Res. Inst., Tokyo Univ., 199-216, 1973(in Japanese).

Mogi, K, Earthquakes and fractures, Tectonoplysics, 5, 35-55, 1967.

Nishida, R., M. Hirano and K. Shiono, Seismological re-evaluation of regional stress orientation and fracture angle in the Kinki district, southwest Japan with reference to developmental process of conjugate faults, Bull. Disas. Prev. Res. Inst., Kyoto Univ., 24, 25-47, 1974.

Oike, K., On a list of hypocenters compiled by the Tottori Micro-earthquake Observatory, Zisin, 28, 331-346, 1975 (in Japanese).

Oike, K., Spatial and temporal distribution of micro-earthquakes and active faults, Memoirs Geol. Soc. Japan, No. 12, 59-73, 1976(in Japanese).

Okada, H., Fine structure of the upper mantle beneath Japanese Island arcs as revealed from body wave analyses, Ph. D. Thesis, Hokkaido Univ., 1977.

Sasatani, T., Source process of a large deep-focus earthquake of 1970 in the Sea of Okhotsk, J. Phys. Earth, 24, 27-42, 1976.

Sato, T. and T. Hirasawa, Body wave spectra from propagating shear cracks, J. Phys. Earth, 21, 415-431, 1973.

Sato, R., Fast computation of theoretical seismograms for an infinite medium Part I. Rectangular fault, J. Phys. Earth, 23, 323-331, 1975.

Sato, R., Fast computation of theoretical seismograms for an infinite medium Part II. Fault with an arbitrary shape, J. Phys. Earth, 24, 43-49, 1976.

Tsukuda, T., Microearthquake waveforms recorded at Tottori Microearthquake Observatory and their relation to hypocentral distributions and the upper-crustal structure, Bull. Disas. Prev. Res. Inst., Kyoto Univ., 26, 17-55, 1976 a.

Tsukuda, T. and S. Nakao, Study on microearthquake sequences in eastern chugoku and northern Kinki districts, southwest Japan(I), Zisin, 29, 395-410, 1976b(in Japanese).

Tsukuda, T., K. Nakamura, and Y. Kishimoto, The earthquake on September 21, 1973 in the vicinity of the Yamasaki fault and its aftershock activity, Zisin, 30, 151-162, 1977a(in Japanese).

Tsukuda, T., Sequences of micrieathquakes near the Yamasaki fault, Bull. Disas. Prev. Res. Inst., Kyoto Univ., 27, 1-22, 1977b.

Tsukuda, T. and S. Nakao, On the accuracy of hypocenter determination by P times at four stations of the Tottori Microearthquake Observatory, Disas. Prev. Res. Inst. Annuals, Kyoto Univ., No. 20B, 47-58, 1977c(in Japanese).

Tsukuda, T. and S. Nakao, Study on microearthquake sequences in the eastern Chugoku and northern Kinki districts, southwest Japan(II), Zisin, 30, 339-358, 1977d(in Japanese).

Tsukuda, T., On the use of analog filters in evaluating amplitude spectra of seismic waves, Bull. Disas. Prev. Res. Inst., Kyoto Univ., 28, 1-8, 1978a.

Tsukuda, T., Seismicity near the Shikano and Yoshioka faults, Disas. Prev. Res. Inst. Annuals, No. 21B, 47-56, 1978b.

Watanabe, H., On the sequence of earthquakes, Special Contributions, Geophysical Institute, Kyoto Univ., No. 4, 153-192, 1964.

TABLES

Table 1 List of earthquakes concerned. Magnitude is given by the formula: M=2.97log(F-P)-2.56, where F-P is the duration time of earthquake motion measured in seconds (Oike, 1975). A, B and C for the Kuchihosomi sequence refer to the regions indicated in Fig. 24. a, b and c indicate earthquake groups with almost the same waveforms.

No.	Date Y	M	D	Origin time H	M	Mag.		No.	Date Y	M	D	Origin time H	M	Mag.	
Horadani, Shikano fault															
1	1976	11	1	12	24	0.4									
Kuchihosomi, Shikano fault															
1	1976	8	17	05	05	0.1	B	35	1977	6	27	08	32	0.4	A
2		11	27	15	39	0.1	B	36				08	33	-0.5	A
3	1977	2	2	07	20	0.9		37				08	33	-1.1	
4		2	5	02	54	-0.2	C	38				08	34	0.6	A
5		3	23	07	28	-0.2	C	39				08	34	0.1	B
6		5	31	05	59	0.4	C	40				08	35	-0.8	
7		6	27	07	50	-0.2	A	41				08	35	-0.8	B
8				08	04	-1.1		42				08	35	-1.1	
9				08	05	-1.1		43				08	35	-0.8	B
10				08	05	0.1	B	44				08	35	-1.1	
11				08	06	0.1		45				08	35	-1.1	
12				08	06	0.1		46				08	35	-0.8	
13				08	07	0.4	B	47				08	35	0.1	
14				08	07	-0.8	A	48				08	35	0.1	
15				08	11	0.1	B	49				08	37	-0.5	B
16				08	11	0.4	B	50				08	37	-1.1	
17				08	14	-0.8	B	51				08	37	-0.5	
18				08	14	0.1	A	52				08	47	0.1	A
19				08	15	0.1	A	53				08	48	-1.1	
20				08	16	0.1	B	54				08	59	-0.5	

No.	Date Y	M	D	Origin time H	M	Mag.		No.	Date Y	M	D	Origin time H	M	Mag.	
21	1977	6	27	08	17	-0.8	B	55	1977	6	27	09	06	-0.5	
22				08	17	-0.5	B	56				09	32	0.7	B
23				08	17	0.1	B	57				09	33	0.4	B
24				08	17	-1.1		58				09	35	-0.2	B
25				08	21	-0.8	B	59				09	49	1.2	B
26				08	22	-1.1		60				10	21	-0.5	A
27				08	26	0.4	B	61				11	32	0.4	B
28				08	26	-1.1		62				12	04	0.4	B
29				08	29	0.1	A	63				12	08	0.7	B
30				08	30	0.9	A	64				12	21	0.1	B
31				08	31	0.4		65		6	28	07	34	-0.8	B
32				08	31	-0.8		66				07	52	0.1	B
33				08	31	-1.1		67		7	26	02	22	0.6	B
34				08	31	-0.8	A	68				02	24	0.4	B
						Tottori									
1	1976	8	22	17	49	0.6		12	1976	9	4	05	31	-0.5	
2		8	28	17	11	2.0		13				05	45	0.9	
3		8	31	00	12	2.0		14		9	5	09	19	0.6	
4				07	28	-0.3		15		9	7	02	25	1.6	
5				08	19	0.7	a	16		10	4	23	05	0.7	
6				22	56	2.2		17		12	19	14	31	1.3	
7				22	57	1.4	a	18		12	31	21	07	1.1	
8		9	1	01	50	0.6		19				21	07	1.6	
9		9	2	07	18	0.6		20	1977	1	9	19	33	0.7	
10		9	3	22	17	1.3	a	21		1	12	12	32	0.7	
11		9	4	05	29	2.1									
						Yamasaki									
1	1979	9	11	23	02	1.6		3	1979	9	12	03	37	-0.3	
2				23	05	-0.8									

No.	Date Y	M	D	Origin time H	M	Mag.		No.	Date Y	M	D	Origin time H	M	Mag.	
							Yasutomi, Yamasaki fault								
1	1977	9	30	16	23	3.7		19	1977	10	2	19	38	0.1	
2				18	29	0.1	a	20		10	3	07	42	0.4	
3				18	30	0.4	a	21		10	4	03	56	-0.1	
4				19	52	-0.1		22		10	5	03	11	1.3	b
5				20	26	3.1		23				17	56	0.4	b
6				20	30	0.9		24		10	6	13	19	-0.1	
7				21	35	0.7		25		10	8	23	25	0.1	
8				22	11	0.4		26		10	10	17	14	0.6	
9		10	1	02	07	0.4		27		10	12	04	36	0.1	
10				10	41	1.3		28				09	17	0.4	b
11		10	2	01	08	0.4		29				11	46	0.6	
12				02	44	-0.1		30		10	13	11	28	1.3	
13				03	52	0.1		31		10	16	11	45	0.1	
14				03	52	0.9		32		10	17	20	37	1.2	c
15				03	52	3.1		33				21	04	0.1	c
16				04	11	1.8		34		10	20	23	49	0.1	c
17				04	29	-0.1		35		10	28	07	36	0.4	
18				04	35	0.9									

Table 2 Hypocentral and attenuation parameters. Bracketed numerals indicate hypocentral errors; reading error in P times in milli-second, E-W component epicentral error in meter, N-S component epicentral error in meter, and focal depth error in meter are given in order. Epicentral azimuths are measured clockwise from the north.

Station	Epicentral distance (km)	Epicentral azimuth (°)	Hypocentral distance (km)	$\frac{r}{V \cdot Q \cdot \Delta t}$
Horadani, Shikano fault H=5.80km Q=200 (10, 40, 60, 90)				
SN	8.63	-135.3	10.40	1.73
CZ	28.74	139.2	29.32	4.89
TT	14.70	68.3	15.80	2.63
Kuchihosomi, Shikano fault H=6.05km Q=200 (10, 60, 90, 320)				
KY	26.70	-95.0	27.38	4.57
SN	11.14	-119.8	12.68	2.12
CZ	26.05	144.4	26.74	4.46
TT	11.73	59.1	13.20	2.20
Tottori H=10.88km Q=200 (5, 20, 70, 150)				
SN	24.34	-108.4	26.66	4.44
CZ	23.43	175.8	25.83	4.31
OY	39,63	116.2	41.10	6.82
TT	5.09	-41.1	12.01	2.00

Station	Epicentral distance (km)	Epicentral azimuth (°)	Hypocentral distance (km)	$\frac{r}{V \cdot Q \cdot \Delta t}$
Yamasaki		H=13.89km (10, 50, 40, 500)		Q=300
CZ	28.31	-47.8	31.53	3.50
MZ	14.37	-149.6	19.99	2.22
IZ	36.00	112.8	38.59	3.47
OY	27.94	27.5	31.20	4.29
Yasutomi, Yamasaki fault		H=18.19km (5, 40, 90, 270)		Q=300
CZ	41.02	-44.0	44.87	4.99
MZ	14.94	-97.4	23.54	2.62
IZ	25.87	97.8	31.62	4.45
OY	35.65	8.6	40.02	3.51

Table 3 Models of fault plane solution. Strike direction is measured clockwise from the north. Notations refer to Fig. 15.

Region	Model	Fault plane A strike direction (°)	Fault plane A dip angle (°)	Fault plane B strike direction (°)	Fault plane B dip angle (°)
Horadani	H	139.2	45.0	-40.8	45.0
Kuchihosomi	K1	-90.0	90.0	180.0	90.0
	K2	-120.5	80.0	152.9	80.6
Tottori	T1	180.0	60.0	90.0	90.0
	T2	-170.0	90.0	100.0	85.0
	T3	-30.0	90.0	60.0	90.0
Yamasaki	YS	-80.0	90.0	10.0	90.0
Yasitomi	Y1	-78.0	90.0	-168.0	55.0
	Y2	-72.0	75.0	-162.0	90.0
	Y3	-72.0	75.0	180.0	60.0

Table 4 Evaluated source parameters. Fault plane solutions refer to Fig. 25. Rupture mode T means a triangular fault; R, rectangular unilateral fault; and B, rectangular bilateral fault. Stations concerned are shown by the initial letter of their code. Bracketed stations are not used in calculating $\bar{D}$. *shows the model of best fit.

No.	Mag.	Fault plane solution	Rupture mode	τ (ms)	a (m)	Stations used	Average $\bar{D}$ (cm)	Mo (10^{17} dyne-cm)	$\Delta\sigma$ (bar)	
						Horadani				
1	0.4	H	T	10	40	S (c) T	0.46	6.1	100	
				10	60		0.27	8.0	41	
				20	40		0.68	9.0	150	*
			R	10	40		0.29	7.7	66	
				20	40		0.34	9.0	77	
			B	10	40		0.16	8.5	18	
				20	40		0.18	9.5	20	
						Kuchihosomi				
1	0.1	K1	T	10	60	S C	0.07	1.9	10	
				20	40		0.16	2.1	36	
				20	60		0.08	2.4	12	*
30	0.9	K1	T	20	60	(K) S C T	0.38	11.0	58	
56	0.9	K1	T	10	60		0.31	9.2	47	
				20	40		0.74	9.8	170	
				20	60		0.38	11.0	58	*
67	0.6	K2	T	10	60		0.44	13.0	67	
				20	40		1.1	15.0	260	

No.	Mag.	Fault plane solution	Rupture mode	τ (ms)	a (m)	Stations used	Average $\bar{D}$ (cm)	Mo (10^{17} dyne-cm)	$\Delta\sigma$ (bar)
					Tottori				
3	2.0	T1	B	20	60	S C(O)(T)	0.67	80.0	51
6	2.2	T1	T	20	80	S C(O)(T)	1.46	77.0	170
				20	100		1.08	89.0	98 *
8	1.2	T2	B	20	40	S C T	0.08	4.2	9
10	1.5	T2	B	20	40	S C(O)T	0.38	20.0	43
11	2.1	T1	R	20	40	S C(O)(T)	0.84	22.0	190
		T2	R	20	60	S C(O)(T)	0.83	49.0	125
13	0.8	T1	T	10	20	C T	1.83	6.0	130
		T1	R	10	20	C T	0.92	6.1	420
		T1	R	10	40	C T	0.29	7.7	66
					Yamasaki				
1	1.6	YS	R	10	60	I O	2.20	130.0	332
2	-0.8	YS	R	10	60	C M O	0.07	3.9	10
3	-0.3	YS	R	10	60	C M I O	0.22	13.0	33

FIGURE CAPTIONS

Fig. 1 Block diagram of the observation system of the Tottori Microearthquake Observatory.

Fig. 2 Overall characteristic of the observation system operated at the Tottori Microearthquake Observatory.

Fig. 3 Typical example of initial portions of microearthquake seismograms(vertical component). Date, origin time(H:M), and the pertinent station(MZ,SN) are attached to each head of the trace. Epicentral sites are as follow: Horadani, Shikano fault, for SN station; and Yamasaki and Sayo,for MZ station. Step like irregularity appearing on the wave traces is due to temporary A-D conversion and D-A conversion in the data accumulating system, sampling frequency of which is 195 Hz.

Fig. 4 Another type of P waveforms originated from the Yamasaki region near the Yamasaki fault.

Fig. 5 Comparison of vertical component seismograms of microearthquakes from almost the same origin at Tottori. Excellent agreement of the crests and troughs on late arrivals and slight difference of pulse widths of the initial P waves are observed. Encircled numerals indicate the event number(Table 1). The observation station is TT(Tottori).

Fig. 6 Comparison of normalized P waveforms on the seismograms. Data source is the same as that of Fig. 5. Closed and broken curves are from the event 10 and event 5, respectively, with their amplitude ratio being 1.6.

Fig. 7 Comparison of normalized P waveforms on the seismograms of the events from almost the same origin at Yamasaki. The observation station is MZ(Mikazuki).

Fig. 8 Seismograms for ultra-microearthquakes of nearly the same origin at Matsushiro(after Ito, 1977). The diamater of the circle that encloses the initial P wave is taken as 30ms. The duration time of the P wave with large amplitude is longer than that with small amplitude.

Fig. 9 Comparison of the two events from quarry blasts at the sites about 500m apart from each other. The shot points are located at Aoya, Tottori prefecture. The events of upper and lower traces for each station were detonated on Jun. 29, 1976 and May 8, 1978, respectively. Epicentral distances range from about 8km to 24km.

Fig. 10 Outline of the "hypocenter locus". The hypocenter, which satisfies P arrival times observed at three stations(a tripartite), moves from the vicinity of the tripartite to the point of ground surface far beyond the stations travelling deep beneath the surface as the origin time of corresponding to the hypocenter decreases.

Fig. 11 Characteristic of the transfer function for attenuation.

Fig. 12 Waveforms of the synthesized seismograms. The triangular displacement pulse(top) is inputted into the absorptive medium and then the observation system of the Tottori Micro-earthquake Observatory. Convolution with the transfer functions,

differentiation and interpolation are operated.

Fig. 13 Same as Fig. 12 but for various pulse widths of input wave and fixed value of the attenuation parameter. Numerals attached to each waveform indicate the time interval of the input triangular pulse from the initial point to the peak.with a unit of ms.

Fig. 14 Observed and deconvolved P waveforms for a microearthquake that originated at Horadani, near the Shikano fault. This event is treated in detail in Chap. II. The vertical components are shown. Ground up is taken upward. The observation station is SN(Shikano). It was confirmed that the inverse operation reproduced the original waveform correctly.

Fig. 15 Fault geometry and fault shapes. Fault plane is specified by dip angle δ, strike direction(x axis) and slip angle λ measured from the horizontal x axis indicating the motion of the hanging wall side with respect to the foot wall block.

Fig. 16 Theoretical displacement P pulses for various fault parameters and stations. Radial components of the displacement vectors are shown. Compression and dilatation are taken upward and downward in the figure, respectively. The numerals attached to each pulse represent the absolute maximum amplitude of the pulse its unit being $10^{-6}\times\bar{D}$, where $\bar{D}$ denotes the final dislocation displacement. The rupture velocity is assumed to be 2.0km/s.The source region is located at Tottori(Tables 2, 3 in Chap. II).

(a) for triangular fault(unilateral), τ =10ms,
(b) for triangular fault(unilateral), τ =20ms,
(c) for rectangular fault(unilateral), τ =10ms

(d) for rectangular fault(unilateral), τ =20ms

Fig. 17 Comparison of displacement response characteristic of the observation system for microearthquakes with that of large earthquakes. B1 and B2 are for the long -period seismograph of WWSSN(Willmore et al., Manual of seismological observatory practice, Report SE-20, World Data Center A for Solid Earth Geophysics, 1979).

Fig. 18 Block diagram of the general procedure presented in Chap. I.

Fig. 19 Regions concerned together with distribution of the observation stations. Broken lines indicate the Shikano fault near Tottori, and the Yamasaki fault in the south.

Fig. 20 Epicentral distribution of earthquakes in the eastern Chugoku and northern Kinki districts. Observation period is from Jul. 1, 1965 to Dec. 31, 1978.

Fig. 21 Hypocentral distribution around the Shikano and Yoshioka faults region(after Tsukuda, 1978b). Only accurate data are plotted. In the concentrated region of foci, for instance, near Kuchihosomi many ultra -microearthquakes occurred, most of the hypocenters of which cannot be precisely determined.

Fig. 22 Hypocentral distribution around the Yamasaki and Yasutomi region. Encircled regions indicate earthquake clusters.

Fig. 23 Map showing the source - station geometry for each region. North is taken upward in the map. Broken curves are active fault traces; Shikano and Yoshioka

faults for Horadani and Kuchihosomi; and Yamasaki fault for Yamasaki and Yasutomi.

Fig. 24 Epicentral map for each spot. Hypocentral depths are about 6km, 11km and 18km for Kuchihosomi, Tottori and Yasutomi, respectively. The depth distribution is given for Yasutomi. Generally the accuracy of focal depth is considerablly low compared to that of epicenter(Table 2). The marks A, B, etc. exhibit regions in the epicentral distribution, and a, b, etc. exhibit regions of clustered events of small magnitude. Source areas of individual events of large magnitude are shown by an elliptic zone. The area for event 11 at Tottori was not definitely determined. At Yasutomi, source areas of the main shock(No. 1) and the two largest aftershocks(M3.1) are shown.

Fig. 25 Fault plane solutions for respective regions(equal area projections of initial motion on the upper focal -hemishere). Open and closed circles indicate dilatation and compression at observing site, respectively. The directions of rupture propagation assumed in the modelling of source are indicated by arrows. The solution for Horadani was determined in reference to the solution of the event of Jan. 22, 1977(M2.2).

Fig. 26 General view of microearthquake seismograms(vertical component). The events from Tottori are shown(up: No. 3, below: No. 10).

Fig. 27 Seismogram P waveforms for the shock that originated at Horadani.

Fig. 28 Q-deconvolved ground displacement of P for the events from Kuchihosami (Upward in the graph ground up). Encircled is the event number in Table 1. Peak amplitude(absolute value) of each displacement waveform is given in the unit of 10^{-6}cm.

Fig. 29 Q-deconvolved ground displacement of P from Tottori as similar as Fig. 28. Dotted curve(OY) indicate the smoothed waveform taking a running average over 10ms. The broken curve is an estimated waveform from the saturated record. In this estimation such diagrams as Figs. 12, 13 were used assuming the original displacement as a triangular pulse(section 1.5).
(a) event 3
(b) event 6
(c) event 11

Fig. 30 Q-deconvolved ground displacement of P from Tottori as similar as Fig. 28.

Fig. 31 Q-deconvolved ground sicplacement of P from Yasutomi as similar as Fig. 28.

Fig. 32 Fitting between the theoretical and observed P displacement waveforms from Horadani. All waveforms are normalized in amplitude. Theoretical and observed waves are indicated by closed and dotted curves, respectively.

Fig. 33 Final fit for the P pulses from Yamasaki as similar as Fig. 32.

Fig. 34 Final fit for the P pulses from Kuchihosomi as similar as Fig. 32.

Fig. 35 Final fit for the P pulses from Tottori as similar as Fig. 32.

Fig. 36 Final fit for the P pulses from Tottori as similar as Fig. 32.

Fig. 37 Maximum trace amplitude as a function of time for the events(No. 3, No. 6, No. 11) from Tottori.

Fig. 38 Simulated P pulses for random barrier model, line barrier model, block barrier model and constant strength model(after Miyatake, 1979).

Fig. 39 Transfer function(amplitude) for the superficial layer. Assumed model is given in the right. A P wave is incident at the bottom of the layer and transformed into vertical ground motion.

Fig. 40 Arrival times of the Aoya quarry blasts(after Tsukuda, 1976a).

Fig. 41 Splitting of SH and SV waves. The source is near Horadani, the Shikano fault.

Fig. 42 Q determination by the comparative path method. The top shows an example of spectral ratio obtained by using analog filters and the bottom is obtained by digital processing.

FIGURES

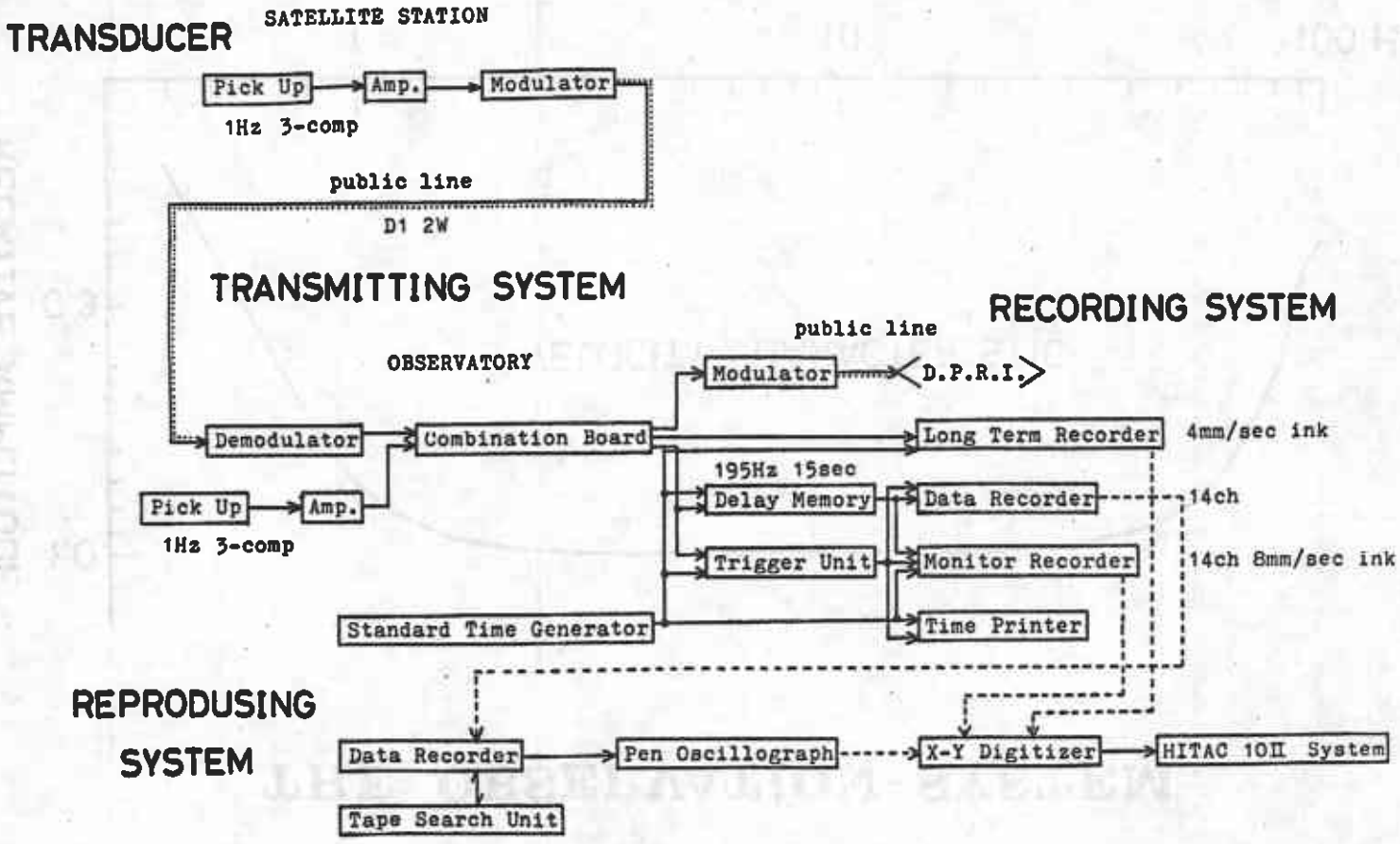
TRANSDUCER
SATELLITE STATION
Pick Up
Amp.
Modulator
1Hz 3-comp
public line
D1 2W
TRANSMITTING SYSTEM
RECORDING SYSTEM
public line
OBSERVATORY
Modulator
D.P.R.I.
Demodulator
Combination Board
Long Term Recorder
4mm/sec ink
195Hz 15sec
Delay Memory
Data Recorder
14ch
Pick Up
Amp.
1Hz 3-comp
Trigger Unit
Monitor Recorder
14ch 8mm/sec ink
Standard Time Generator
Time Printer
REPRODUSING
SYSTEM
Data Recorder
Pen Oscillograph
X-Y Digitizer
HITAC 10II System
Tape Search Unit

Fig. 1

OVERALL RESPONSE CURVE OF THE OBSERVATION-SYSTEM

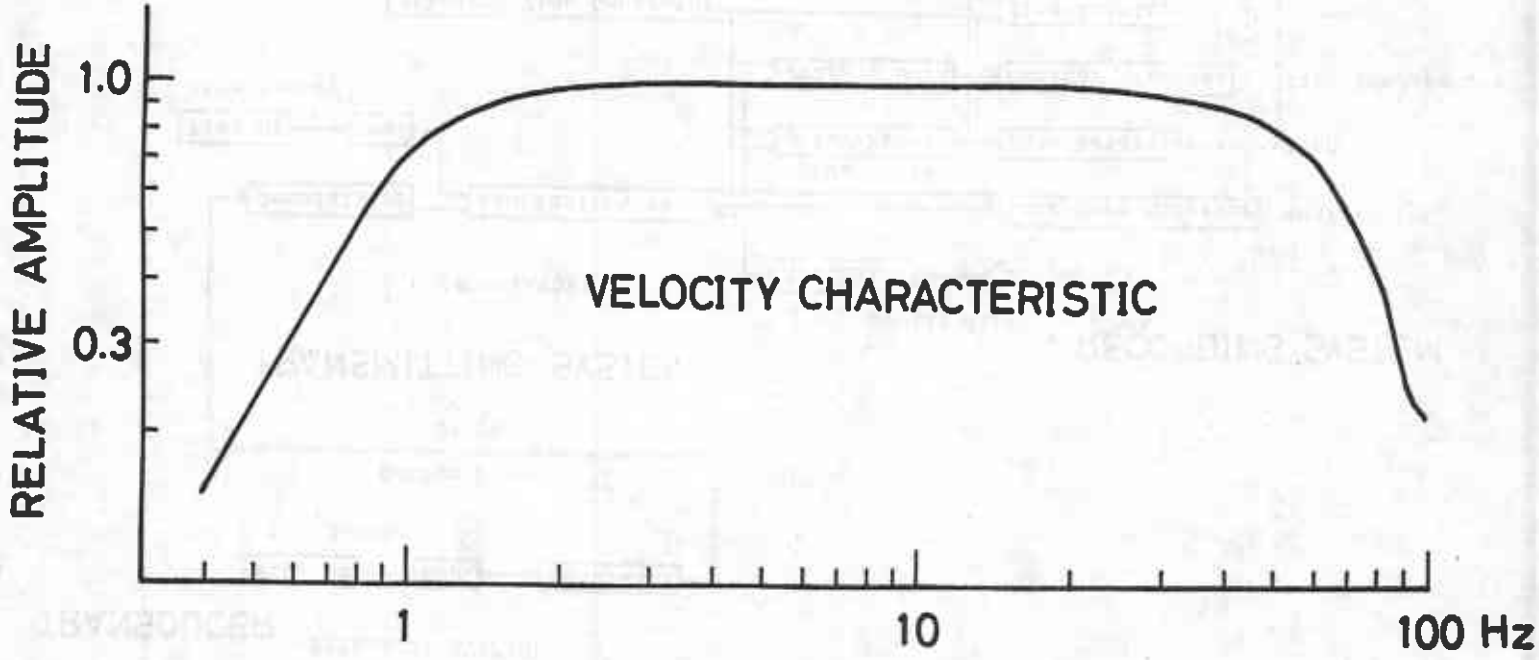

Fig. 2

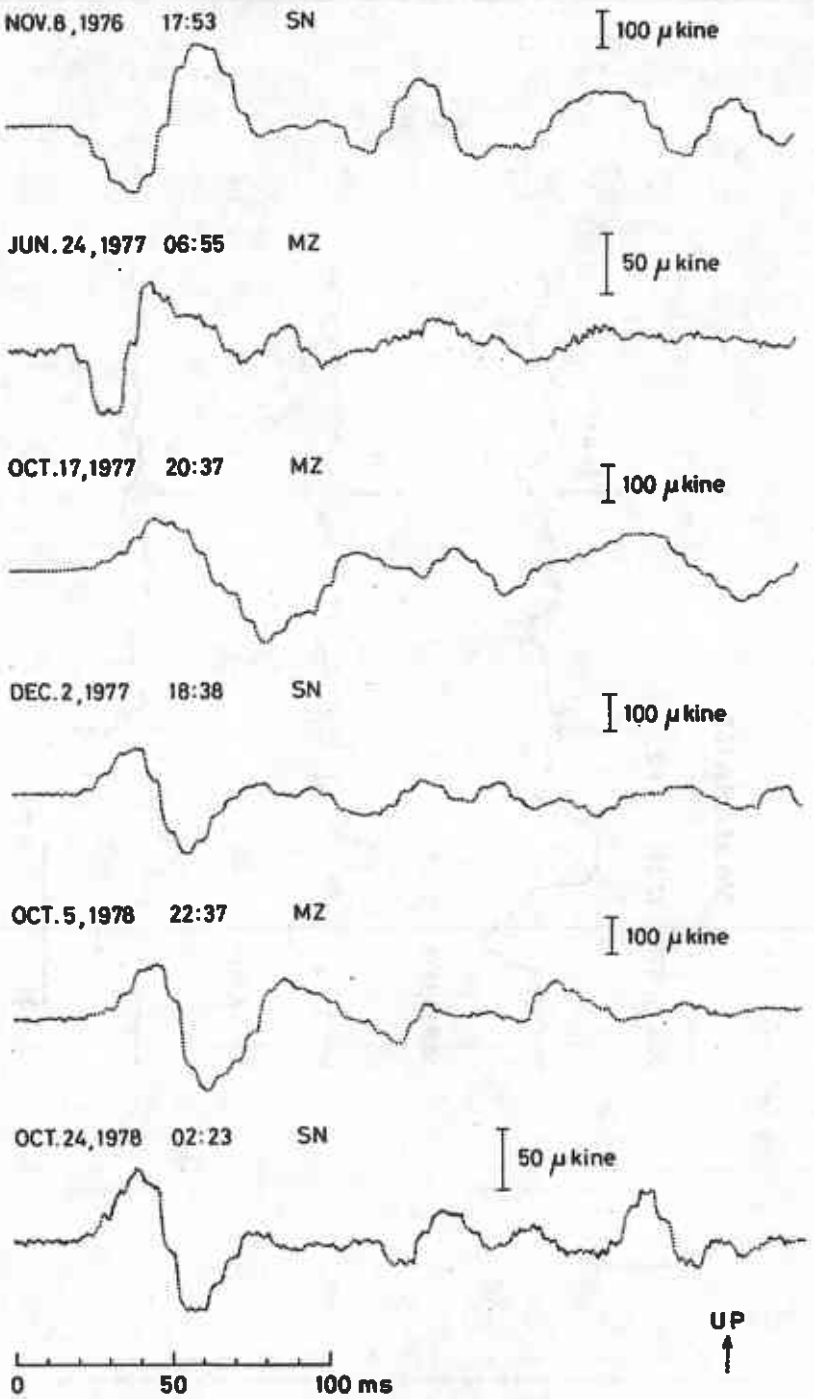
NOV.8, 1976 17:53 SN
100 μkine
JUN. 24, 1977 06:55 MZ
50 μkine
OCT.17, 1977 20:37 MZ
100 μkine
DEC. 2, 1977 18:38 SN
100 μkine
OCT. 5, 1978 22:37 MZ
100 μkine
OCT. 24, 1978 02:23 SN
50 μkine
UP
0
50
100 ms

Fig. 3

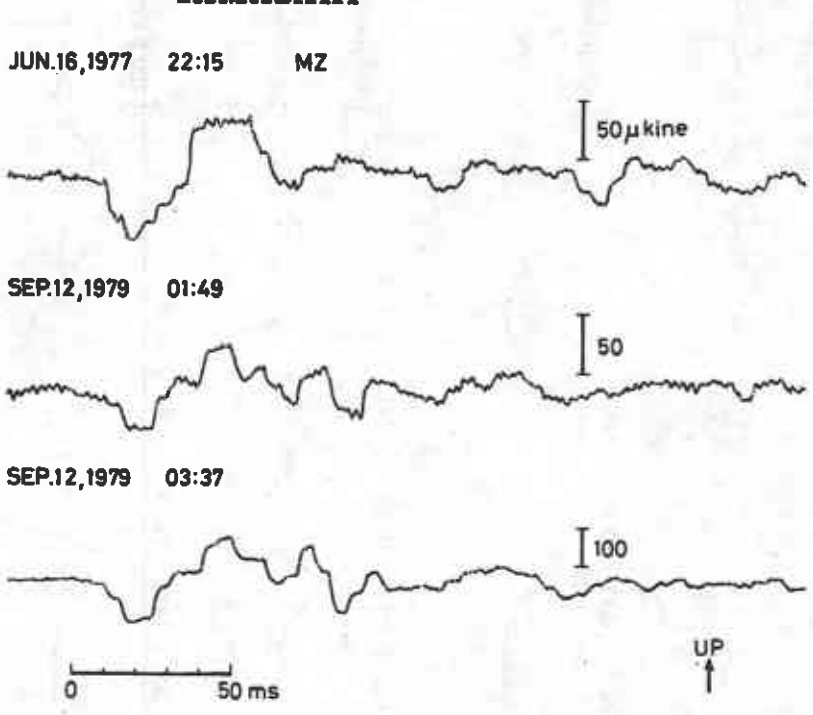
YAMASAKI
JUN.16,1977 22:15 MZ
50μkine
SEP.12,1979 01:49
50
SEP.12,1979 03:37
100
UP
0
50 ms

Fig. 4

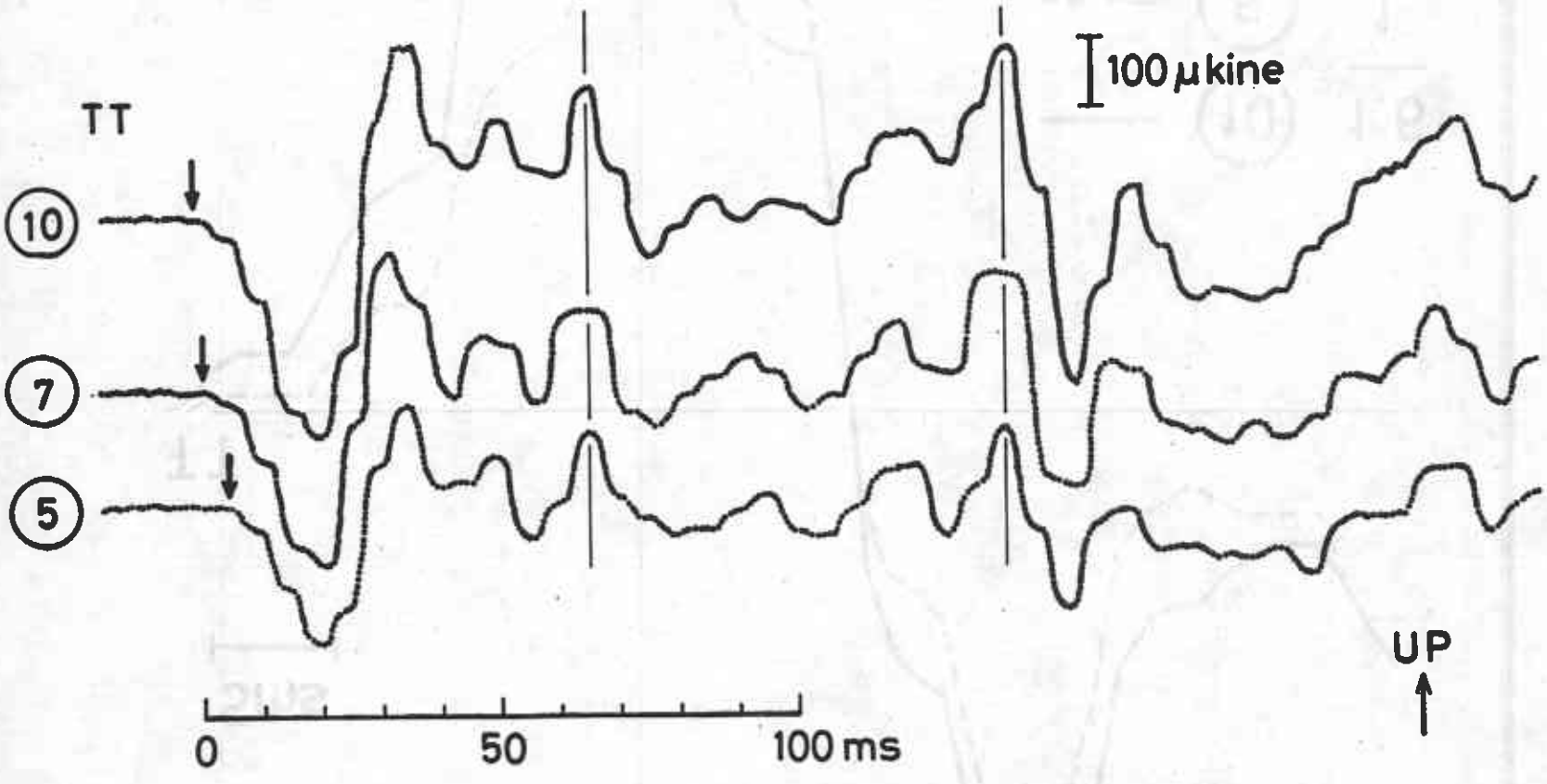

Fig. 5

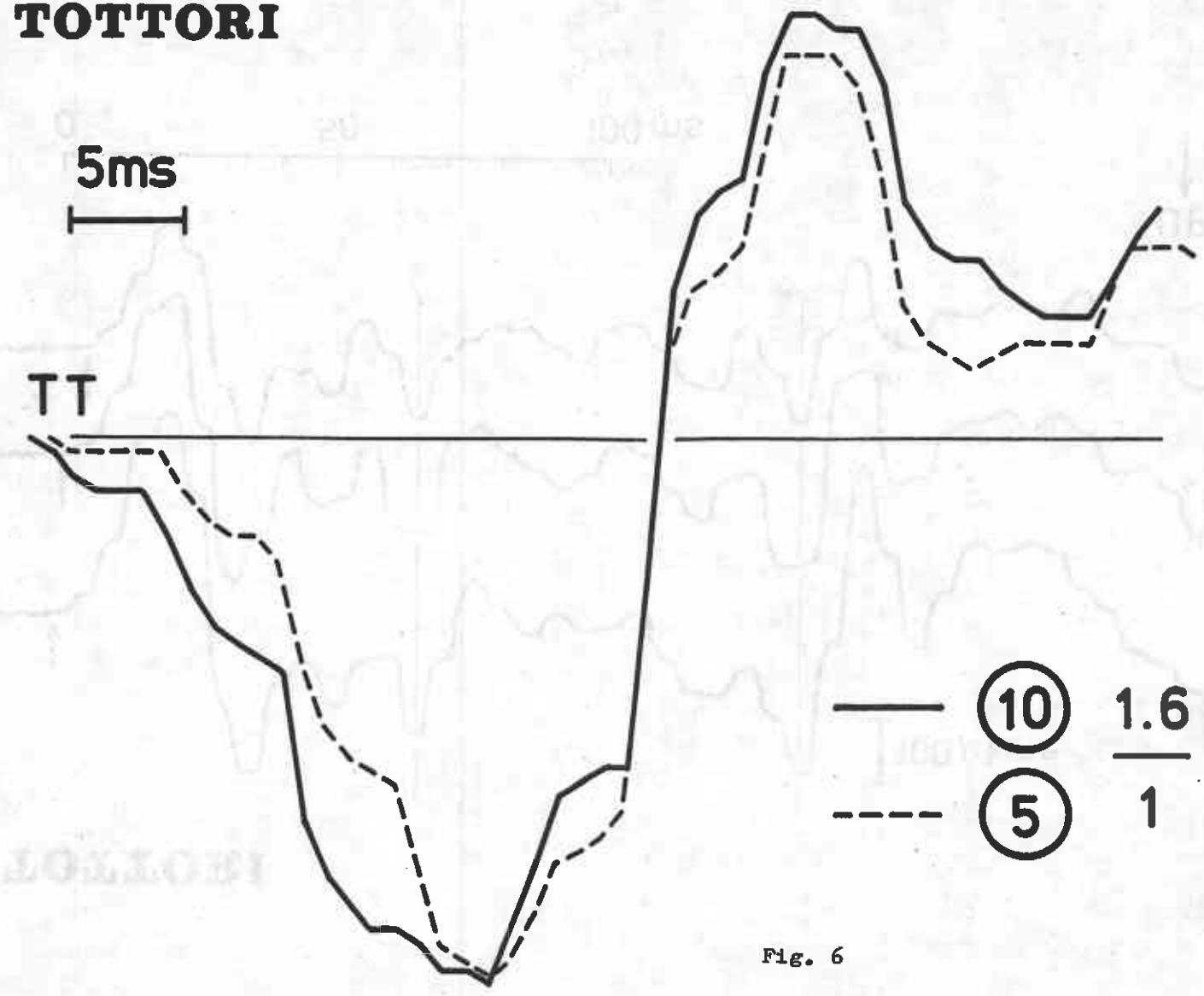

Fig. 6

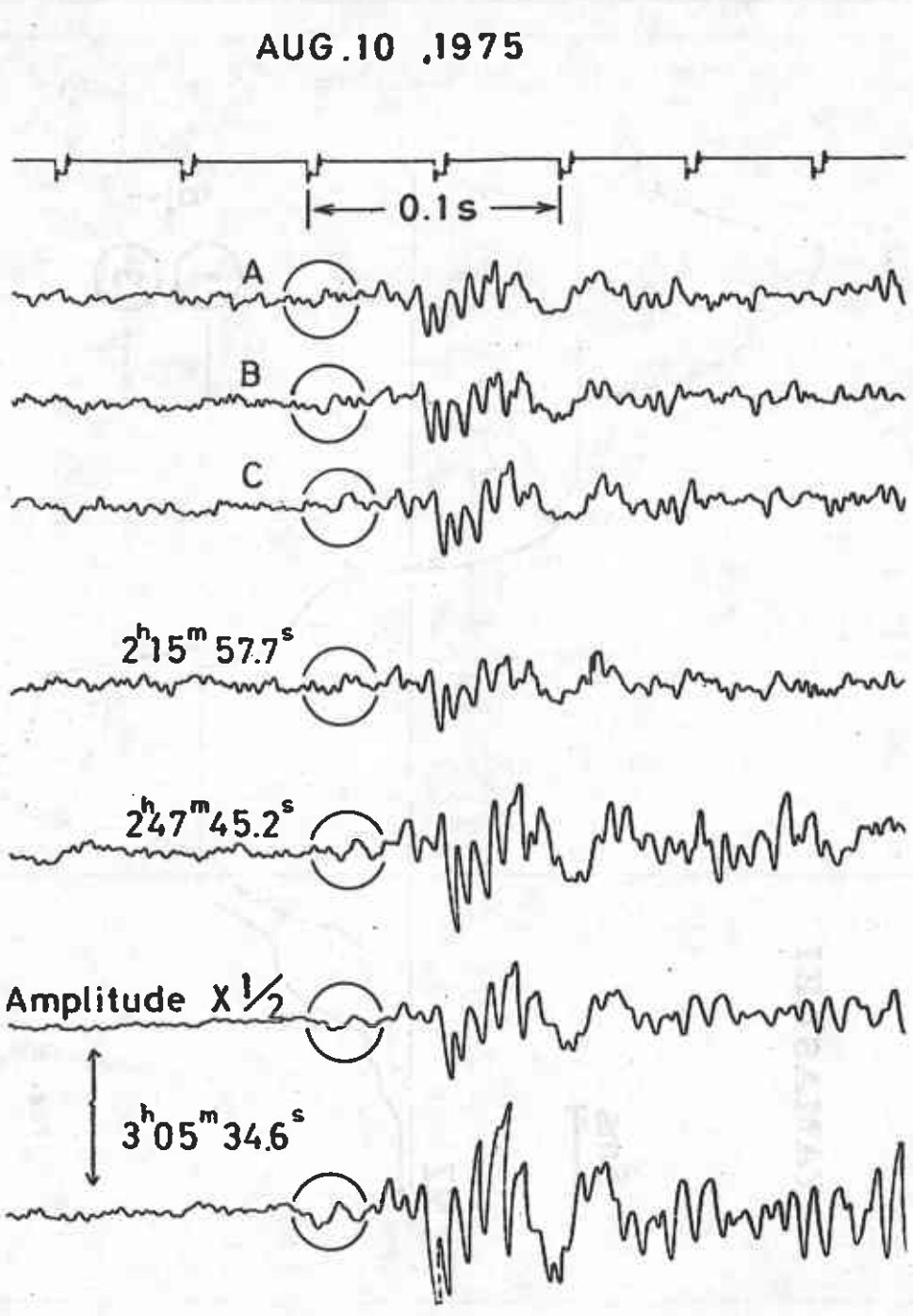
AUG.10 ,1975
0.1s
A
B
C
2h15m57.7s
2h47m45.2s
Amplitude X 1/2
3h05m34.6s

Fig. 7

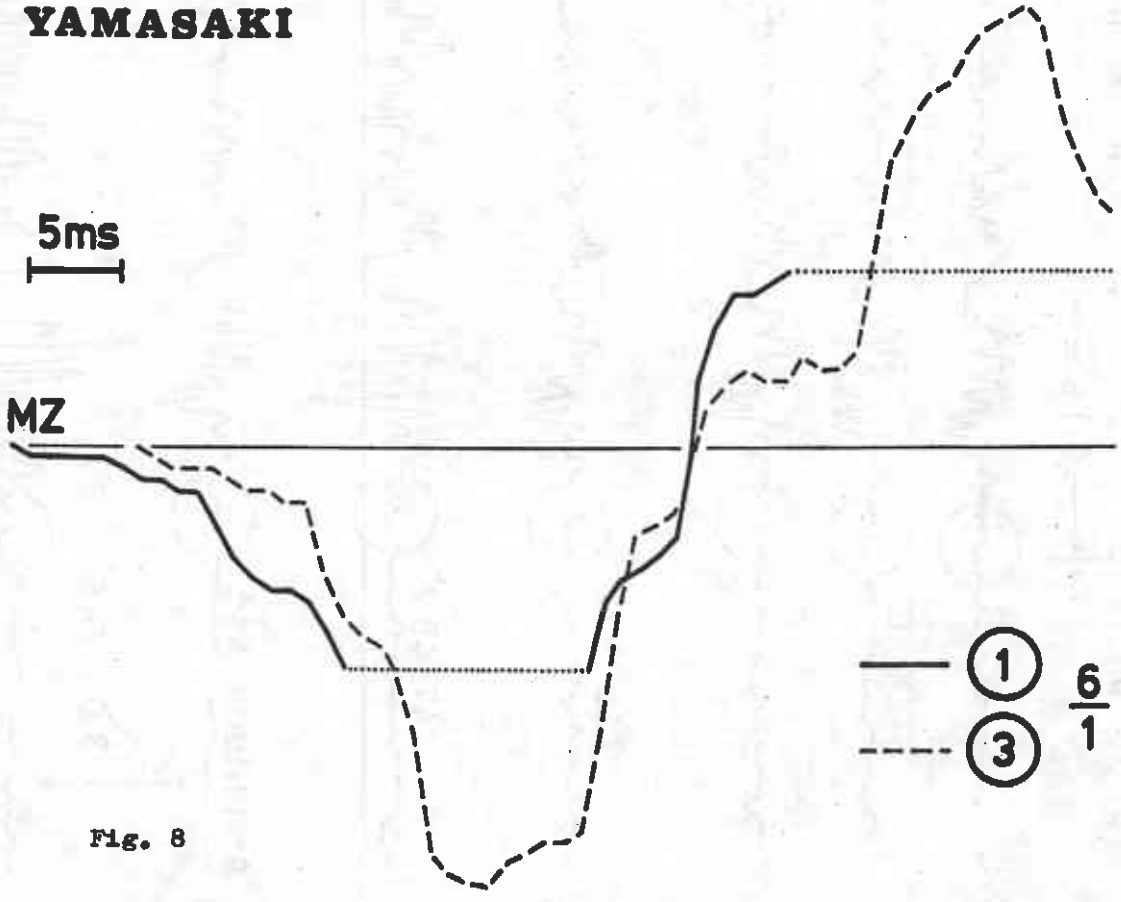

Fig. 8

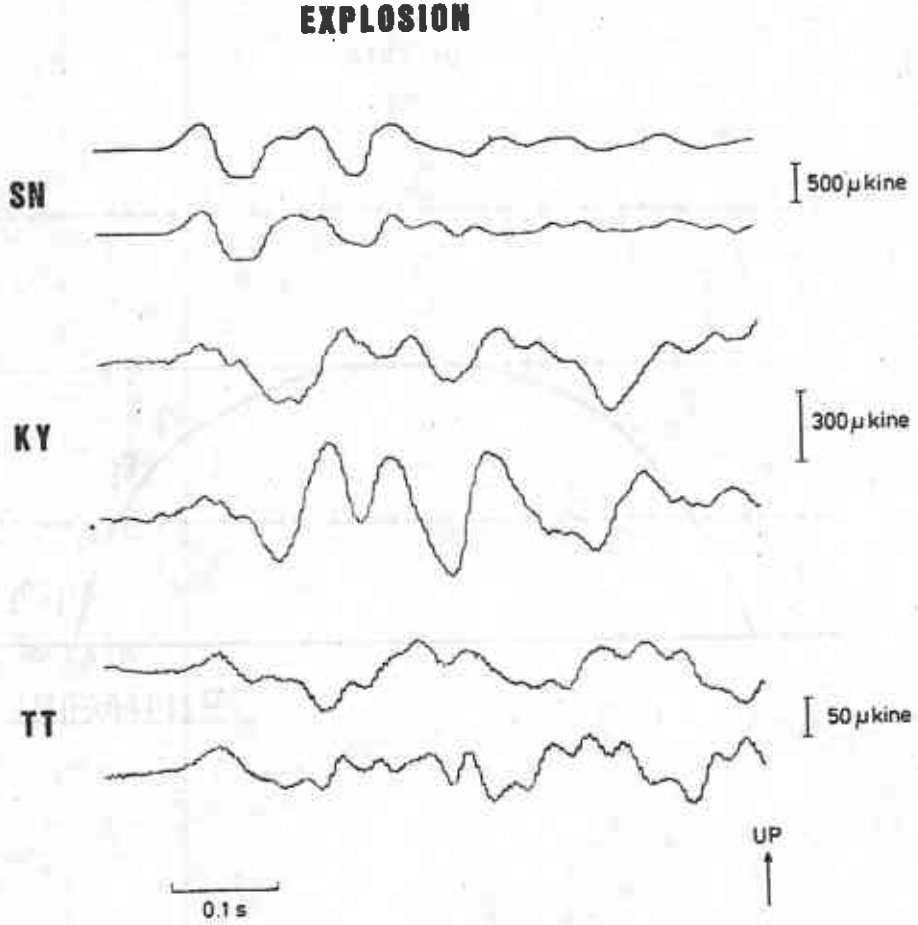

Fig. 9

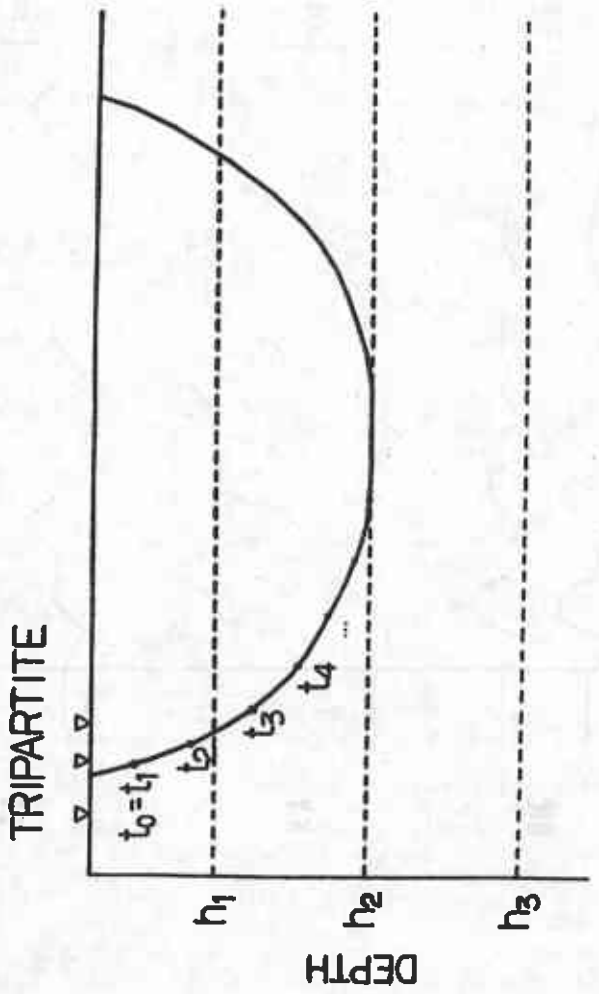

Fig. 10

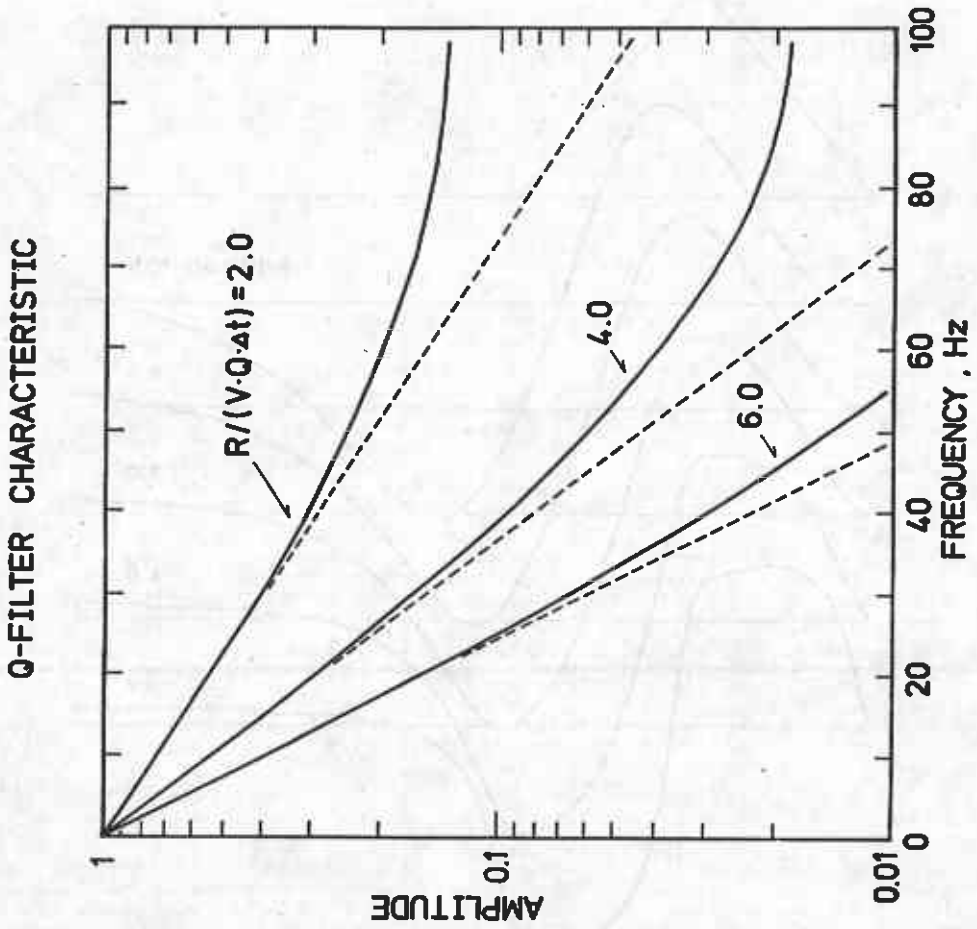
Q-FILTER CHARACTERISTIC
R/(V·Q·Δt) = 2.0
4.0
6.0
AMPLITUDE
1
0.1
0.01
0
20
40
60
80
100
FREQUENCY, Hz

Fig. 11

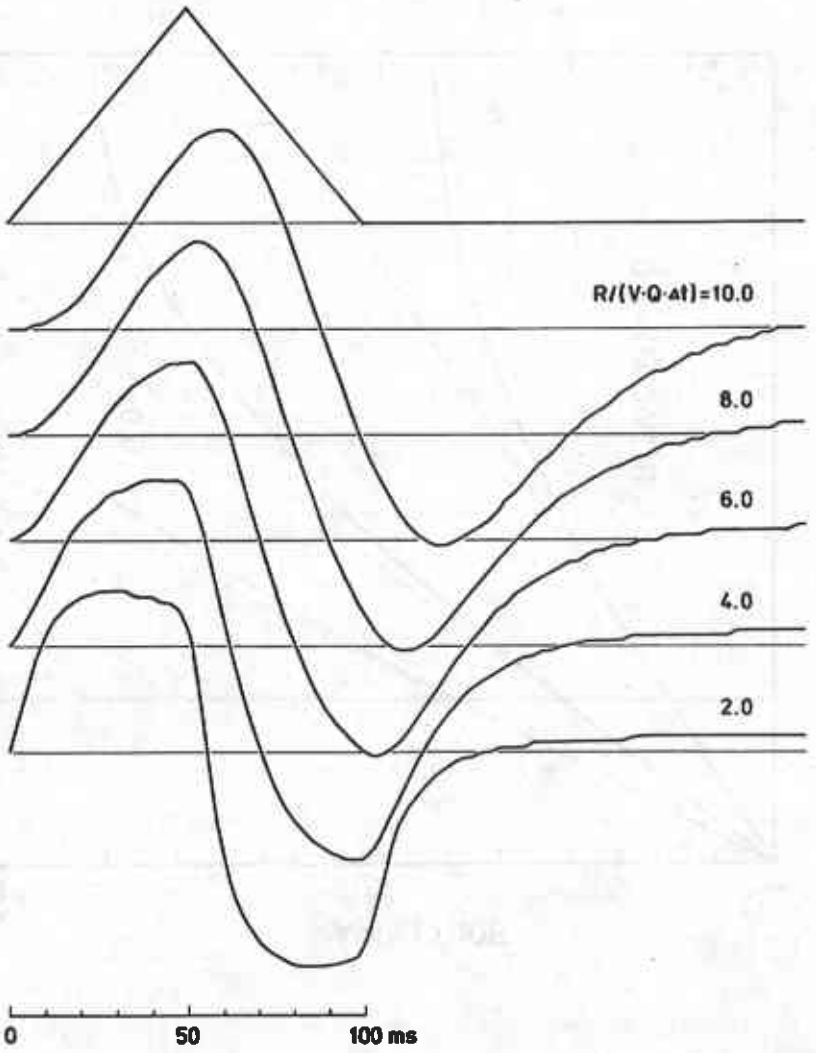

Fig. 12

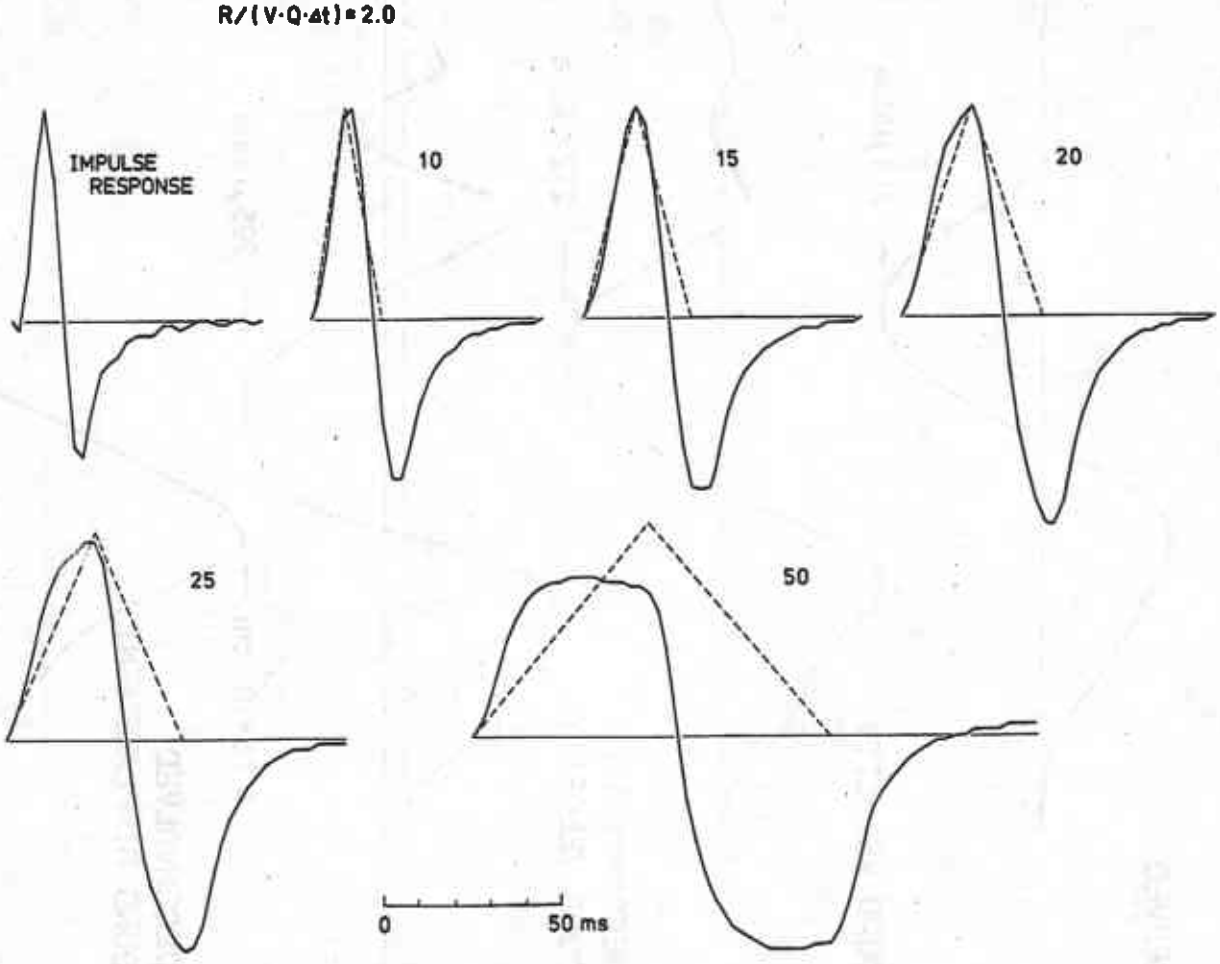

Fig. 13

HORADANI , SHIKANO FAULT

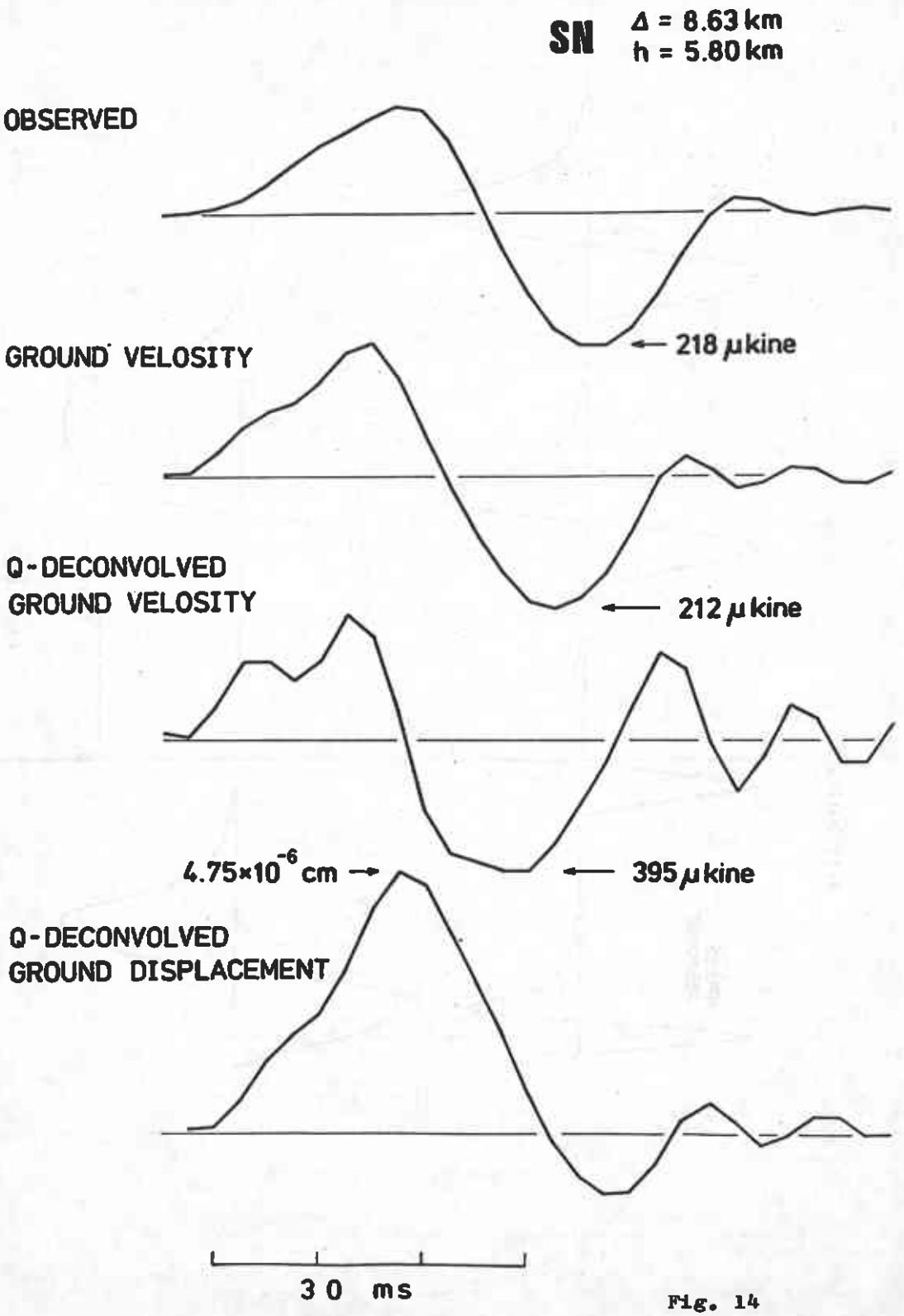

Fig. 14

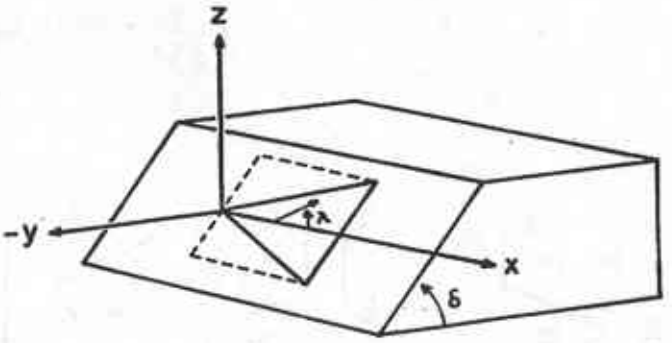
z
-y
x
δ

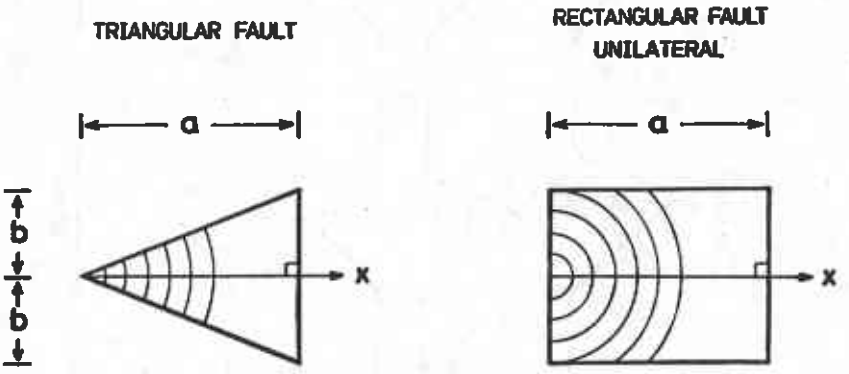
TRIANGULAR FAULT
RECTANGULAR FAULT
UNILATERAL
a
a
b
b
x
x

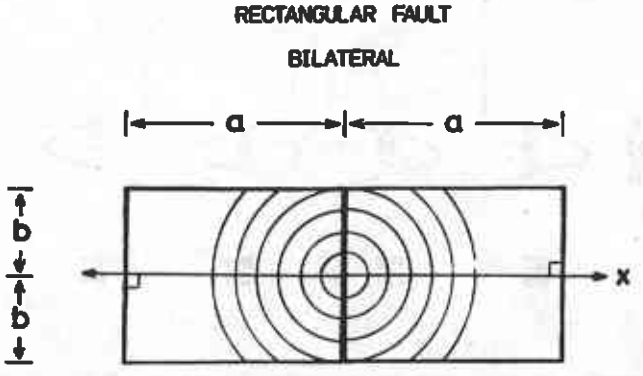
RECTANGULAR FAULT
BILATERAL
a
a
b
b
x

Fig. 15

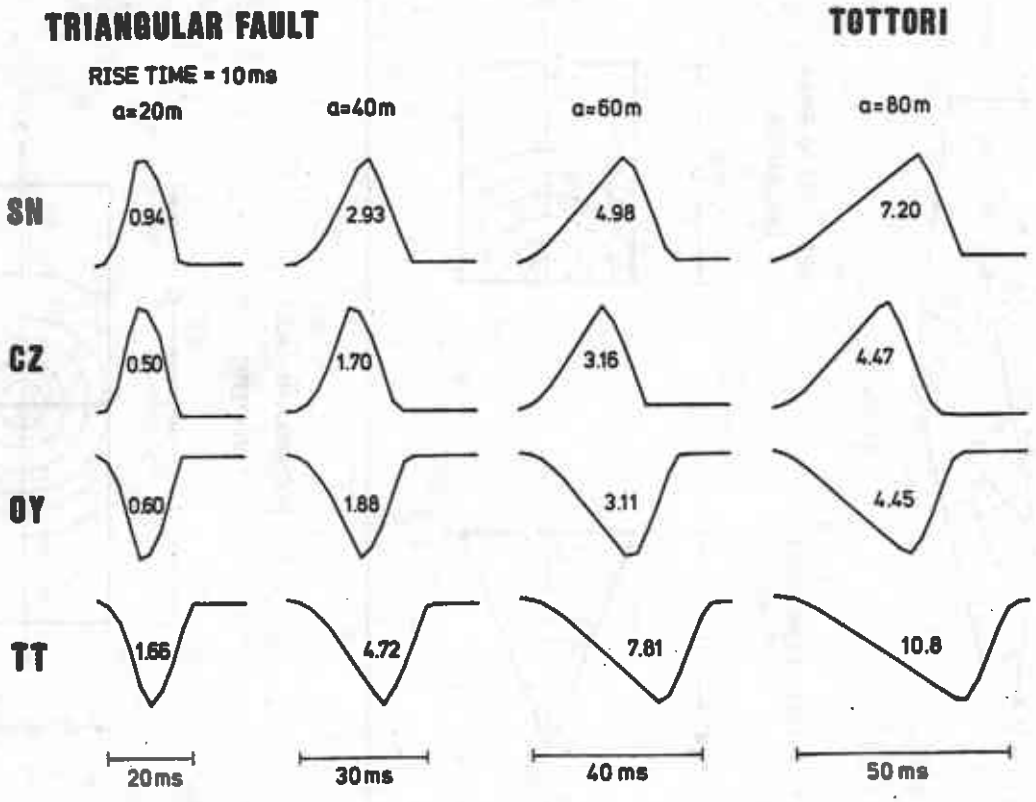
TRIANGULAR FAULT
TOTTORI
RISE TIME = 10ms
a=20m
a=40m
a=60m
a=80m
SN
CZ
OY
TT
0.94
2.93
4.98
7.20
0.50
1.70
3.16
4.47
0.60
1.88
3.11
4.45
1.66
4.72
7.81
10.8
20ms
30ms
40 ms
50 ms

Fig. 16(a)

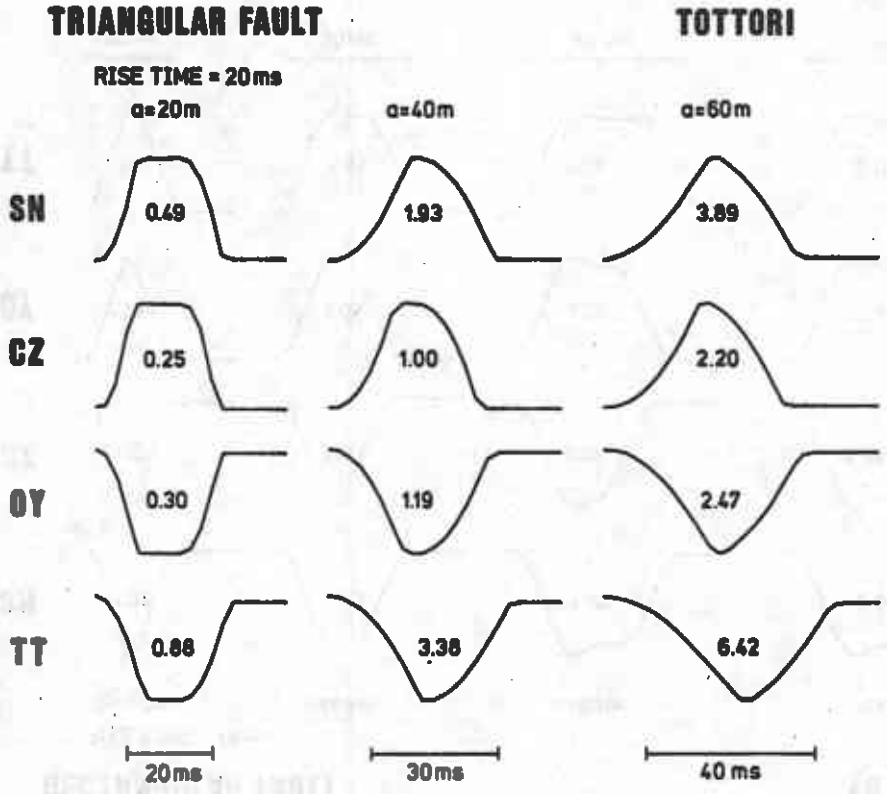
TRIANGULAR FAULT
TOTTORI
RISE TIME = 20ms
a=20m
a=40m
a=60m
SN
CZ
OY
TT
0.49
1.93
3.89
0.25
1.00
2.20
0.30
1.19
2.47
0.88
3.38
6.42
20ms
30ms
40 ms

Fig. 16(b)

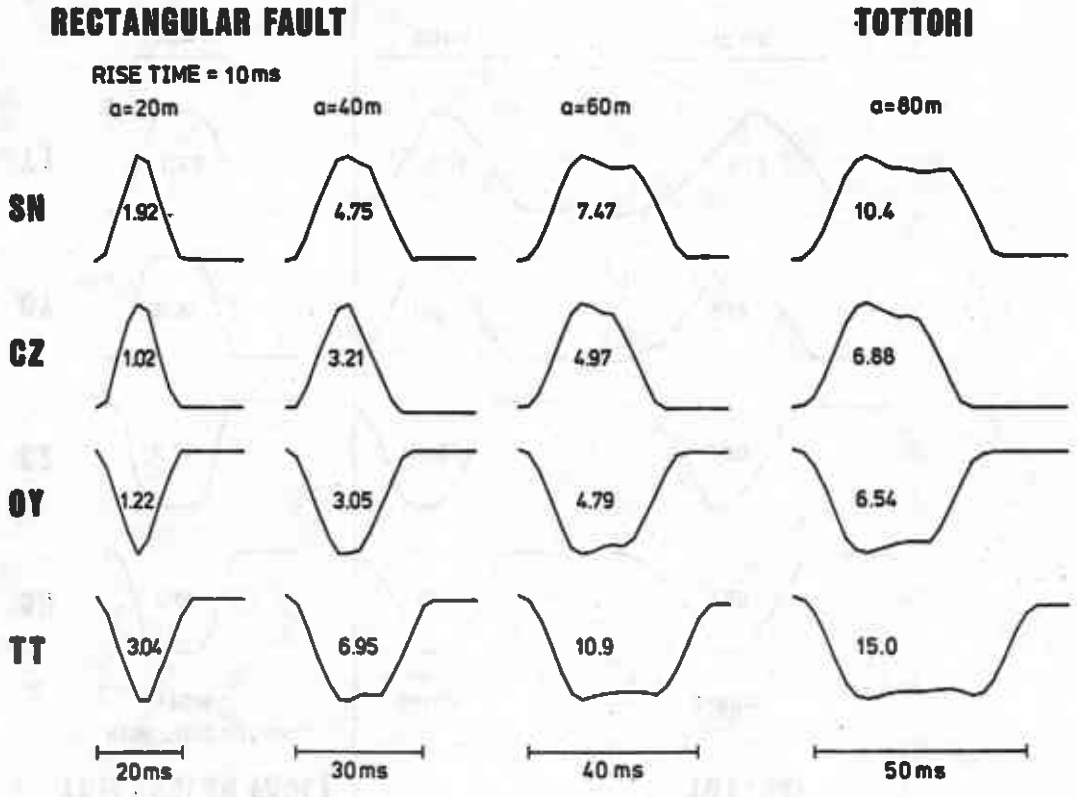
RECTANGULAR FAULT
TOTTORI
RISE TIME = 10ms
a=20m
a=40m
a=60m
a=80m
SN
CZ
OY
TT
1.92
4.75
7.47
10.4
1.02
3.21
4.97
6.88
1.22
3.05
4.79
6.54
3.04
6.95
10.9
15.0
20ms
30ms
40 ms
50ms

Fig. 16(c)

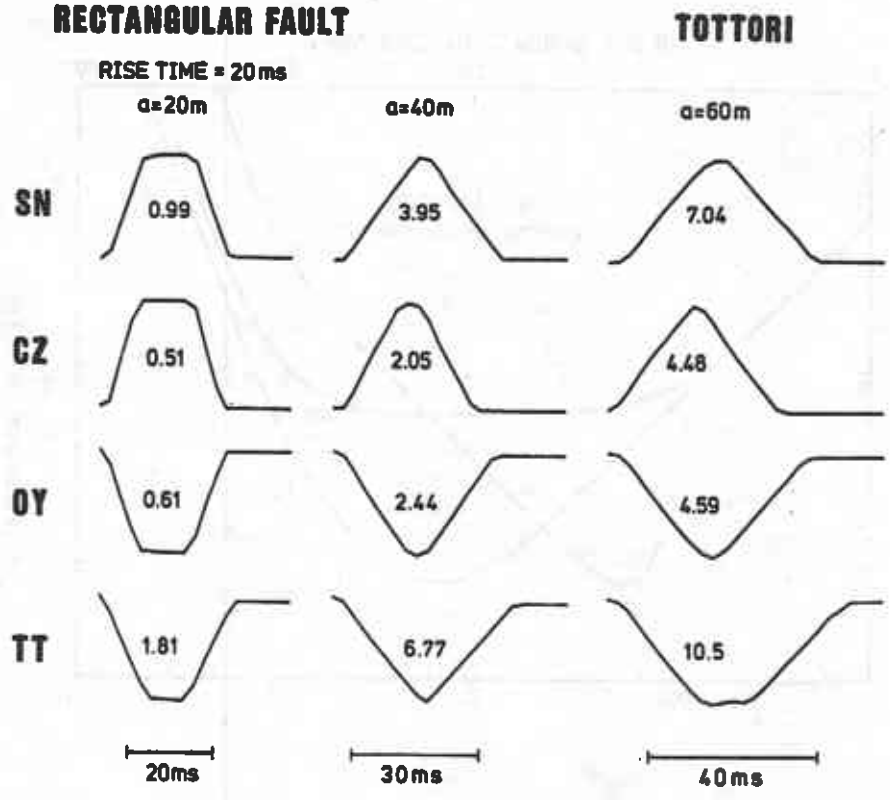
RECTANGULAR FAULT
TOTTORI
RISE TIME = 20ms
a=20m
a=40m
a=60m
SN
CZ
OY
TT
0.99
3.95
7.04
0.51
2.05
4.48
0.61
2.44
4.59
1.81
6.77
10.5
20ms
30ms
40ms

Fig. 16(d)

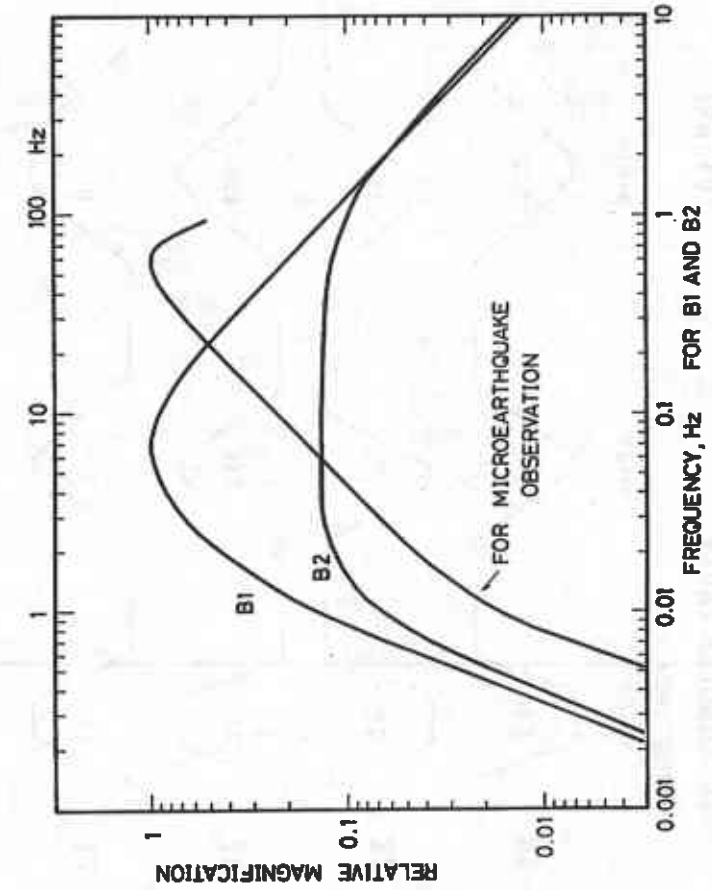
RELATIVE MAGNIFICATION
1
0.1
0.01
0.001
1
10
100
Hz
0.01
0.1
1
10
FREQUENCY, Hz
B1
B2
FOR MICROEARTHQUAKE OBSERVATION
FOR B1 AND B2

Fig. 17

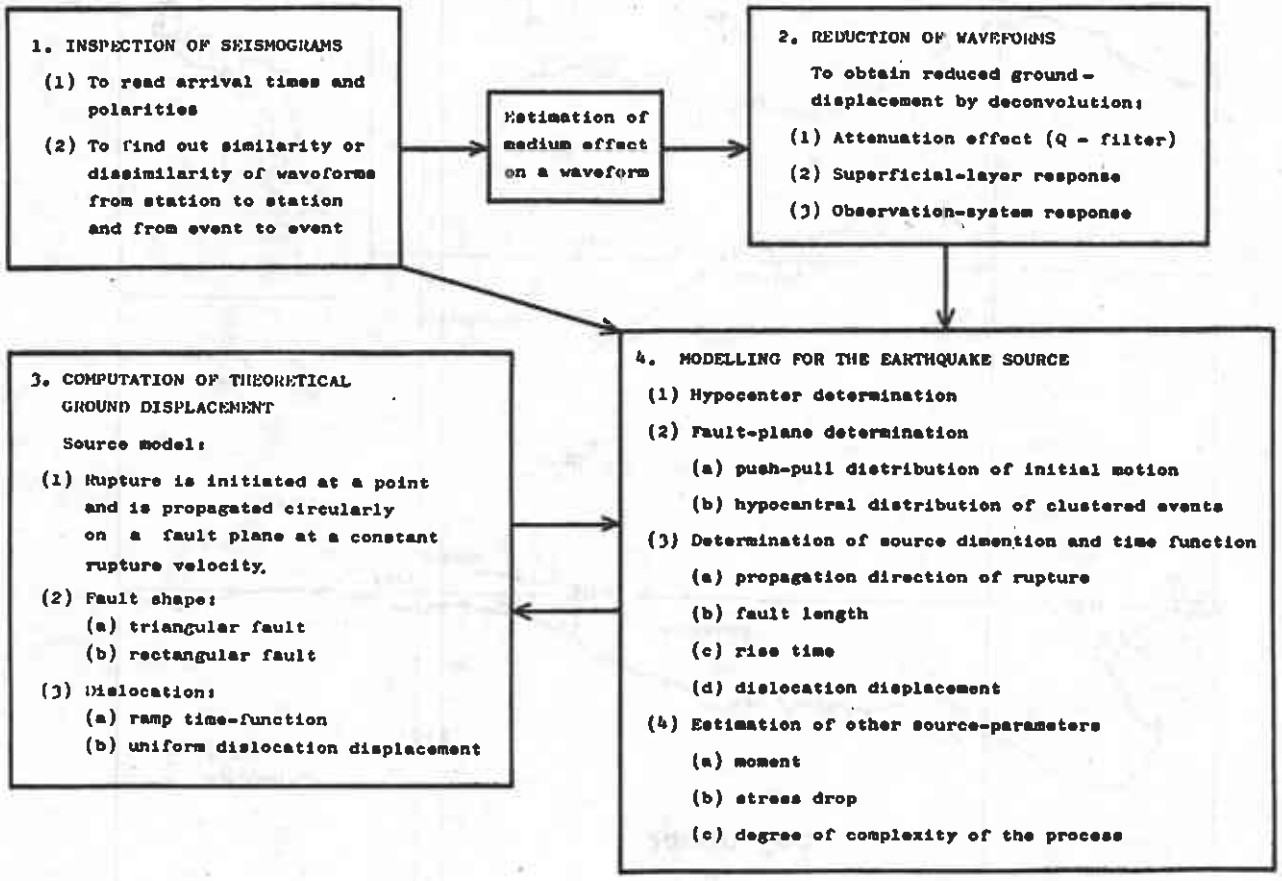
1. INSPECTION OF SEISMOGRAMS
(1) To read arrival times and polarities
(2) To find out similarity or dissimilarity of waveforms from station to station and from event to event
Estimation of medium effect on a waveform
2. REDUCTION OF WAVEFORMS
To obtain reduced ground-displacement by deconvolution:
(1) Attenuation effect (Q - filter)
(2) Superficial-layer response
(3) Observation-system response
3. COMPUTATION OF THEORETICAL GROUND DISPLACEMENT
Source model:
(1) Rupture is initiated at a point and is propagated circularly on a fault plane at a constant rupture velocity.
(2) Fault shape:
(a) triangular fault
(b) rectangular fault
(3) Dislocation:
(a) ramp time-function
(b) uniform dislocation displacement
4. MODELLING FOR THE EARTHQUAKE SOURCE
(1) Hypocenter determination
(2) Fault-plane determination
(a) push-pull distribution of initial motion
(b) hypocentral distribution of clustered events
(3) Determination of source dimention and time function
(a) propagation direction of rupture
(b) fault length
(c) rise time
(d) dislocation displacement
(4) Estimation of other source-parameters
(a) moment
(b) stress drop
(c) degree of complexity of the process

Fig. 18

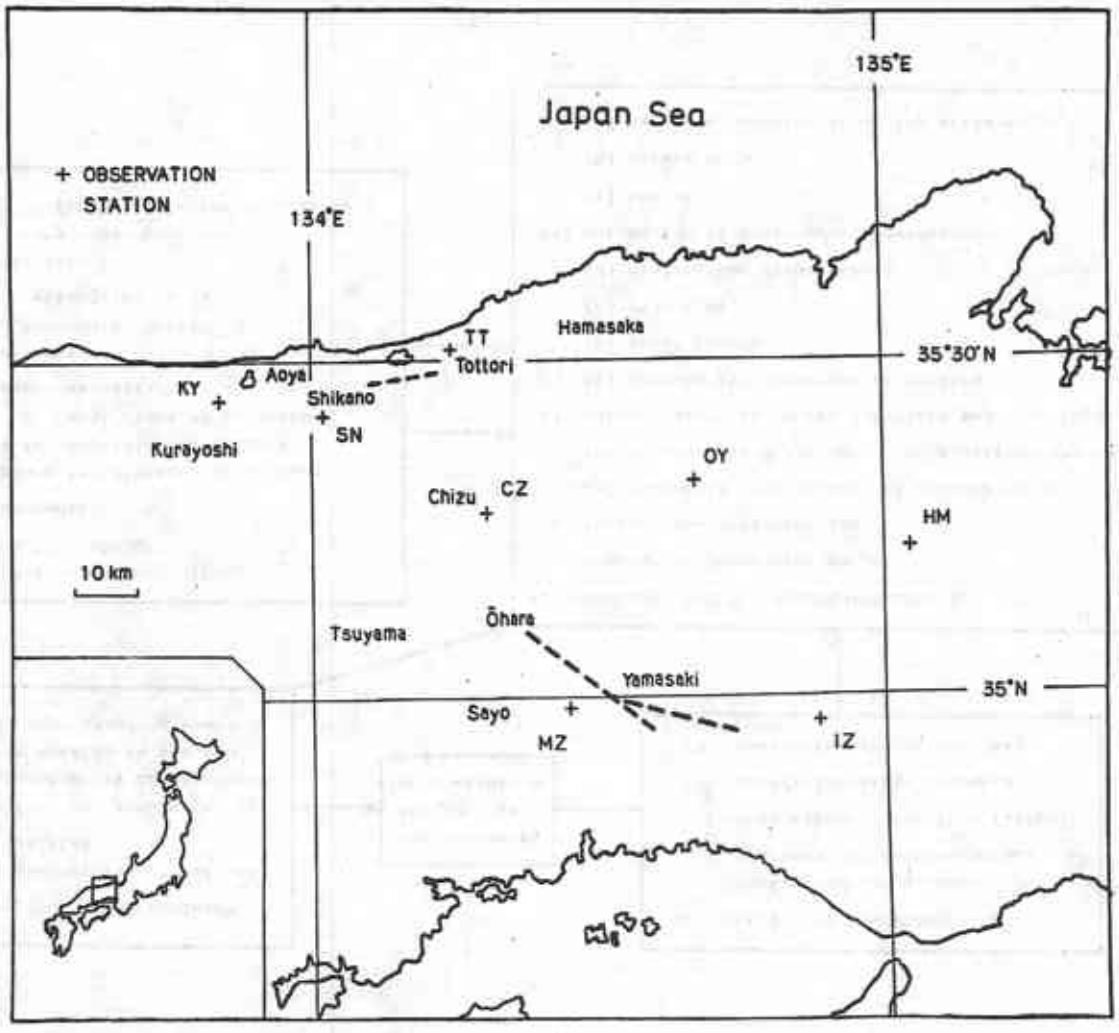
Japan Sea
+ OBSERVATION STATION
135°E
134°E
35°30'N
35°N
TT
Tottori
Hamasaka
KY
Aoya
Shikano
SN
Kurayoshi
OY
Chizu
CZ
HM
10 km
Tsuyama
Ōhara
Yamasaki
Sayo
MZ
IZ

Fig. 19

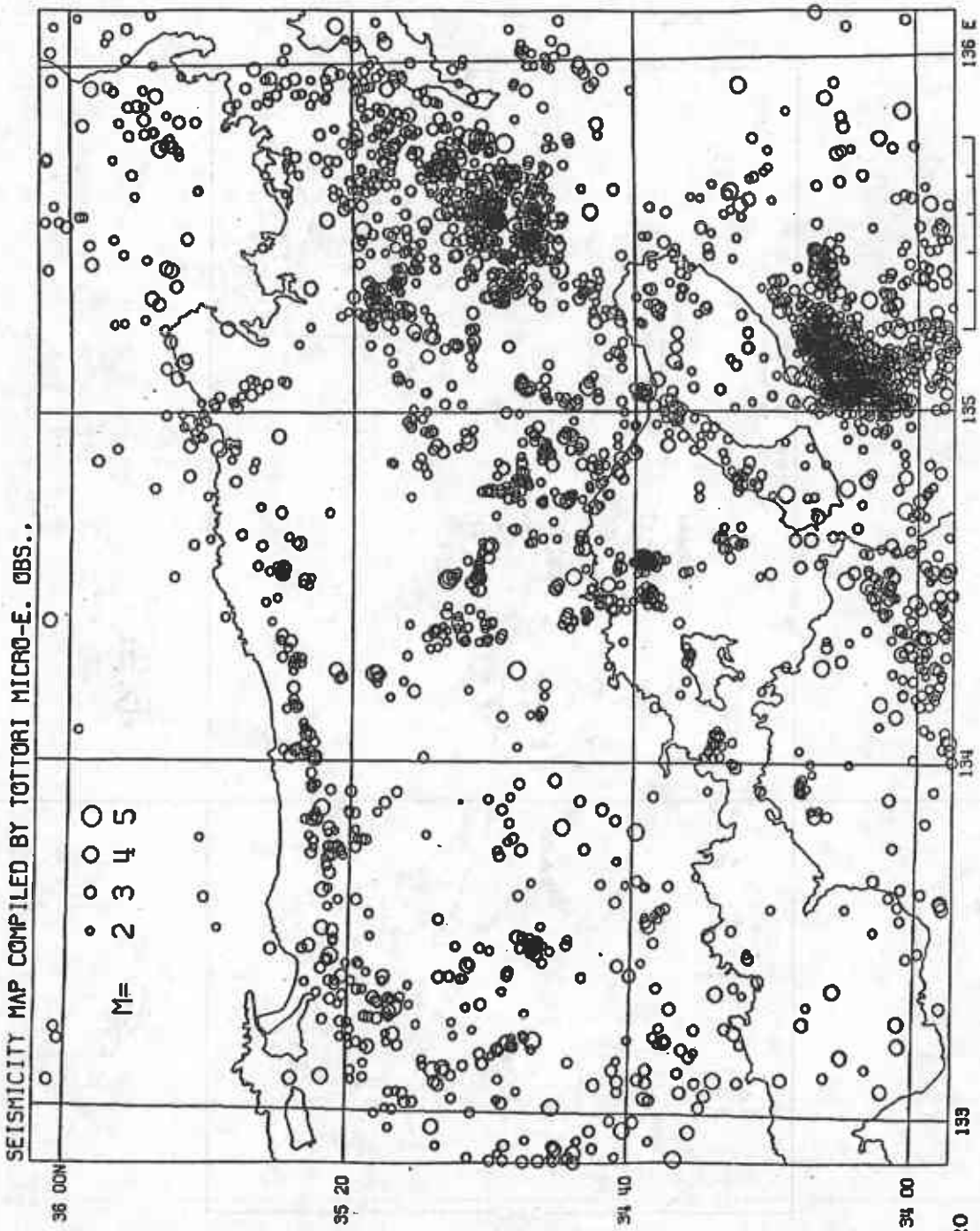
SEISMICITY MAP COMPILED BY TOTTORI MICRO-E. OBS..
M= 2 3 4 5
36 00N
35 20
34 40
34 00
133
134
135
136 E
50 KM

Fig. 20

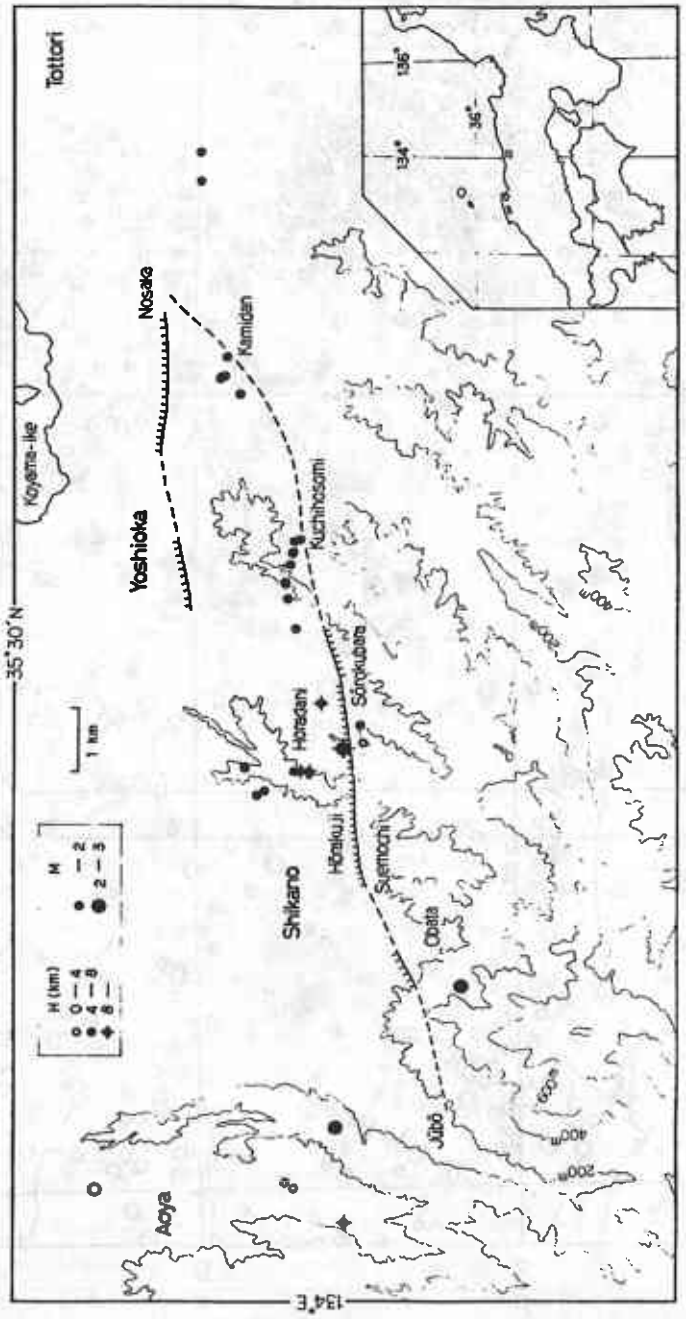
Tottori
Koyama-ike
Nosaka
Yoshioka
Kamidan
Kuchihosomi
Sonokubara
Horadani
Hōraiguji
Shikano
Sugimochi
Obata
Jūbō
Aoya
35°30'N
134°E
1 km
H (km)
0 — 4
4 — 8
8 —
M
— 2
2 — 3
200m
400m
600m
800m
134°
135°
136°
35°

Fig. 21

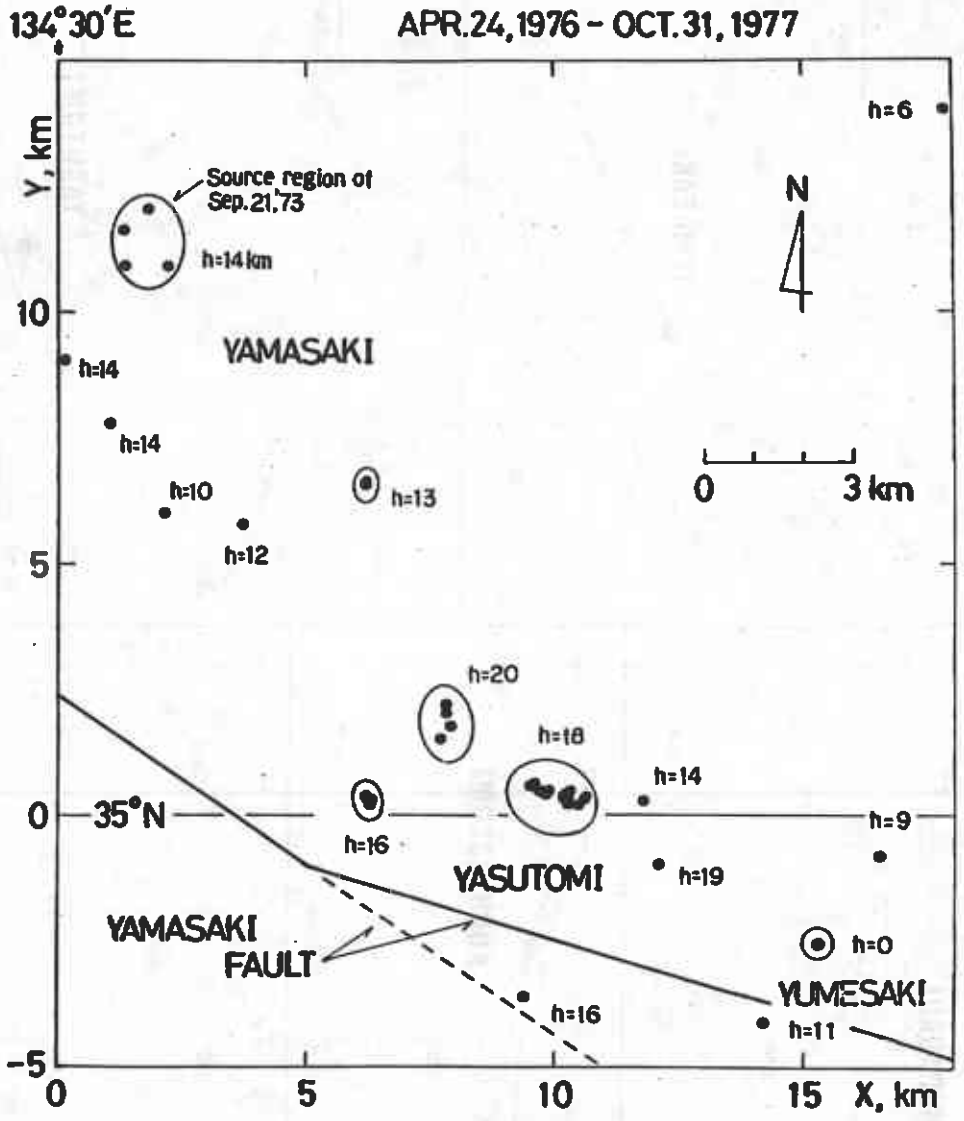
134°30'E
APR.24,1976 - OCT.31,1977
Y, km
X, km
Source region of Sep.21,'73
h=14 km
N
h=6
YAMASAKI
h=14
h=14
h=10
h=12
h=13
0
3 km
h=20
h=18
h=14
h=16
35°N
h=9
YASUTOMI
h=19
YAMASAKI FAULT
h=0
YUMESAKI
h=16
h=11
10
5
0
-5
0
5
10
15

Fig. 22

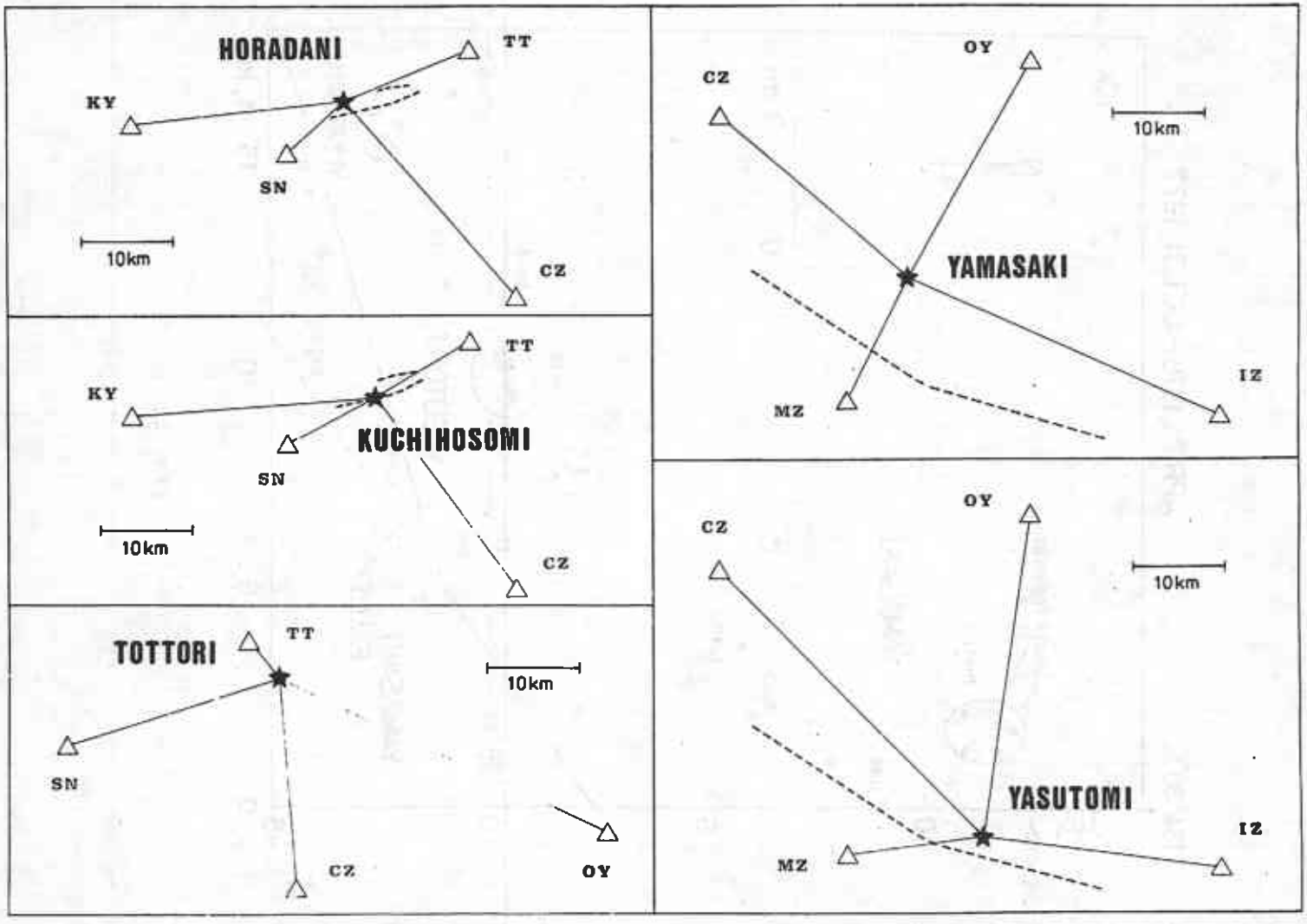
HORADANI
TT
KY
SN
10km
CZ
KUCHIHOSOMI
TT
KY
SN
10km
CZ
TOTTORI
TT
10km
SN
CZ
OY
OY
CZ
10km
YAMASAKI
MZ
IZ
OY
CZ
10km
YASUTOMI
MZ
IZ

Fig. 23

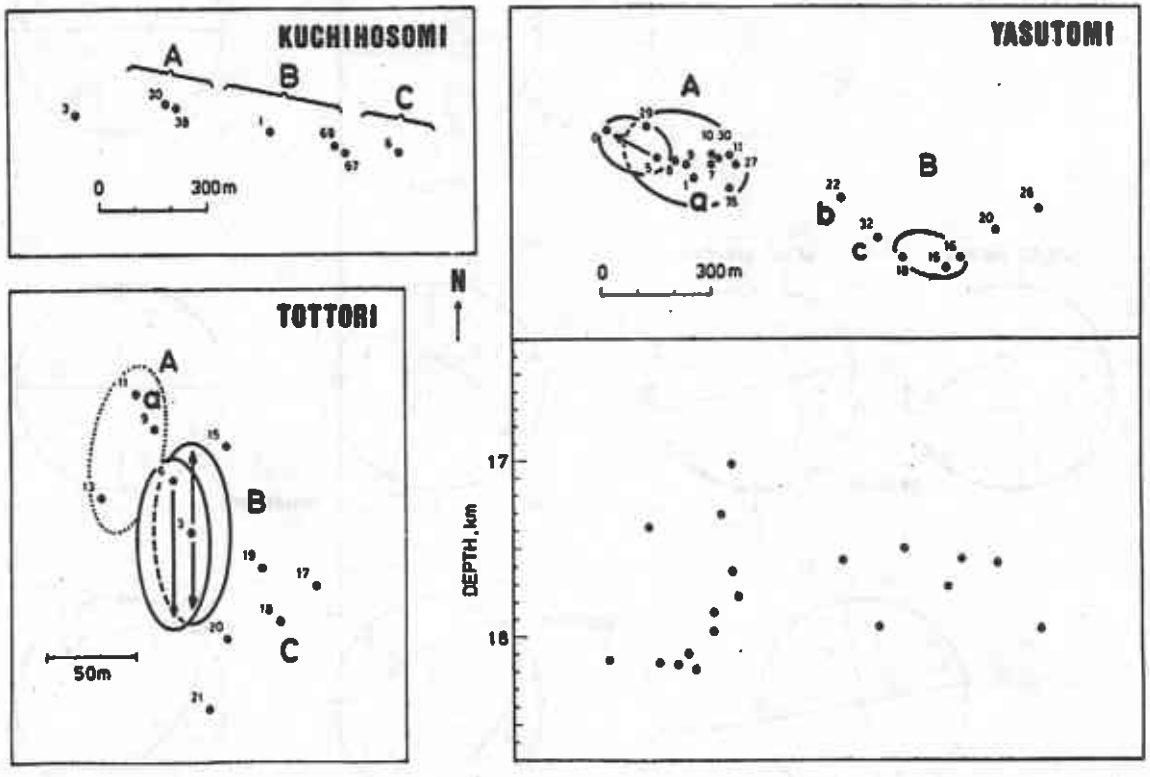
KUCHIHOSOMI
A
B
C
0
300m
YASUTOMI
A
B
a
b
c
0
300m
N
TOTTORI
A
B
C
50m
DEPTH, km
17
18

Fig. 24

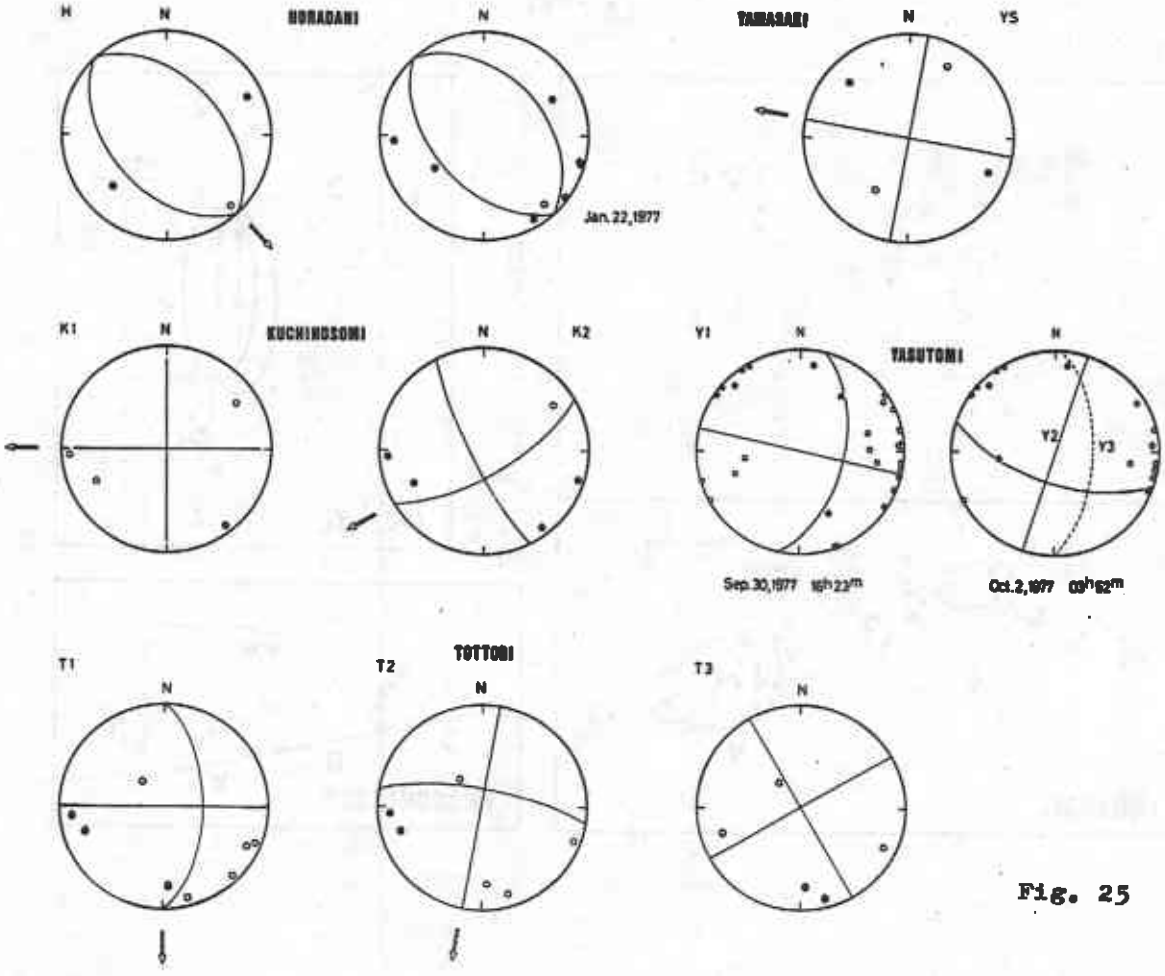
H
N
HORADANI
N
Jan. 22, 1977
YAMASAKI
N
YS
K1
N
KUCHINOSOMI
N
K2
Y1
N
YASUTOMI
N
Y2
Y3
Sep. 30, 1977 16h22m
Oct. 2, 1977 03h52m
T1
N
TOTTORI
T2
N
T3
N

Fig. 25

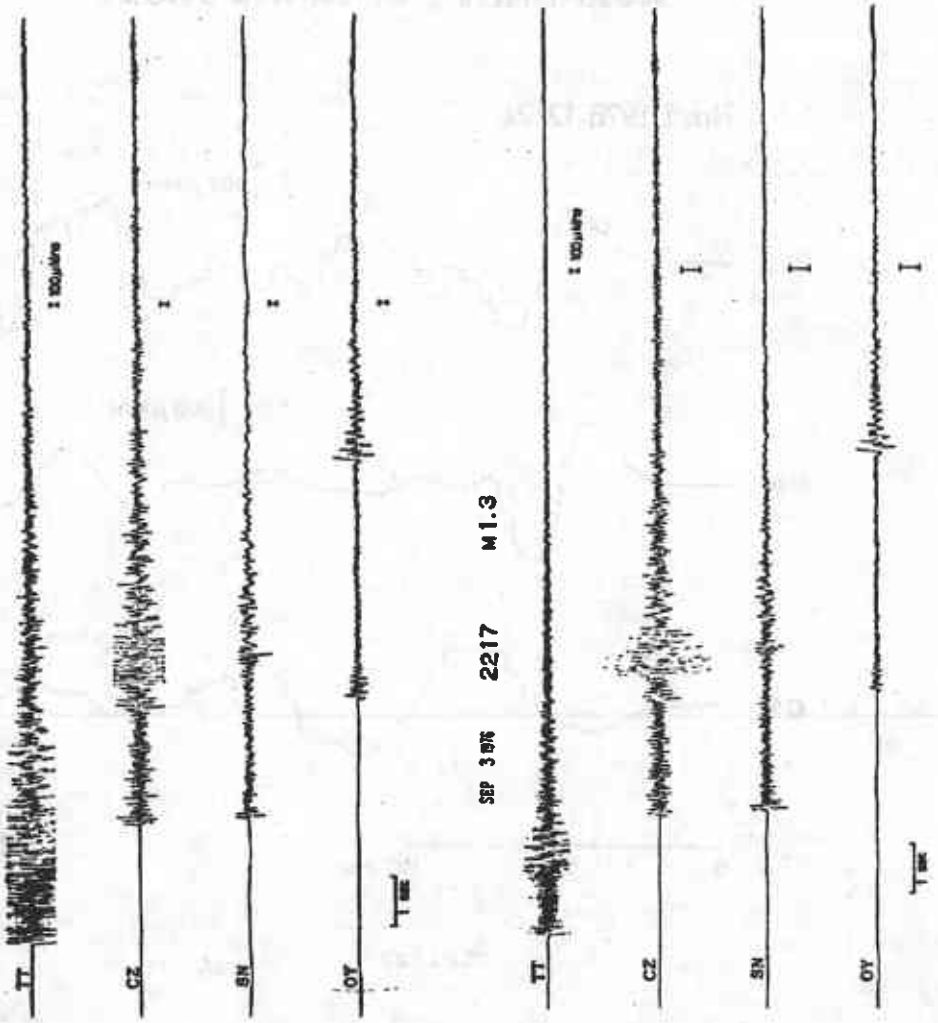

Fig. 26

HORADANI , SHIKANO FAULT

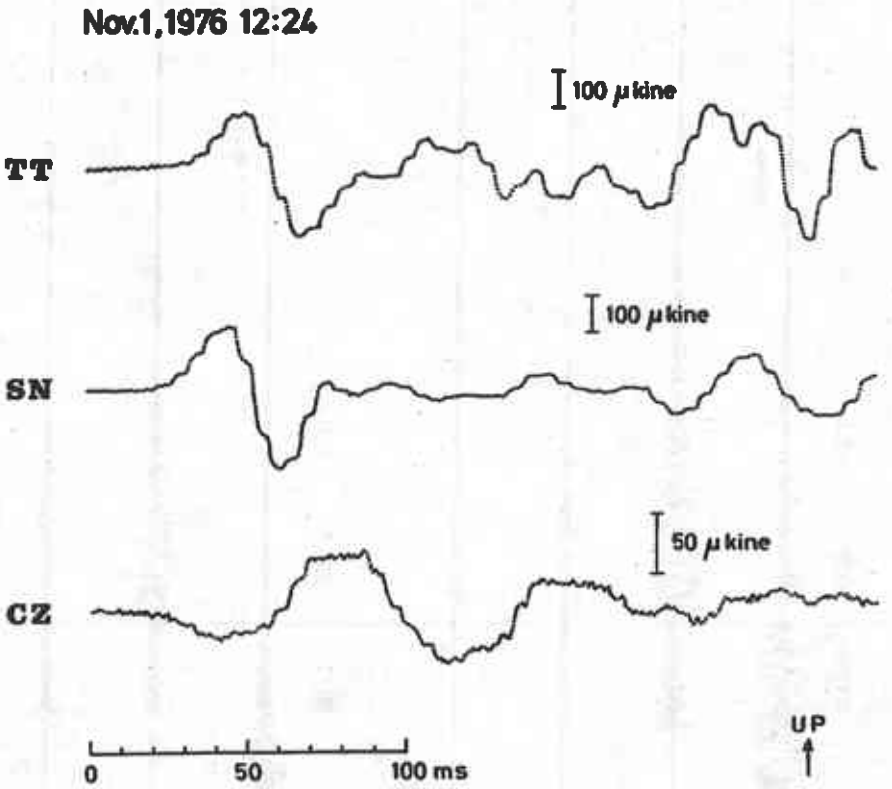

Fig. 27

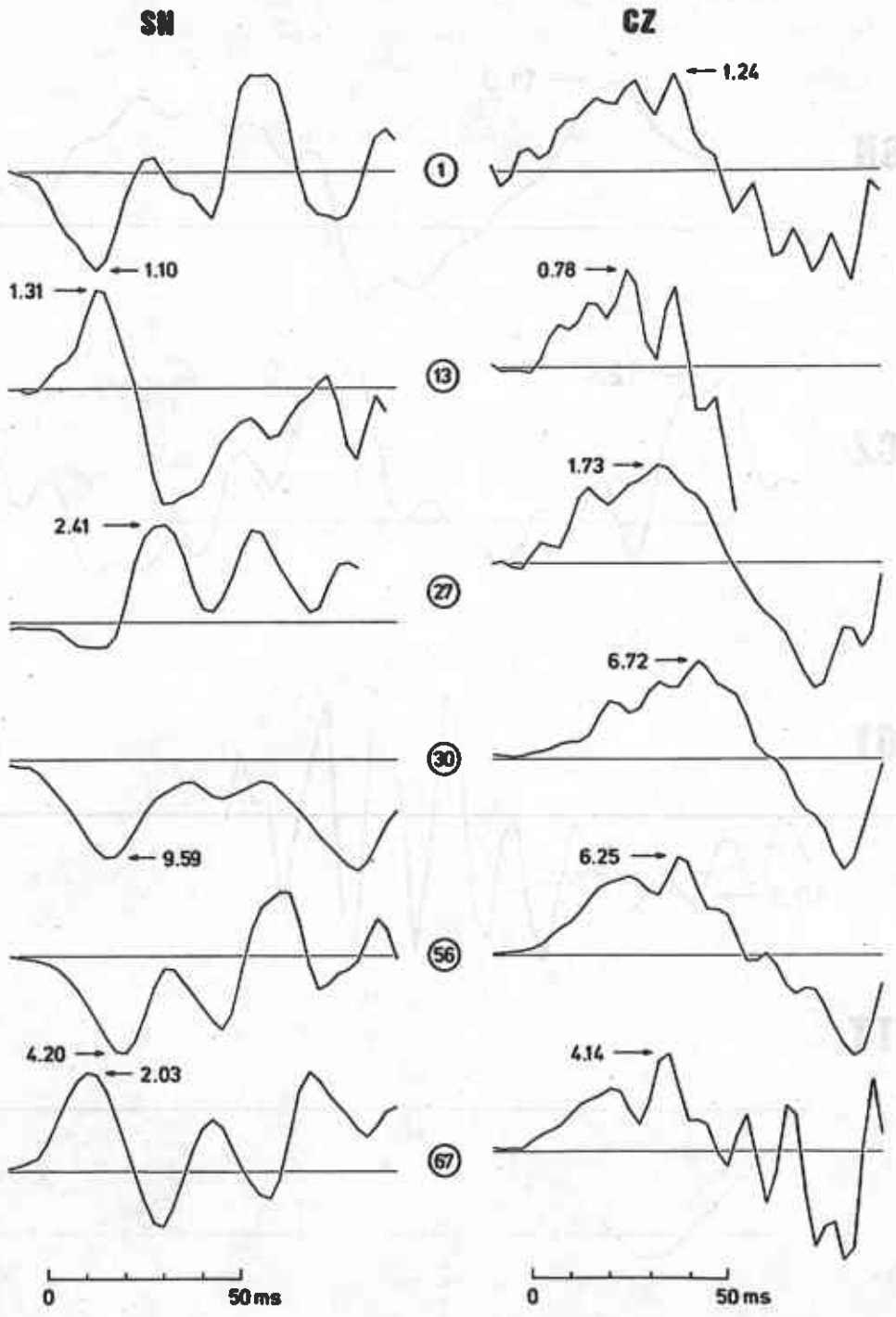
KUCHIHOSOMI , SHIKANO FAULT
SN
CZ
1.24
1.10
1.31
0.78
1.73
2.41
6.72
9.59
6.25
4.20
2.03
4.14
1
13
27
30
56
67
0
50 ms
0
50 ms

Fig. 28

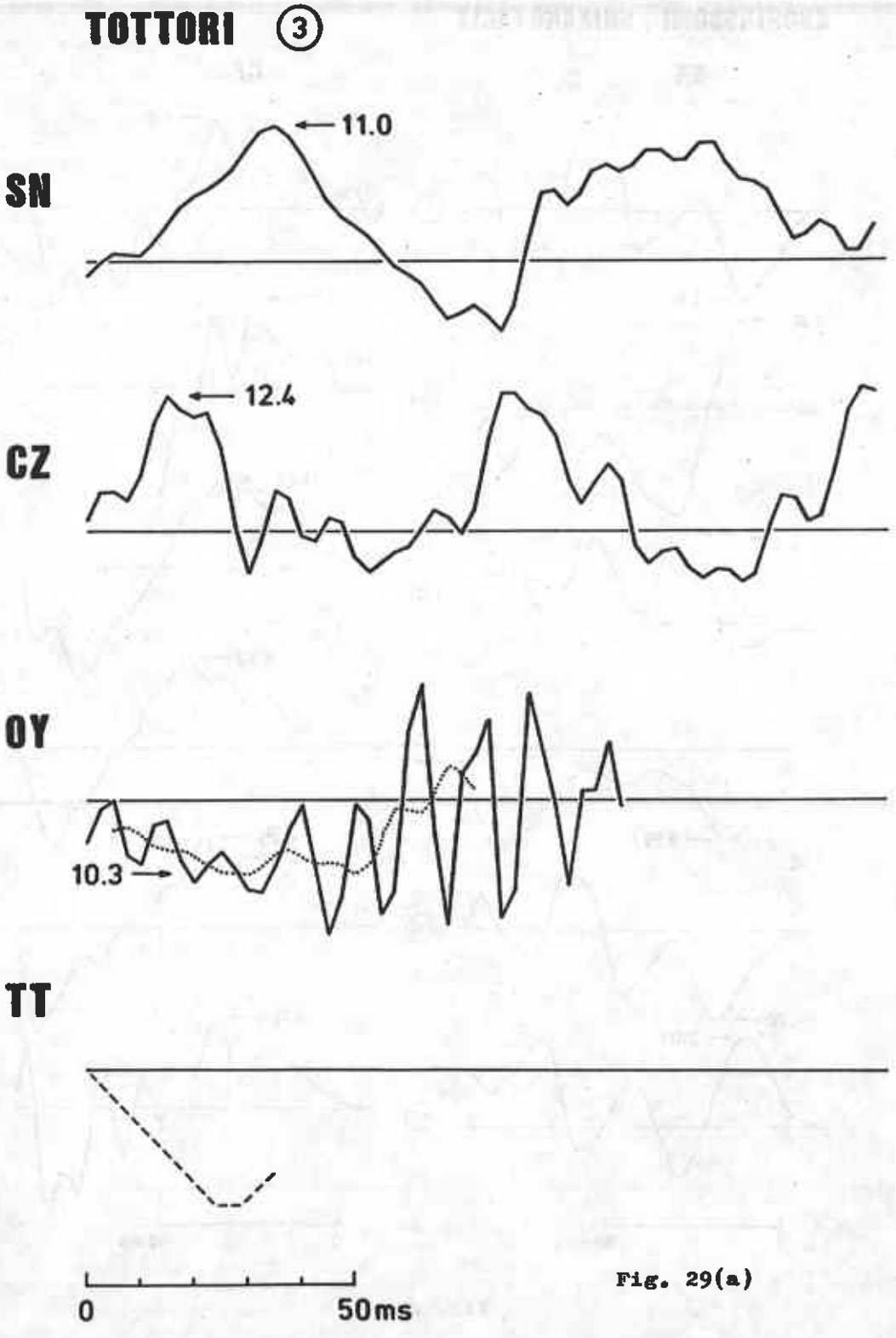

Fig. 29(a)

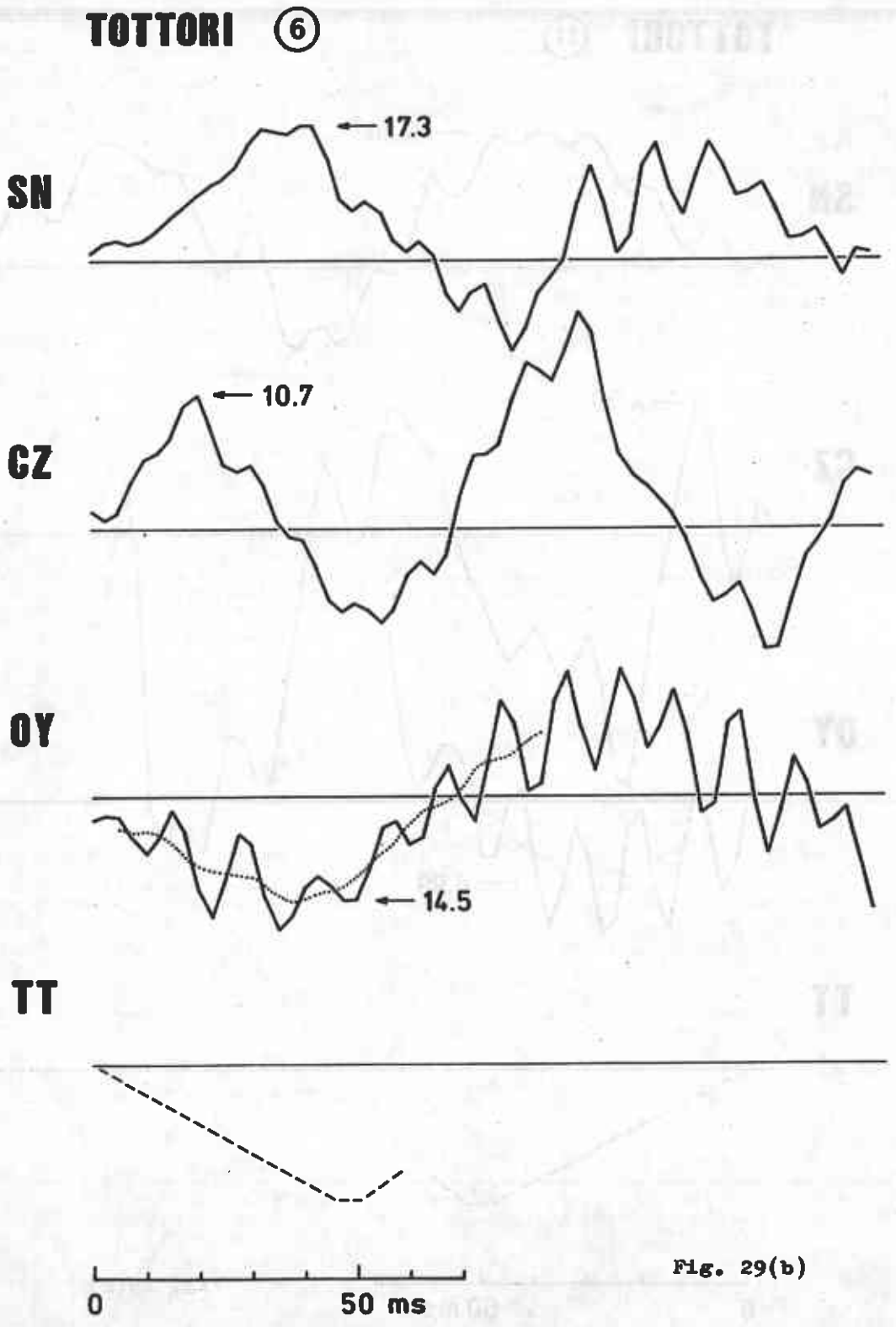

Fig. 29(b)

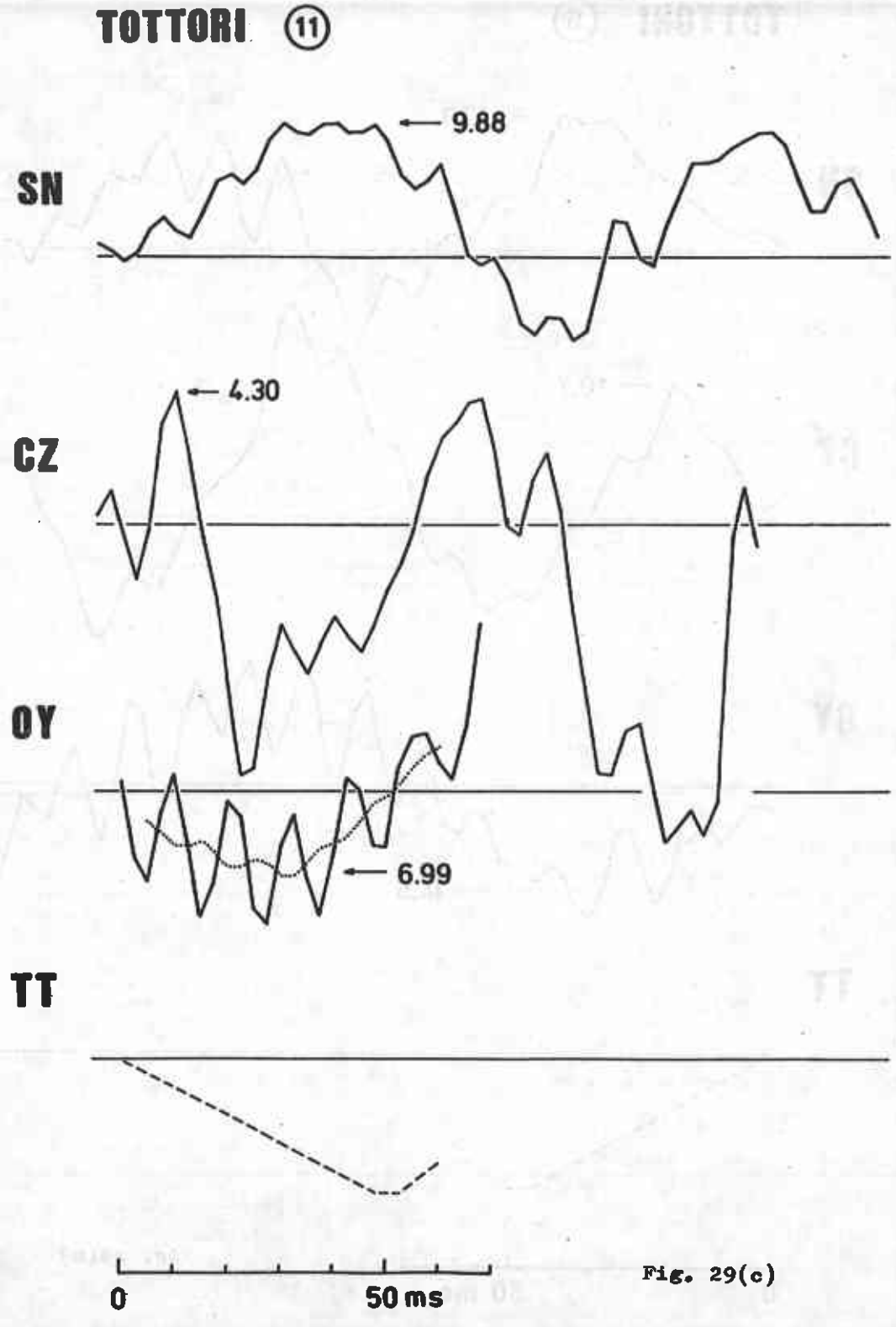

Fig. 29(c)

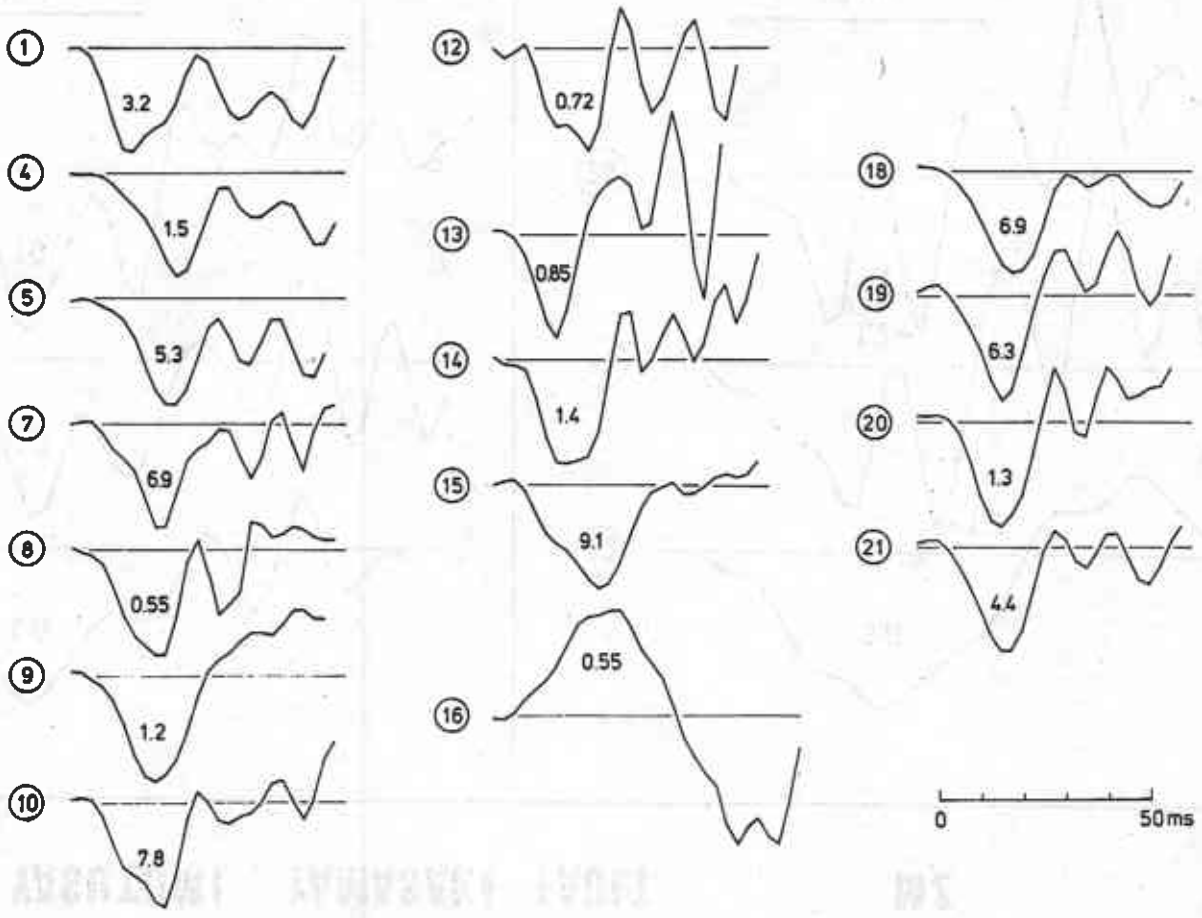
TOTTORI
TT
1
3.2
4
1.5
5
5.3
7
6.9
8
0.55
9
1.2
10
7.8
12
0.72
13
0.85
14
1.4
15
9.1
16
0.55
18
6.9
19
6.3
20
1.3
21
4.4
0
50ms

Fig. 30

YASUTOMI , YAMASAKI FAULT MZ

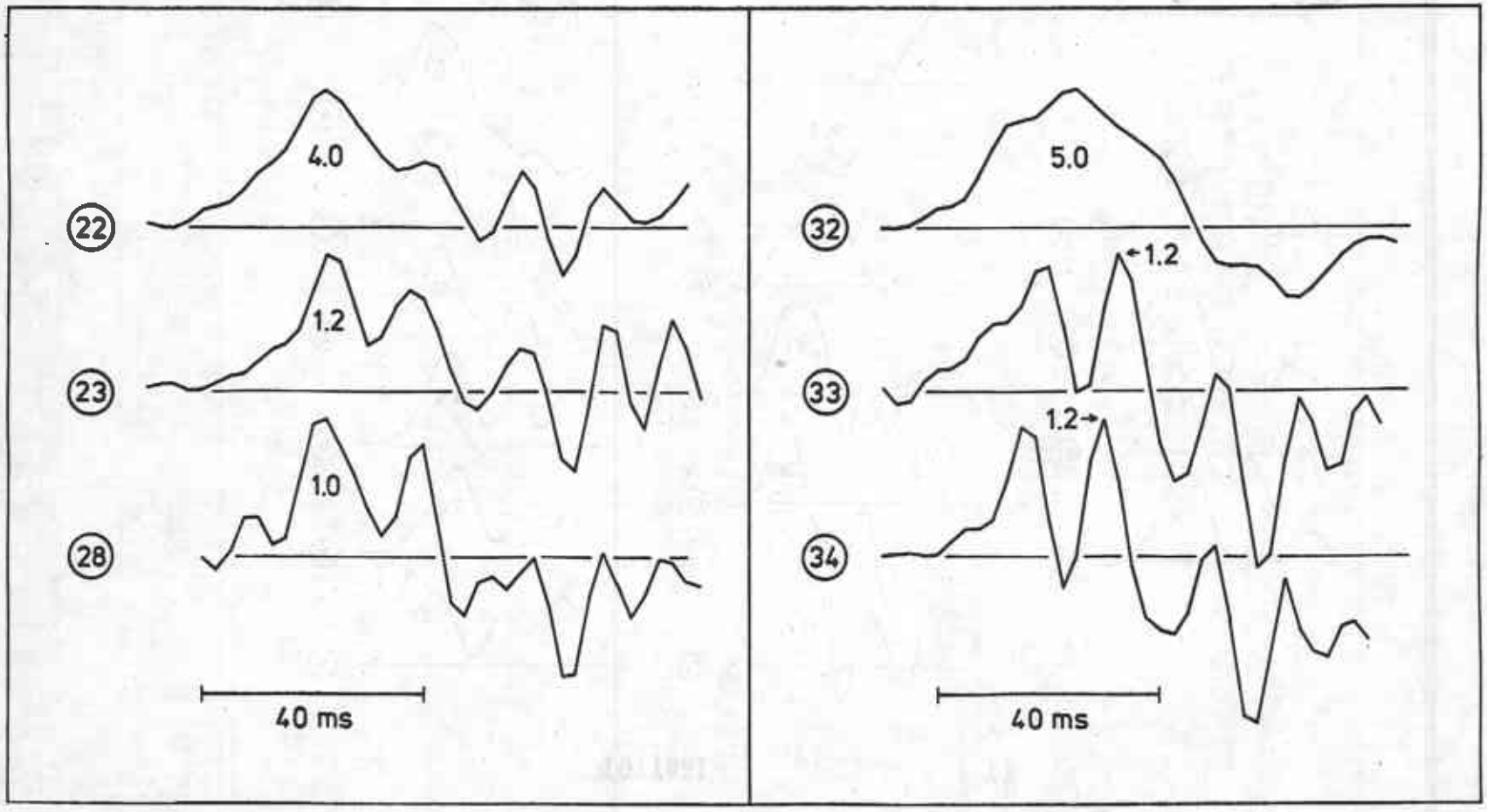

Fig. 31

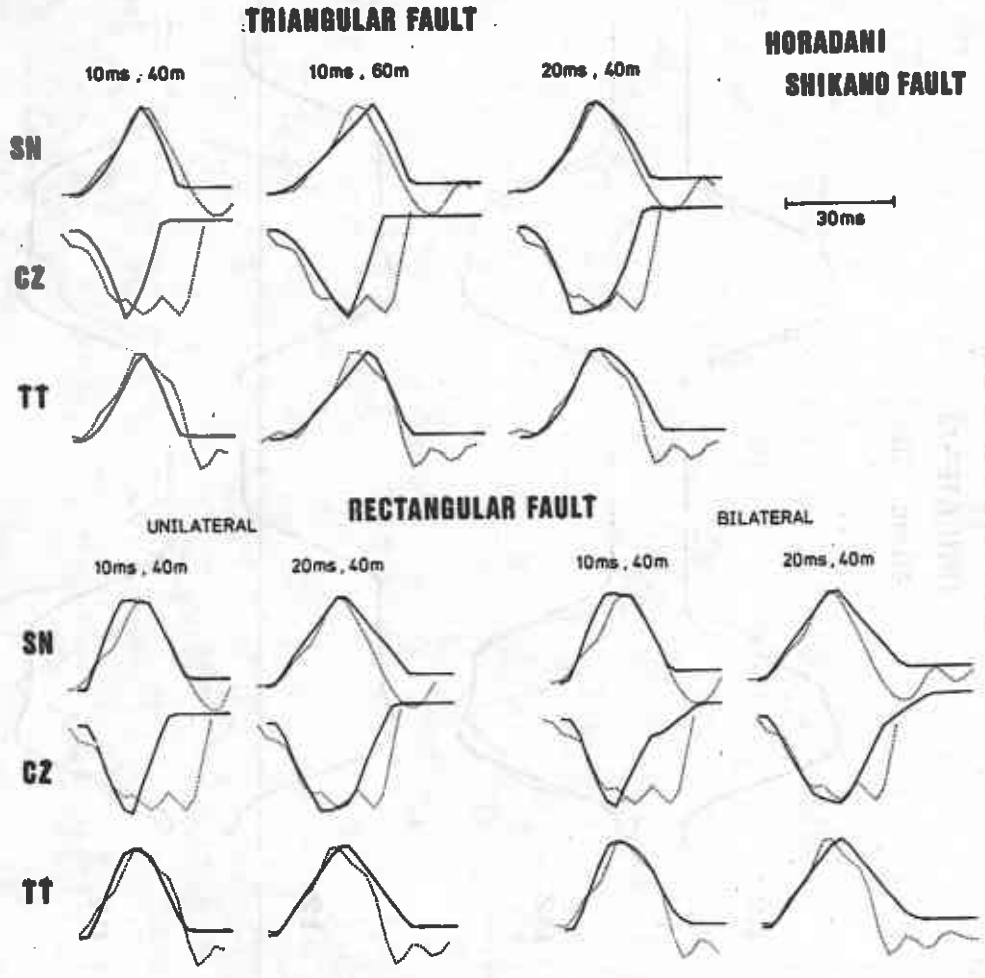
TRIANGULAR FAULT
HORADANI
SHIKANO FAULT
10ms , 40m
10ms , 60m
20ms , 40m
SN
CZ
TT
30ms
RECTANGULAR FAULT
UNILATERAL
BILATERAL
10ms , 40m
20ms , 40m
10ms , 40m
20ms , 40m
SN
CZ
TT

Fig. 32

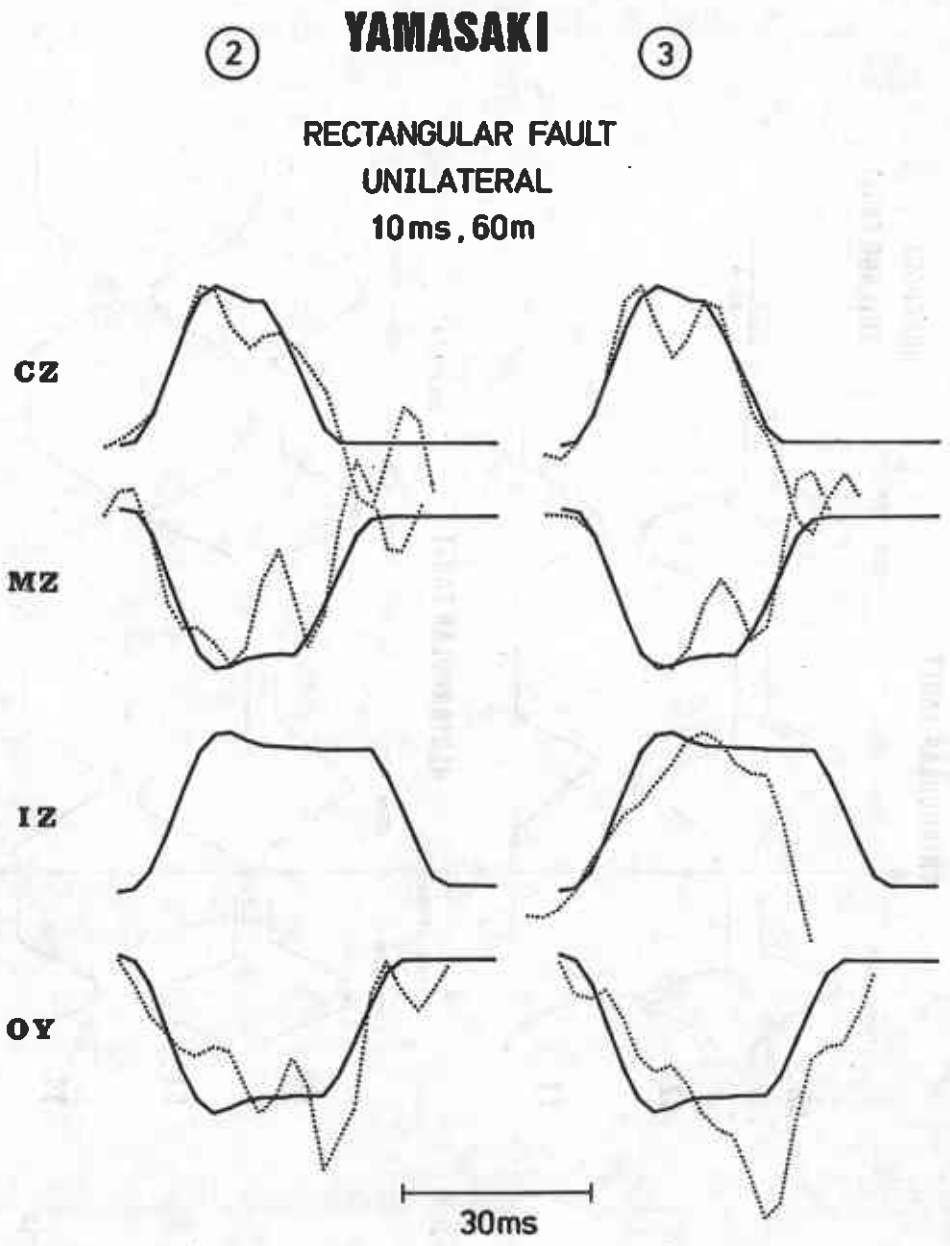
②
YAMASAKI
③
RECTANGULAR FAULT
UNILATERAL
10ms, 60m
CZ
MZ
IZ
OY
30ms

Fig. 33

KUCHIHOSOMI (30)

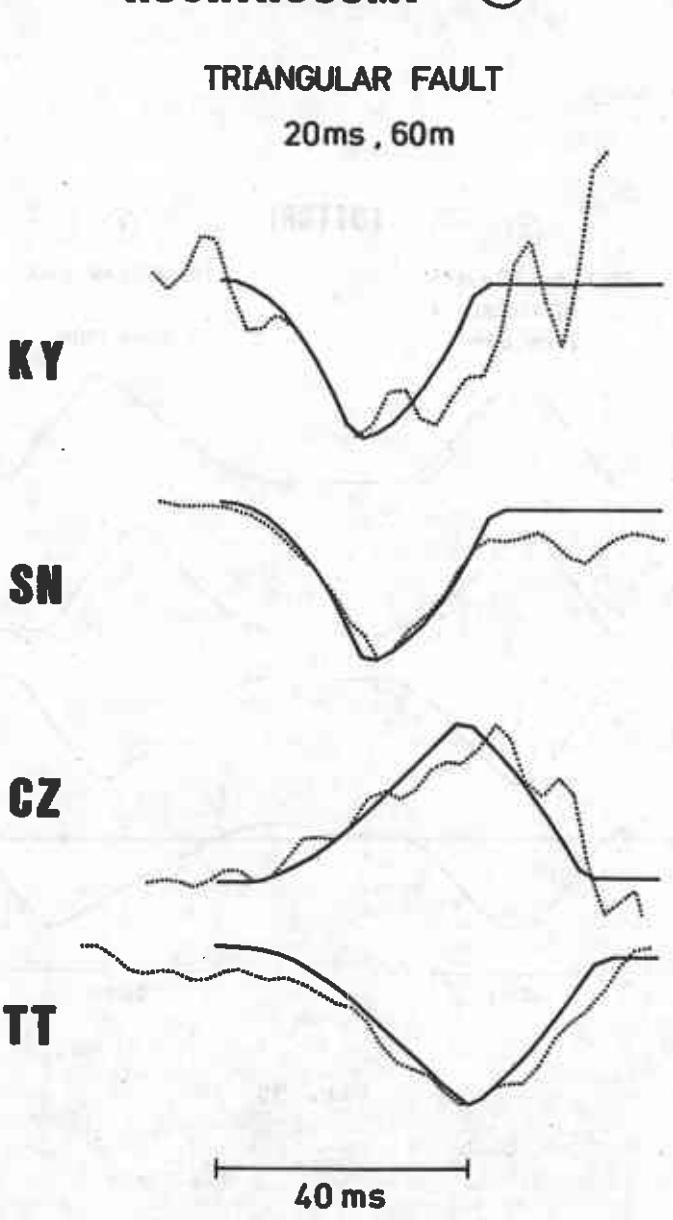

Fig. 34

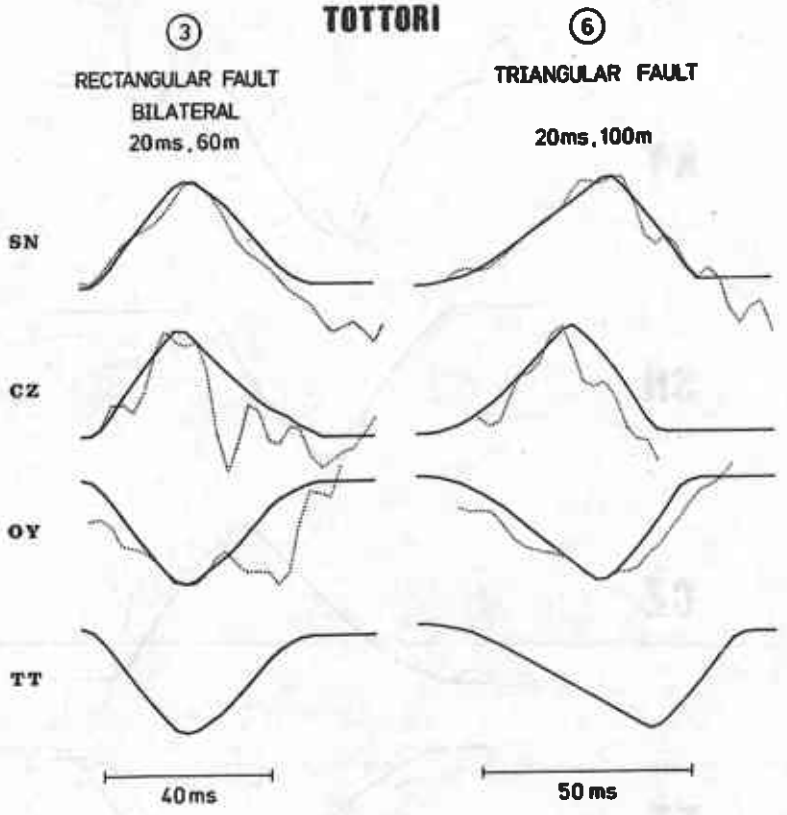
TOTTORI
③
RECTANGULAR FAULT
BILATERAL
20ms, 60m
⑥
TRIANGULAR FAULT
20ms, 100m
SN
CZ
OY
TT
40ms
50ms

Fig. 35

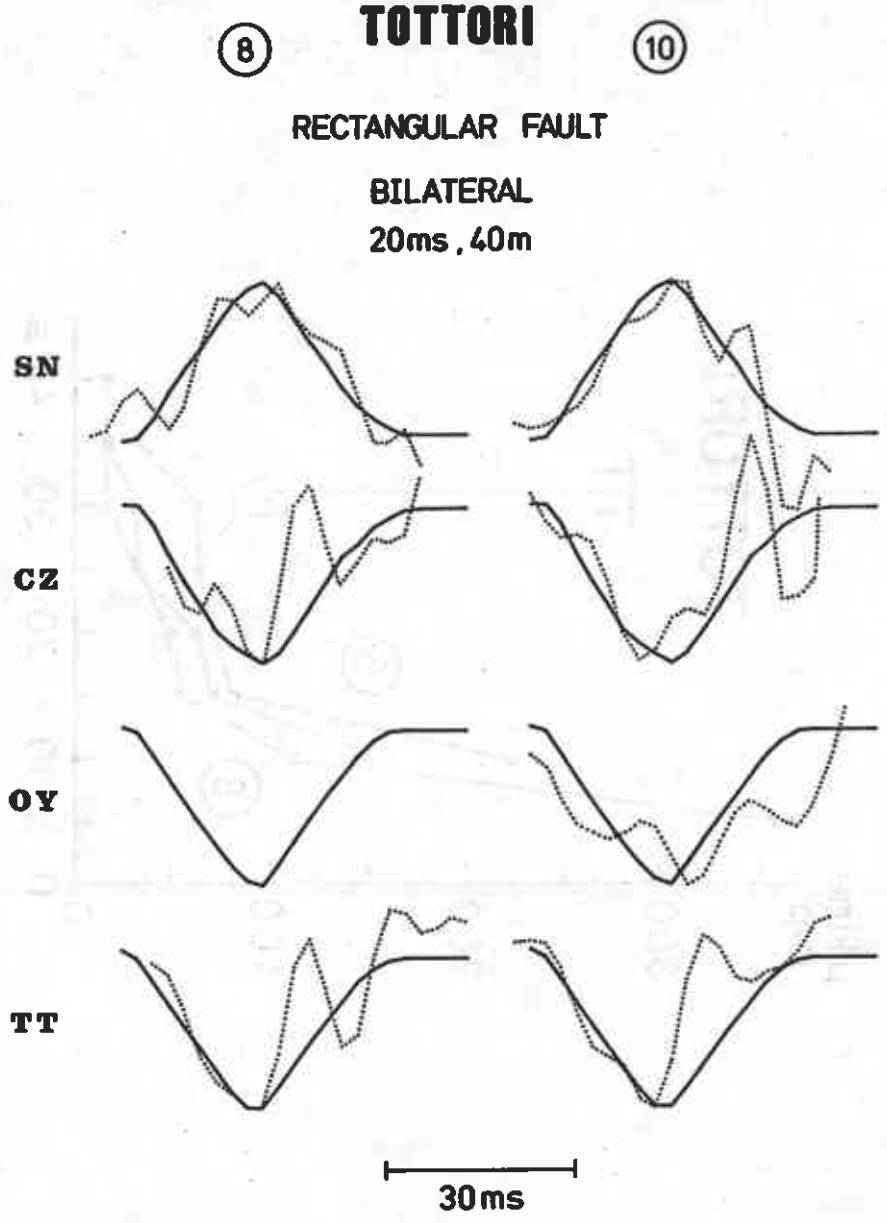
8
TOTTORI
10
RECTANGULAR FAULT
BILATERAL
20ms, 40m
SN
CZ
OY
TT
30ms

Fig. 36

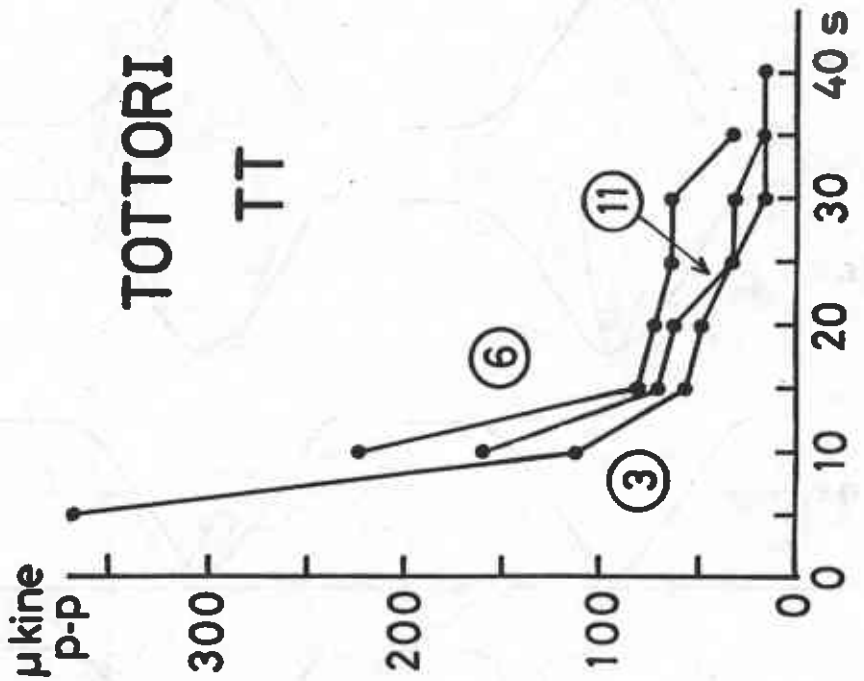

Fig. 37

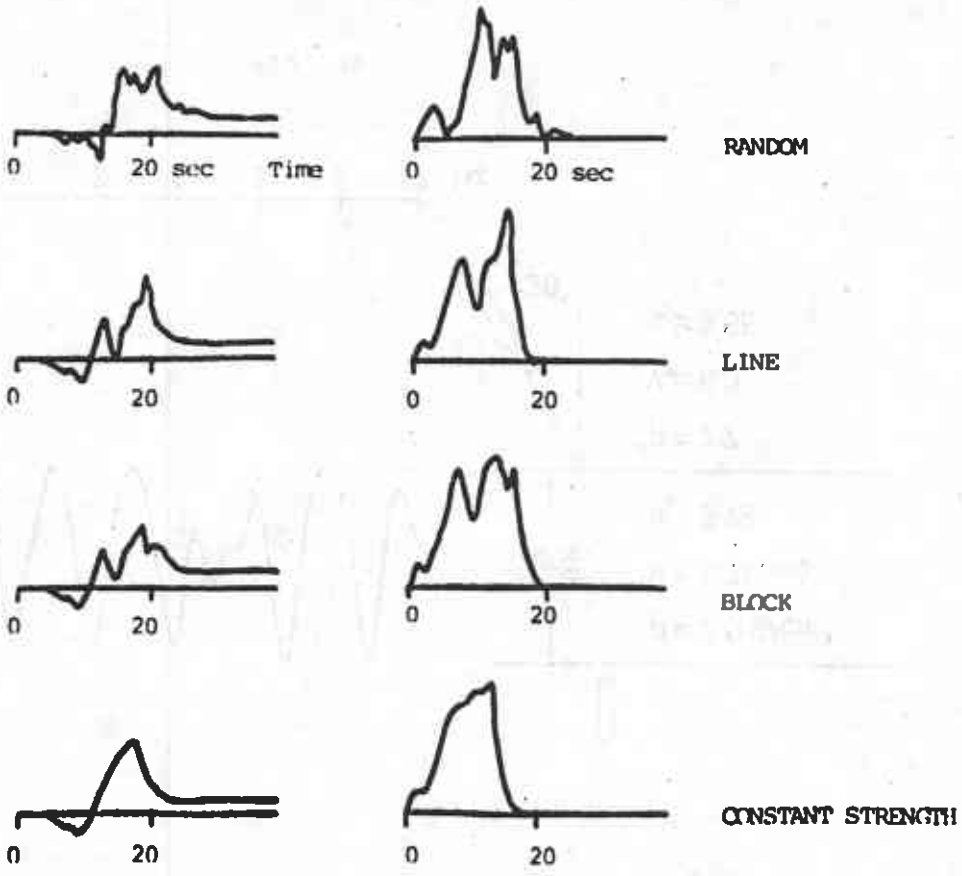
0
20 sec
Time
0
20 sec
RANDOM
0
20
0
20
LINE
0
20
0
20
BLOCK
0
20
0
20
CONSTANT STRENGTH
NEAR FIELD DISPLACEMENTS
FAR FIELD DISPLACEMENTS

Fig. 38

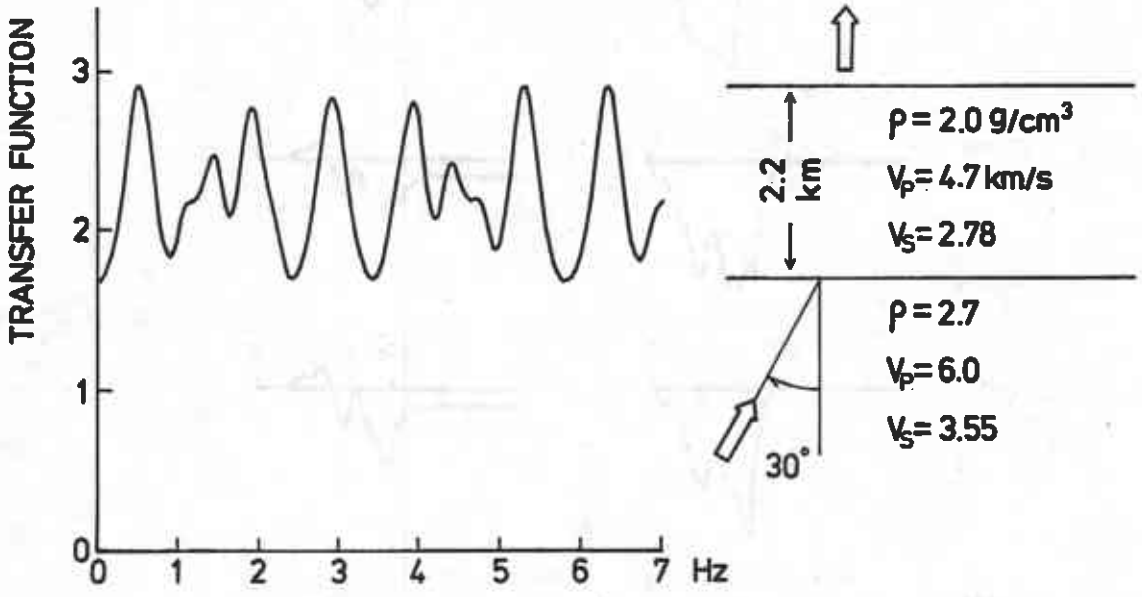
TRANSFER FUNCTION
3
2
1
0
0 1 2 3 4 5 6 7 Hz
2.2 km
ρ = 2.0 g/cm³
Vp = 4.7 km/s
Vs = 2.78
ρ = 2.7
Vp = 6.0
Vs = 3.55
30°

Fig. 39

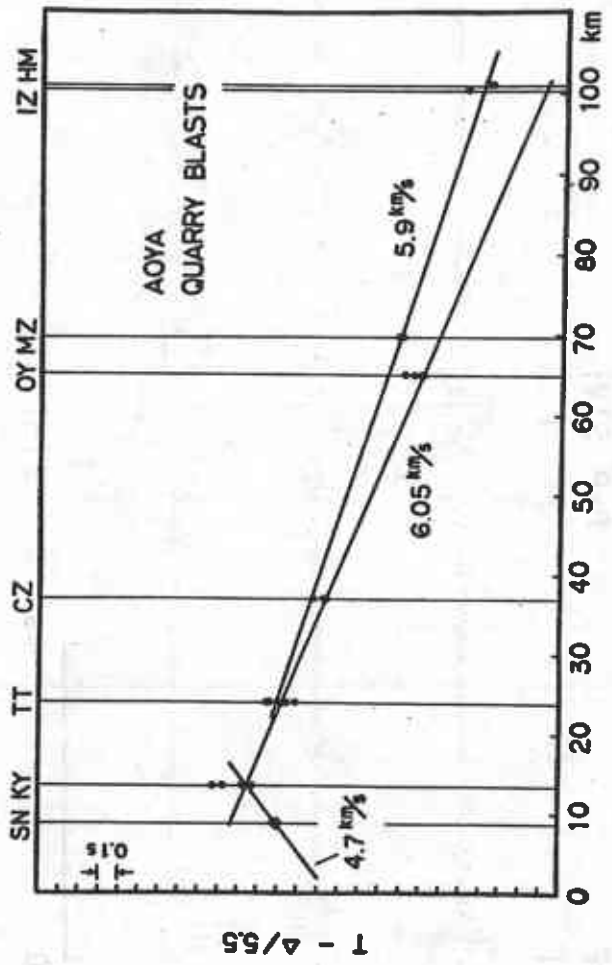
IZ HM
OY MZ
CZ
TT
SN KY
AOYA
QUARRY BLASTS
5.9 km/s
6.05 km/s
4.7 km/s
0.1s
1
T
0
10
20
30
40
50
60
70
80
90
100 km
DISTANCE (Δ)
T - Δ/5.5

Fig. 40

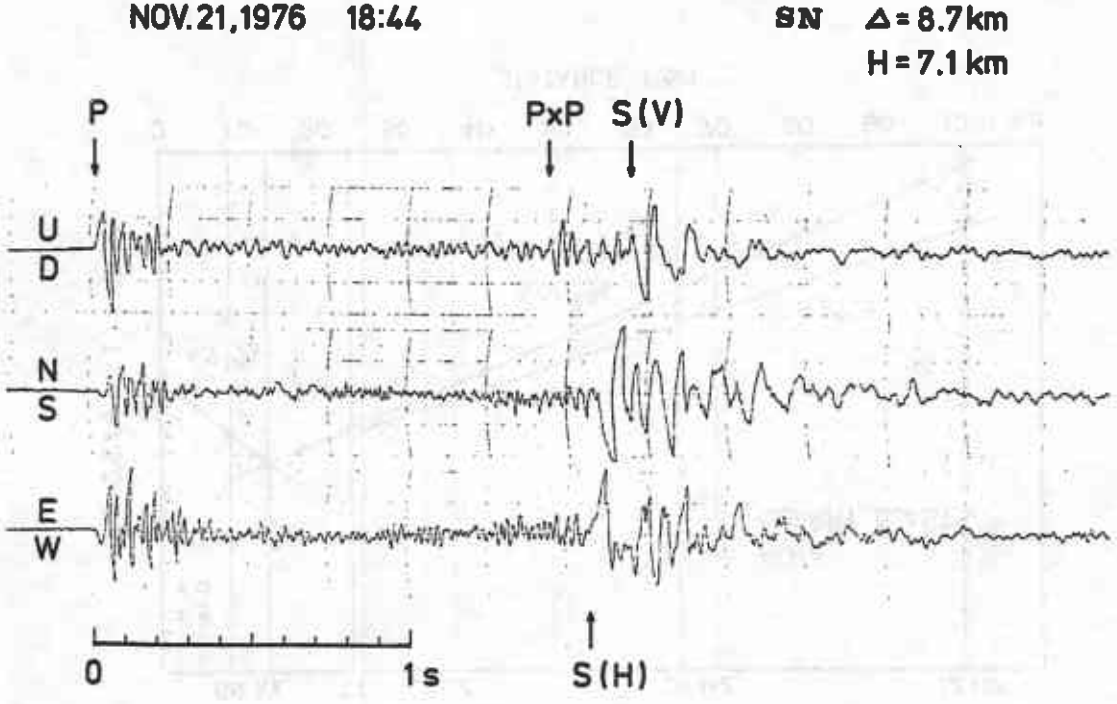

Fig. 41

AUG.4, 1976 00:57

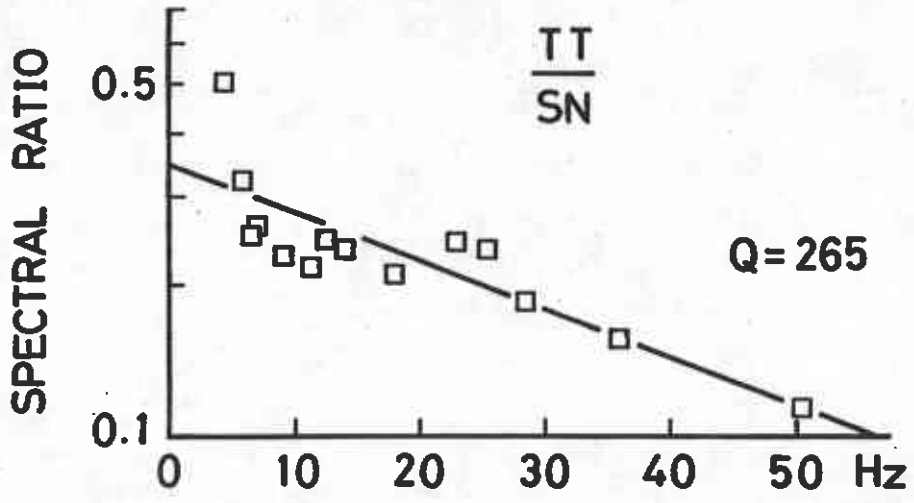

NOV.1, 1976 12:24

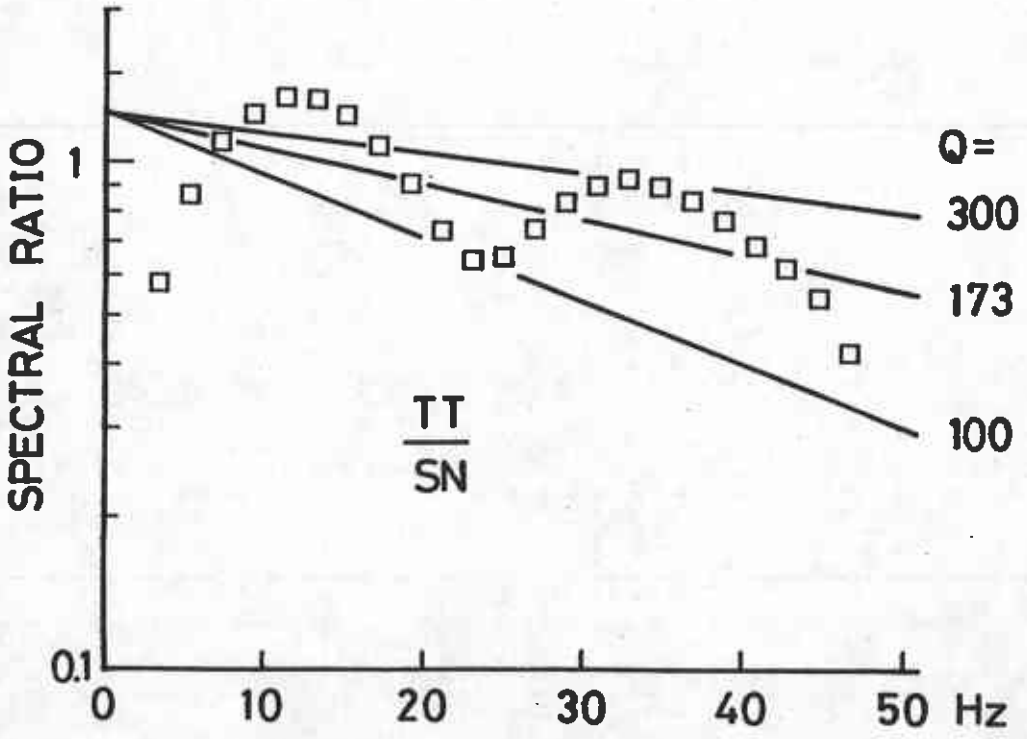

Fig. 42